RADIATION-INDUCED CURRENTS AND CONDUCTIVITY IN POLYETHYLENE

by

JEFFREY CLAIR RYMAN

B.S., Kansas State University, 1969

A MASTER'S THESIS

submitted in partial fulfillment of the

requirements for the degree

MASTER OF SCIENCE

Department of Nuclear Engineering

KANSAS STATE UNIVERSITY
Manhattan, Kansas

1974

Approved by

Richard E. Faw

Major Professor

Table of Contents

ILLEGIBLE DOCUMENT

THE FOLLOWING DOCUMENT(S) IS OF POOR LEGIBILITY IN THE ORIGINAL

THIS IS THE BEST COPY AVAILABLE

Table of Contents (Continued)

Table of Contents (Continued)

List of Figures

List of Figures (Continued)

List of Tables

List of Tables (Continued)

List of Tables (Continued)

1. Introduction

1.1 Background

An understanding of the phenomenon of transient electrical conductivity induced in dielectric materials by ionizing radiation is important in the design of electrical components and systems which must operate in a radiation environment and in the analysis of component and system operation in such an environment. In particular, an understanding of radiation-induced transient electrical conductivity in common insulators such as polyethylene is important in the analysis of the behavior of components such as coaxial cables which are subjected to a radiation environment.

Much work has been done in the investigation of radiation-induced conductivity in organic insulators subjected to X and gamma radiation. Faw and Robinson (1) provide an excellent review of selected literature concerning the effects of X and gamma radiation on dielectrics, as well as a comparison of the various theoretical models which are currently used to describe the phenomenon of radiation-induced electrical conductivity.

In contrast, very few studies of neutron-induced electrical conductivity in insulators have been done. A search of the literature revealed only two reports of investigations in this area. Harrison et al. (2) studied the conductivity of several dielectric materials exposed to pulses of neutron and gamma radiation from the Sandia Pulsed Reactor and the TRIGA Mk-F Reactor. Frankovsky and Shatzkes (3) investigated the radiation-induced currents in several capacitors with different dielectrics exposed to radiation pulses from the Sandia Pulsed Reactor. Although Harrison et al. (2) studied the conductivity during "transient equilibrium" with the pulsed-irradiation

sources, it appears that no work has been done on steady-state neutron-induced electrical conductivity in dielectrics.

1.2 Purpose of the Investigation

During the work of Faw and Robinson (1) currents were observed during and after irradiation of polyethylene at zero applied voltage which had nearly the same magnitude as the currents observed with several hundred volts constant applied voltage. It was found that post-irradiation recovery under constant applied voltage could not be interpreted unless the "short-circuit" current was subtracted from the currents observed with an applied voltage across the specimen. This short-circuit current has also been observed by Fellers (4) and by Yahagi and Danno (5) during gamma-irradiation studies. In addition, Mizutani et al. (6) observed transient currents in polyethylene under short-circuit conditions during irradiation with ultra-violet light.

The first purpose of this work was to investigate the nature of this short-circuit current, to propose a plausible explanation of its origin, and to determine, if possible, whether the corrections made by Faw and Robinson (1) to the post-irradiation data with an applied voltage have a sound theoretical basis.

The second purpose of this work was to study neutron-induced conductivity in polyethylene, since the presence of the 24 Ci KSU ^{252}Cf Facility (7) provided an excellent opportunity to investigate this phenomenon.

2. Theory

2.1 Radiation-Induced Currents Considering Charge Injection and Space-Charge Effects

A survey of the literature indicated that short-circuit currents might be the result of charge injection and non-uniform spatial distribution of trapped charge, but no comprehensive discussion of the equations governing these processes was found. Since a knowledge of these equations is essential to an understanding of the possible origins of the short-circuit currents, a detailed development of the equations will be presented here.

2.1.1 Basic Governing Equations

Several researchers (8-11) have presented some of the equations describing the space-charge-induced fields and currents produced in dielectrics subjected to charge-carrier injection. Lindmayer (8) intuitively relates the current in a short-circuited dielectric sandwiched between two conductors to the motion of the zero-field plane present in the dielectric. Gross and Perlman (9) derive the equations for short-circuit currents in charged insulators from first principles. Monteith and Hauser (10) present numerical solutions to the equations governing the space charge distribution and the electric field in electron-irradiated polyethylene terephthalate. Murphy and Gross (11) discuss the buildup and decay of space charge in a dielectric exposed to a beam of ^{60}Co gamma rays. The common denominator in these investigations is that a spatially non-uniform space charge or non-uniform charge injection can give rise to externally-measurable currents, even under short-circuit conditions. However, one feature absent from all the investigations is consideration of recombination, since only electrons were assumed to be trapped in the insulators.

The equations describing the space-charge distribution, the electric field, and the induced currents will be developed for the specimen and coaxial cable geometries used in this work, which are shown in Fig. 2.1.

The equations relating the electric field and the charge distribution within the dielectric are Poisson's equation and the continuity equations for free and trapped charge carriers. A cylindrical coordinate system is employed, and azimuthal symmetry is assumed.

The charge density $\rho(x,r,t)$ {C m^{-3}} is given by

$$\rho(x,r,t) = e[p(x,r,t) - p_o(x,r) + p_t(x,r,t) - p_{to}(x,r)] - e[n(x,r,t) - n_o(x,r) + n_t(x,r,t) - n_{to}(x,r)] \qquad (2.1)$$

where

e = charge per carrier {1.6×10^{-19} C}

$p(x,r,t)$ = density of free holes {m^{-3}}

$p_o(x,r)$ = density of free holes at equilibrium {m^{-3}}

$p_t(x,r,t)$ = density of trapped holes {m^{-3}}

$p_{to}(x,r)$ = density of trapped holes at equilibrium {m^{-3}}

$n(x,r,t)$ = density of free electrons {m^{-3}}

$n_o(x,r)$ = density of free electrons at equilibrium {m^{-3}}

$n_t(x,r,t)$ = density of trapped electrons {m^{-3}}

$n_{to}(x,r)$ = density of trapped electrons at equilibrium {m^{-3}}.

Charge neutrality at equilibrium requires that

$$\int_V [p_o(x,r) + p_{to}(x,r)]dV = \int_V [n_o(x,r) + n_{to}(x,r)]dV \qquad (2.2)$$

where the integration is carried out over the volume of the insulator.

Poisson's equation governs the electric field within the insulator:

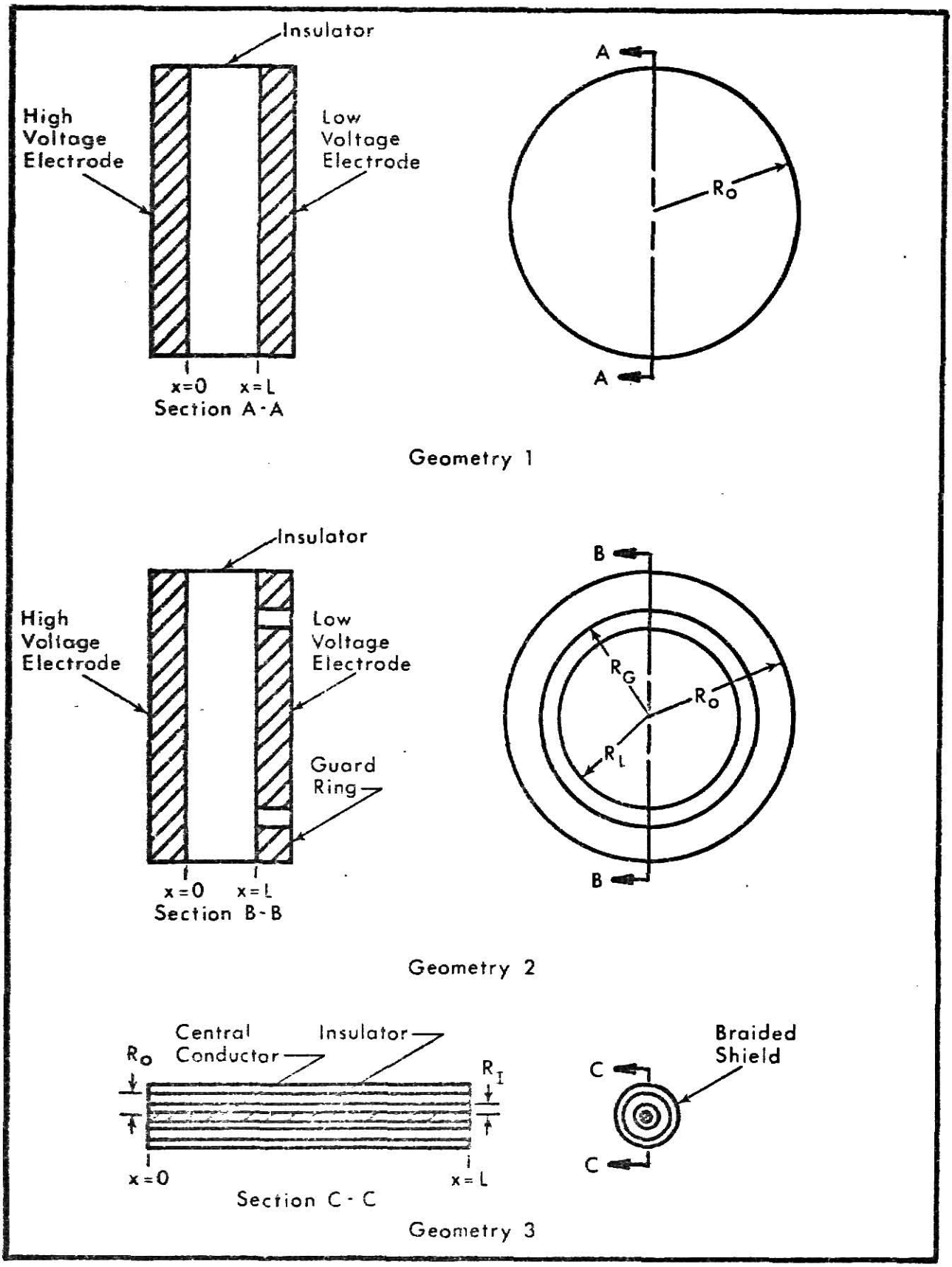

Fig. 2.1 Specimen and coaxial cable geometries.

$$\vec{\nabla} \cdot \vec{E}(x,r,t) = \frac{\rho(x,r,t)}{\varepsilon} \tag{2.3}$$

where

$\vec{E}(x,r,t)$ = electric field vector $\{V\ m^{-1}\}$

ε = permittivity of the insulator $\{C^2\ N^{-1}\ m^{-2}\}$.

The electric field is related to the potential $\phi(x,r,t)$ $\{V\}$ by

$$\vec{E}(x,r,t) = -\vec{\nabla}\,\phi(x,r,t) \tag{2.4}$$

so that

$$\nabla^2\phi(x,r,t) = -\frac{\rho(x,r,t)}{\varepsilon}\ . \tag{2.5}$$

The boundary conditions for the experiments carried out during this investigation are

(1) Geometry 1:

$\phi(0,r,t) = V$ (constant applied voltage) , $0 \le r \le R_o$

$\phi(L,r,t) = 0$, $0 \le r \le R_o$.

(2) Geometry 2:

$\phi(0,r,t) = V$, $0 \le r \le R_o$

$\phi(L,r,t) = 0$, $0 \le r \le R_L$ and $R_G \le r \le R_o$.

(3) Geometry 3:

$\phi(x,R_I,t) = \phi(x,R_o,t) = 0$, $0 \le x \le L$.

To write the continuity equations for free and trapped charge carriers, it is assumed that the insulator may be described in terms of energy bands. Electron and hole traps are assumed to have a continuous energy distribution throughout the forbidden energy gap, and are assumed to have a uniform spatial distribution in the insulator. For convenience, the energy of electron traps is measured downward from the conduction band, while the energy of hole traps is measured upward from the valence band.

The continuity equation for electrons trapped at energy E is

$$\frac{\partial n_t(x,r,t,E)}{\partial t} = \alpha_n(E)n(x,r,t)[n_T(E) - n_t(x,r,t,E)] - \alpha_p(E)p(x,r,t)n_t(x,r,t,E) - \nu_n(E)n_t(x,r,t,E)\exp(-E/kT) \tag{2.6}$$

where

$n_T(E)$ = electron trap density per unit energy $\{m^{-3}\ eV^{-1}\}$

$n_t(x,r,t,E)$ = trapped electron density per unit energy $\{m^{-3}\ eV^{-1}\}$

$\alpha_n(E)$ = electron capture coefficient for traps at energy E $\{m^3\ sec^{-1}\}$

$\alpha_p(E)$ = hole capture coefficient for traps at energy E $\{m^3\ sec^{-1}\}$

$\nu_n(E)$ = "attempt to escape" frequency for electrons trapped at energy E $\{sec^{-1}\}$

k = Boltzmann constant $\{8.617 \times 10^{-5}\ eV\ °K^{-1}\}$

T = absolute temperature $\{°K\}$.

Integrated over the energy gap, Eq. (2.6) becomes

$$\frac{\partial n_t(x,r,t)}{\partial t} = \langle\alpha_n\rangle\, n(x,r,t) \int_0^{E_g} [n_T(E) - n_t(x,r,t,E)]dE - \langle\alpha_p\rangle\, p(x,r,t) \int_0^{E_g} n_t(x,r,t,E)dE - \langle\nu_n\rangle \int_0^{E_g} n_t(x,r,t,E)e^{-E/kT}dE\ , \tag{2.7}$$

where $\langle\alpha_n\rangle$, $\langle\alpha_p\rangle$, and $\langle\nu_n\rangle$ are energy-averaged values, and E_g is the width of the forbidden energy gap $\{eV\}$.

Similarly, the continuity equation for trapped holes, integrated over the energy gap, is

$$\frac{\partial p_t(x,r,t)}{\partial t} = \langle \alpha_p \rangle\, p(x,r,t) \int_0^{E_g} [p_T(E) - p_t(x,r,t,E)]$$

$$- \langle \alpha_n \rangle\, n(x,r,t) \int_0^{E_g} p_t(x,r,t,E)dE - \langle \nu_p \rangle \int_0^{E_g} p_t(x,r,t,E)e^{-E/kT}dE \qquad (2.8)$$

where

$p_T(E)$ = hole trap density per unit energy $\{m^{-3}\ eV^{-1}\}$

$p_t(x,r,t,E)$ = trapped hole density per unit energy $\{m^{-3}\ eV^{-1}\}$

$\langle \nu_p \rangle$ = "attempt to escape" frequency for trapped holes averaged over the forbidden energy gap $\{sec^{-1}\}$.

The capture coefficients $\langle \alpha_n \rangle$ and $\langle \alpha_p \rangle$ are the products of the carrier thermal velocities and their capture cross sections. It is usually assumed that identical cross sections govern trapping and recombination. The attempt to escape frequencies $\langle \nu_n \rangle$ and $\langle \nu_p \rangle$ may be thought of as the probabilities that an electron or hole energetically excited to the conduction or valence band will actually pass into the band. Rose (12) has shown that $\langle \nu_n \rangle = \langle \alpha_n \rangle N_C$ and $\langle \nu_p \rangle = \langle \alpha_p \rangle N_V$, where N_C and N_V are the effective densities of states in the conduction and valence bands, respectively.

The continuity equations for free electrons and free holes are

$$\frac{\partial n(x,r,t)}{\partial t} = g_n(x,r,t) - \frac{\partial n_t(x,r,t)}{\partial t} - \langle \alpha_n \rangle\, n(x,r,t) \int_0^{E_g} p_t(x,r,t,E)dE$$

$$+ \vec{\nabla} \cdot [\mu_n(\vec{E})\, n(x,r,t)\, \vec{E}(x,r,t)] \ , \qquad (2.9)$$

and

$$\frac{\partial p(x,r,t)}{\partial t} = g_p(x,r,t) - \frac{\partial p_t(x,r,t)}{\partial t} - \langle \alpha_p \rangle \, p(x,r,t) \int_0^{E_g} n_t(x,r,t,E)\,dE$$

$$+ \vec{\nabla} \cdot [\mu_p(\vec{E}) \; p(x,r,t) \; \vec{E}(x,r,t)] \qquad (2.10)$$

where

$g_n(x,r,t)$ = generation rate of free electrons per unit volume $\{m^{-3} \; sec^{-1}\}$

$g_p(x,r,t)$ = generation rate of free holes per unit volume $\{m^{-3} \; sec^{-1}\}$

$\mu_n(\vec{E})$ = mobility of free electrons $\{m^2 \; V^{-1} \; sec^{-1}\}$

$\mu_p(\vec{E})$ = mobility of free holes $\{m^2 \; V^{-1} \; sec^{-1}\}$.

In this work, $g_n(x,r,t)$ and $g_p(x,r,t)$ are the result of gamma irradiation of the insulator, electrode system, and coaxial lead components. In general, $g_n(x,r,t) \neq g_p(x,r,t)$ since Compton electrons are scattered from the electrodes into the insulator, and Compton electrons produced near the edges of the insulator may scatter from the insulator. The carrier generation rates also include the electrons and holes produced by secondary ionization from the Compton electrons.

The total current density $\vec{J}(t)$ $\{A \; m^{-2}\}$ at any point in the insulator is the sum of the displacement and conduction current densities:

$$\vec{J}(t) = \frac{\partial \vec{D}(x,r,t)}{\partial t} + \vec{J}_c(x,r,t) \qquad (2.11)$$

where

$\vec{J}_c(x,r,t)$ = conduction current density $\{A \; m^{-2}\}$

$\vec{D}(x,r,t)$ = electric displacement $\{C \; m^{-2}\}$.

The electric displacement is given by

$$\vec{D}(x,r,t) = \varepsilon_o \, \vec{E}(x,r,t) + \vec{P}(x,r,t) \qquad (2.12a)$$

$$= \varepsilon \, \vec{E}(x,r,t) \qquad (2.12b)$$

where

ε_o = permittivity of free space $\{8.854 \times 10^{-12}\ C^2\ N^{-1}\ m^{-2}\}$

$\vec{P}(x,r,t)$ = polarization $\{C\ m^{-2}\}$ (dipole moment per unit volume).

That $\vec{J}(t)$ is a function of time only follows from Maxwell's relation that

$$\vec{\nabla} \times \vec{H}(x,r,t) = \frac{\partial \vec{D}(x,r,t)}{\partial t} + \vec{J}_c(x,r,t) \tag{2.13}$$

where $\vec{H}(x,r,t)$ is the magnetic field strength. If the divergence is taken of both sides of Eq. (2.13),

$$\vec{\nabla} \cdot [\frac{\partial \vec{D}(x,r,t)}{\partial t} + \vec{J}_c(x,r,t)] = 0 \tag{2.14}$$

and $\vec{J}(t)$ will not vary with position. The conduction current density $\vec{J}_c(x,r,t)$ contains a component due to the drift of charge carriers in the internal electric field, a component due to diffusion of carriers, and a component due to movement of injected and radiation-scattered charges particles. In most solids, the diffusion component is small enough to be neglected (9). Then,

$$\vec{J}_c(x,r,t) = \vec{J}_E(x,r,t) + \vec{J}_g(x,r,t) \tag{2.15}$$

where

$\vec{J}_E(x,r,t)$ = field-induced current density

$\vec{J}_g(x,r,t)$ = injection current density.

2.1.2 Reduced Equations

To carry the development any further, it is necessary to make some assumptions about the energy distributions of traps and trapped charge carriers. It is assumed that holes are trapped immediately, i.e., the concentration of free holes is negligibly small. As in the work of Monteith and Hauser (10), it is assumed that all hole traps below the electron Fermi

level E_{fn} are filled, while all traps between the conduction band and the Fermi level are vacant. Then, the continuity equation for trapped electrons is

$$\frac{\partial n_t(x,r,t)}{\partial t} = \langle \alpha_n \rangle\, n(x,r,t) \int_0^{E_{fn}} n_T(E)dE - \langle \nu_n \rangle \int_{E_{fn}}^{E_g} n_T(E) e^{-E/kT} dE \ . \quad (2.16)$$

The dependent variables are assumed to have no radial dependence for geometry 1, and no x dependence for geometry 3. These assumptions will hold if the irradiation is uniform and if edge effects are not great. Finally, the electron trap distribution is assumed to vary exponentially with energy (10):

$$n_T(E) = \frac{B}{kT_c} \exp(-E/kT_c) \quad (2.17)$$

where B and T_c are constants governing the energy distribution. If $E_g >> kT_c$, as is usually the case, then $B \simeq n_T$, where n_T is the total trap density.

Then, for geometry 1, the governing equations become

$$\frac{\partial E(x,t)}{\partial x} = \frac{\rho(x,t)}{\epsilon} \ , \quad (2.18a)$$

$$\int_0^L E(x,t)dx = V \text{ (or } 0) \ , \quad (2.18b)$$

$$\frac{\partial n_t(x,t)}{\partial t} = \langle \alpha_n \rangle\, n(x,t)[n_T - n_t(x,t)] - \langle \nu_n \rangle\, n_T \left[1 + \frac{T_c}{T}\right]^{-1} \left[\frac{n_t(x,t)}{n_T}\right]^{(1+T_c/T)} \ , \quad (2.18c)$$

$$\frac{\partial p_t(x,t)}{\partial t} = g_p(x,t) - \langle \alpha_n \rangle\, n(x,t)\, p_t(x,t) \quad (2.18d)$$

and

$$\frac{\partial n(x,t)}{\partial t} = g_n(x,t) - \frac{\partial n_t(x,t)}{\partial t} - \langle \alpha_n \rangle\, n(x,t)\, p_t(x,t) + \frac{\partial}{\partial x}[\mu_n\, n(x,t)\, E(x,t)] \quad (2.18e)$$

where E(x,t) is the magnitude of the electric field strength.

For geometry 3, the governing equations are

$$\frac{1}{r}\frac{\partial}{\partial r}\left[r\ E(r,t)\right] = \frac{\rho(r,t)}{\varepsilon}\ , \tag{2.19a}$$

$$\int_{R_I}^{R_o} E(r,t)dr = 0\ , \tag{2.19b}$$

$$\frac{\partial n_t(r,t)}{\partial t} = \langle\alpha_n\rangle\ n(r,t)\ \left[n_T - n_t(r,t)\right] - \langle\nu_n\rangle\ n_T\left[1+\frac{T_c}{T}\right]^{-1}\left[\frac{n_t(r,t)}{n_T}\right]^{(1+T_c/T)}\ , \tag{2.19c}$$

$$\frac{\partial p_t(r,t)}{\partial t} = g_p(r,t) - \langle\alpha_n\rangle\ n(r,t)\ p_t(r,t)\ , \tag{2.19d}$$

and

$$\frac{\partial n(r,t)}{\partial t} = g_n(r,t) - \frac{\partial n_t(r,t)}{\partial t} - \langle\alpha_n\rangle\ n(r,t)\ p_t(r,t) + \frac{1}{r}\frac{\partial}{\partial r}\left[r\ \mu_n n(r,t)\ E(r,t)\right]\ . \tag{2.19e}$$

2.1.3 Currents and the Movement of Zero-Field Surfaces

In many cases, the externally applied field will be small enough to allow the existence of one or more zero-field surfaces within the insulator. The number and location of surfaces depends on the charge distribution $\rho(x,r,t)$. In the case of only one independent spatial variable, it is possible to relate the current density to the motion of the zero-field planes or cylinders. For geometry 1, Gross and Perlman (9) have shown that under short-circuit conditions

$$J(t) = -\rho[x_i(t),t]\ \frac{dx_i}{dt} + J_g[x_i(t),t] \tag{2.20}$$

where $x_i(t)$ is the coordinate of any zero-field plane. For the case of no irradiation (no injection current),

$$J(t) = -\rho[x_i(t),t]\,\frac{dx_i}{dt} \quad , \tag{2.21}$$

and

$$\rho[x_1(t),t]\,\frac{dx_1}{dt} = \rho[x_2(t),t]\,\frac{dx_2}{dt} = \ldots \tag{2.22}$$

which shows that multiple zero-field planes cannot move independently of each other. It should be noted that if $\rho(x,t)$ is separable into a product of functions of time only, and space only, i.e., $\rho(x,t) = f(x)\,h(t)$, then dx_i/dt is zero and the total current density is zero in the absence of any injection current. The same equations are valid in the case of a constant applied voltage, provided the zero-field planes exist.

For geometry 3, it can be shown that (see Appendix 9.2)

$$J(t) = \frac{r_i(t)\ell n(R_o/R_I)}{(R_o - R_I)}\left\{-\rho[r_i(t),t]\,\frac{dr_i}{dt} + J_g[r_i(t),t]\right\} \tag{2.23}$$

where $r_i(t)$ is the coordinate of any zero-field cylinder. If there is no injection current, multiple zero-field cylinders cannot move independently.

2.2 Steady-State Neutron-Induced Conductivity

2.2.1 Basic Principles (1)

Consider a sheet specimen of insulating material of area A{cm^2} and thickness L{cm}. Suppose that a potential difference V{V} is applied across the specimen, resulting in a current flow I{A}. The electrical conductivity σ {$\Omega^{-1}\ cm^{-1}$} is then given by

$$\sigma = \frac{J}{E_o} = \frac{LI}{AV} = \frac{L}{AR} \tag{2.24}$$

where J{$A\ cm^{-2}$} is the magnitude of the current density, E_o {$V\ cm^{-1}$} is the magnitude of the electric field strength, and R{Ω} is the resistance of the specimen.

Suppose that the current I is a result of secondary ionization from neutron irradiation which induces g charge carriers per cm^3 per sec. The current in the specimen is then given by

$$I = gALe\tau/T_r \tag{2.25}$$

where e $\{1.6 \times 10^{-19}$ C$\}$ is the charge per carrier, τ {sec} is the charge carrier lifetime, and T_r {sec} is the charge carrier transit time from electrode to electrode. The transit time is just

$$T_r = \frac{L}{v} = \frac{L}{E_o\mu} = \frac{L^2}{V\mu} \tag{2.26}$$

where v $\{cm\ sec^{-1}\}$ is the charge carrier drift velocity, and μ is the mobility $\{cm^2\ V^{-1}\ sec^{-1}\}$. Then

$$I = gALe\mu\tau V/L \tag{2.27}$$

or

$$\sigma = ge\mu\tau\ . \tag{2.28}$$

The dependence of charge carrier generation rate on neutron flux may be deduced from the following argument.

Neglecting nuclear transmutations, such as the (n,γ) reaction, the primary event of neutron interaction with solids is displacement. Ionization occurs secondarily. The primary knock-on (recoil) atoms can cause further displacements and ionization if they have sufficient energy. Displacement occurs if the target atom receives an energy E_p in excess of E_d, defined as the displacement energy. E_d is of the order of 25 eV for most solids.

In the case of the primary knock-on atom, ionization can occur if the speed of the primary, as it recoils, is greater than the speed of its outermost electrons in their orbits.

When the primary knock-on atom is the projectile, a convenient approximation is the use of an "ionization energy" E_i (13). If the primary

knock-on has energy $E_p \geq E_i$, the most probable interaction is ionization. If $E_p < E_i$, the most probable interaction is displacement. E_i, within a factor of two, is given by

$$E_i \simeq A \times 10^3 \text{ eV} \tag{2.29}$$

where A is the atomic mass number of the target atom.

The number of primary knock-on atoms per cm^3 per sec capable of causing further ionization is

$$N_{pi} = N_A \int_{E_i}^{E_p(max)} dE_p \int_i \phi(E)\, k(E,E_p) dE \tag{2.30}$$

where N_A is the number of target atoms per cm^3, $\phi(E)$ is the neutron flux per unit energy, $k(E,E_p)\, dE_p$ is the probability that a collision between a neutron of energy E and a target atom results in a primary knock-on energy in dE_p about E_p, and the subscript i on the innermost integral indicates that only those values of E capable of causing $E_p \geq E_i$ are considered.

Rearranging,

$$N_{pi} = N_A \int_{E_i}^{E_p(max)} dE_p \int_i \phi(E)\, dE \frac{\int_i \phi(E)\, k(E,E_p)\, dE}{\int_i \phi(E)\, dE} \tag{2.31}$$

or

$$N_{pi} = N_A\, \phi_i \int_{E_i}^{E_p(max)} dE_p\, \bar{k}_i(E_p) \tag{2.32}$$

where $\bar{k}_i(E_p)$ is the displacement cross section averaged over the neutron energy distribution in the range where $E_p \geq E_i$, and ϕ_i is now the neutron fast flux.

Since the charge carrier generation rate will be proportional to N_{pi}, it can be given as

$$g = C_1 \phi_f \tag{2.33}$$

or

$$g = C_2 \dot{\theta} \tag{2.34}$$

where $\dot{\theta}$ is the absorbed dose rate, C_1 and C_2 are appropriate proportionality constants, and the subcript f specifically denotes the fast neutron flux. The conductivity during steady-state irradiation may now be expressed as

$$\sigma = g\tau e\mu = C_1\phi_f\tau e\mu = C_2\dot{\theta}\tau e\mu \ . \tag{2.35}$$

2.2.2 The Rose Model

Probably the most successful model which can explain the dose-rate dependence of radiation-induced conductivity is that of Albert Rose (12,14, 15). His model predicts that $\sigma \propto \dot{\theta}^{\delta}$, where $0.5 \leq \delta \leq 1$.

The model assumes that insulators may be described in terms of energy bands. A continuous distribution of states is postulated in the forbidden energy band. States close to the conduction band behave as traps for electrons and recombination centers for holes. States close to the valence band behave as traps for holes and recombination centers for electrons. States in the middle of the forbidden gap behave as recombination centers for both carriers. Demarcation levels defining these regions can be given in terms of Fermi levels. The demarcation and Fermi levels are shown in Fig. 2.2. Again, for convenience, the energy of electron traps is measured downward from the conduction band, while the energy of hole traps is measured upward from the valence band. Now, let n_r be the density of recombination states occupied by electrons, and p_r the density of recombination states not occupied by electrons. Other notation is the same as in

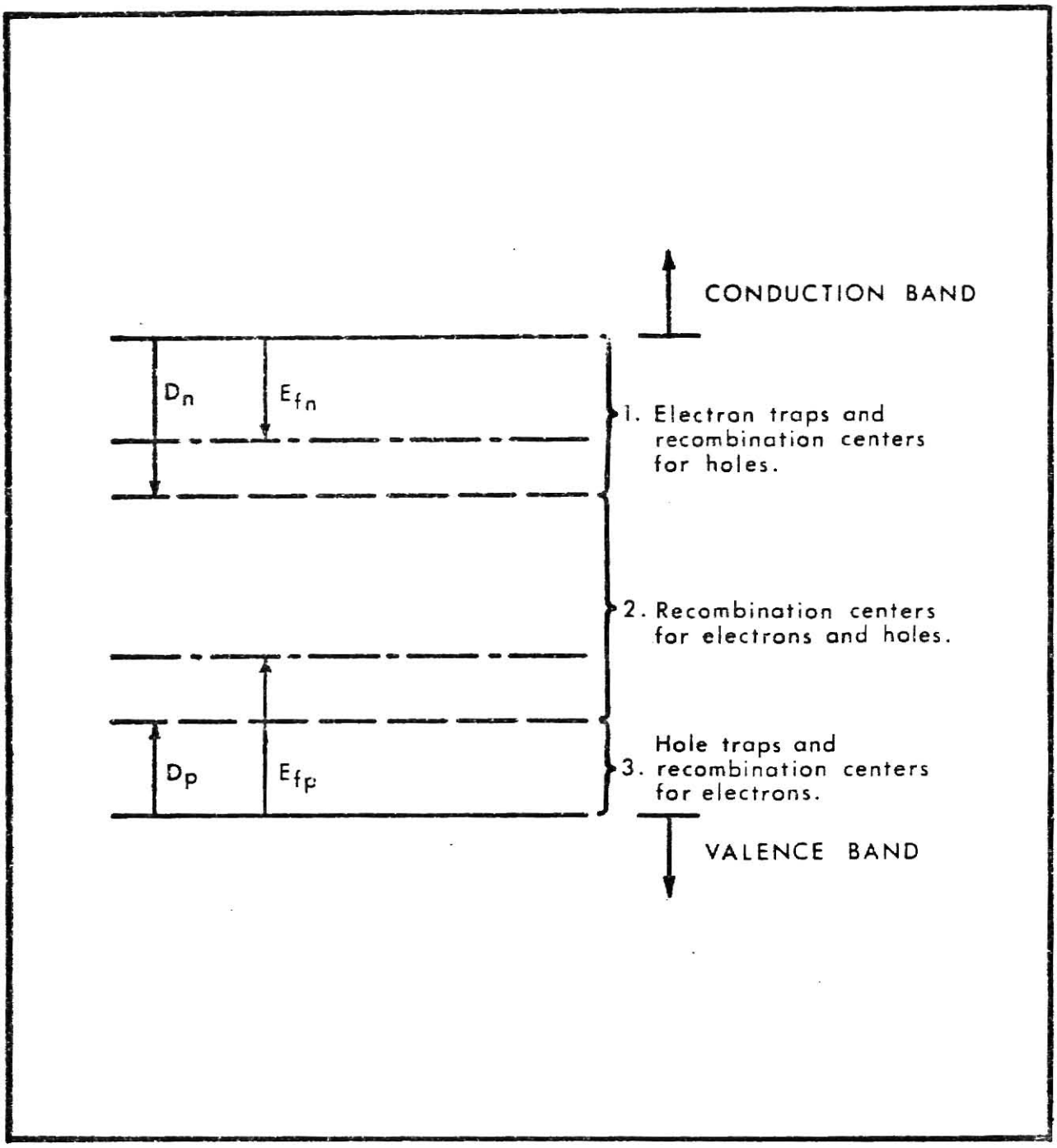

Fig. 2.2 Illustration of demarcation and Fermi levels (15).

Section 2.1. It is assumed that the concentrations of free electrons and free holes are small in comparison to n_r and p_r. Then, under steady-state conditions,

$$n \simeq \frac{g}{p_r \alpha_n} \quad \text{and} \quad p \simeq \frac{g}{n_r \alpha_p} \tag{2.36}$$

so that

$$\frac{p}{n} = \frac{\alpha_n p_r}{\alpha_p n_r} . \tag{2.37}$$

The steady-state electron and hole Fermi levels E_{fn} and E_{fp} are defined by

$$\frac{n}{N_C} = e^{-E_{fn}/kT} \quad \text{and} \quad \frac{p}{N_V} = e^{-E_{fp}/kT} . \tag{2.38}$$

The electron and hole demarcation levels D_n and D_p are defined as those levels at which there is equal probability of reexcitation or hole (electron) capture, i.e.,

$$\alpha_n N_C e^{-D_n/kT} = p\alpha_p \tag{2.39a}$$

and

$$\alpha_p N_V e^{-D_p/kT} = n\alpha_n . \tag{2.39b}$$

Then, from equations (2.37) and (2.38),

$$D_n = E_{fn} + kT \ln(n_r/p_r) \tag{2.40}$$

and

$$D_p = E_{fp} - kT \ln(n_r/p_r) . \tag{2.41}$$

Now, in Fig. 2.2, if an electron is trapped in Region 1, reexcitation is more likely than hole capture. If a hole is trapped in Region 3, reexcitation to the valence band is more likely than electron capture. States in Region 2 are the principal sites for recombination. Rose makes three assumptions: (1) in the absence of radiation, p_r is negligibly small, (2) in Region 1, the electron traps have an energy distribution $n_T(E) = B e^{-aE}$, where $a \leq 1$, and (3) $\alpha_p >> \alpha_n$. These assumptions mean that only one type of

recombination center exists, electron traps have an exponentially decreasing energy distribution, and hole conduction is negligible.

Now, during irradiation,

$$p_r \simeq \int_{E_{fn}}^{\infty} n_T(E)dE = \frac{B}{a} e^{-aE_{fn}} = \frac{B}{a}\left(\frac{n}{N_C}\right)^a \tag{2.42}$$

But,
$$n_T \simeq \int_0^{\infty} n_T(E)dE \simeq \frac{B}{a} . \tag{2.43}$$

Thus,
$$p_r = n_T\left(\frac{n}{N_C}\right)^a . \tag{2.44}$$

However, $p_r = g/n\alpha_n$, so that

$$n = \left[\frac{gN_C^a}{\alpha_n n_T}\right]^{\frac{1}{1+a}} \tag{2.45}$$

Since $a \leq 1$, the exponent δ must lie in the range $0.5 \leq \delta \leq 1.0$ But, $n = g\tau$, so that

$$\tau = \frac{g}{n} \propto g^{\delta-1} \propto \dot{\theta}^{\delta-1} . \tag{2.46}$$

Substitution of these results in Eq. (2.35) gives the expression of Rose for steady-state radiation-induced electrical conductivity:

$$\sigma = A_\theta \dot{\theta}^{\delta} \quad , \quad 0.5 \leq \delta \leq 1 \tag{2.47}$$

where A_θ is a new proportionality constant.

3. Experimental Work

3.1 Current Measurements

The required measurement is that of the current I flowing through the polyethylene specimen as a function of applied voltage, dose, and dose rate. The technique used in this work is that followed by Faw and Robinson (1). The method is illustrated in Fig. 3.1. A stable, high gain, high input-impedance electrometer operational amplifier with precision feedback resistors from 10^9 to 10^{13} ohms is used. The amplifier input is at virtual ground potential. The output signal from the amplifier is fed simultaneously to a strip chart recorder and a digital voltmeter.

3.1.1 Apparatus Used during Gamma Irradiation

The current measurement apparatus used in this work is illustrated in block diagram form in Fig. 3.2. Table 3.1 lists the items of equipment, manufacturers, and model numbers. The Model 300 electrometer was calibrated using the Keithley Model 261 Picoampere Source, and was found to measure correctly to within 0.1 pA.

The gamma ray source was an Atomic Energy of Canada Limited Model 220 Gammacell with a nominal source strength of 3963 Ci as of March 15, 1965. This source consists of several stainless steel pencils containing metallic ^{60}Co slugs which are arranged in a symmetrical array around the outer radius of an 8 in. high by 6 in. diameter cylindrical chamber. The chamber, which is normally in a raised position outside the gammacell, is mechanically lowered to a position within the ^{60}Co source array for irradiation of the specimen. A cross-sectional view of the AECL Model 220 Gammacell is shown in Fig. 3.3.

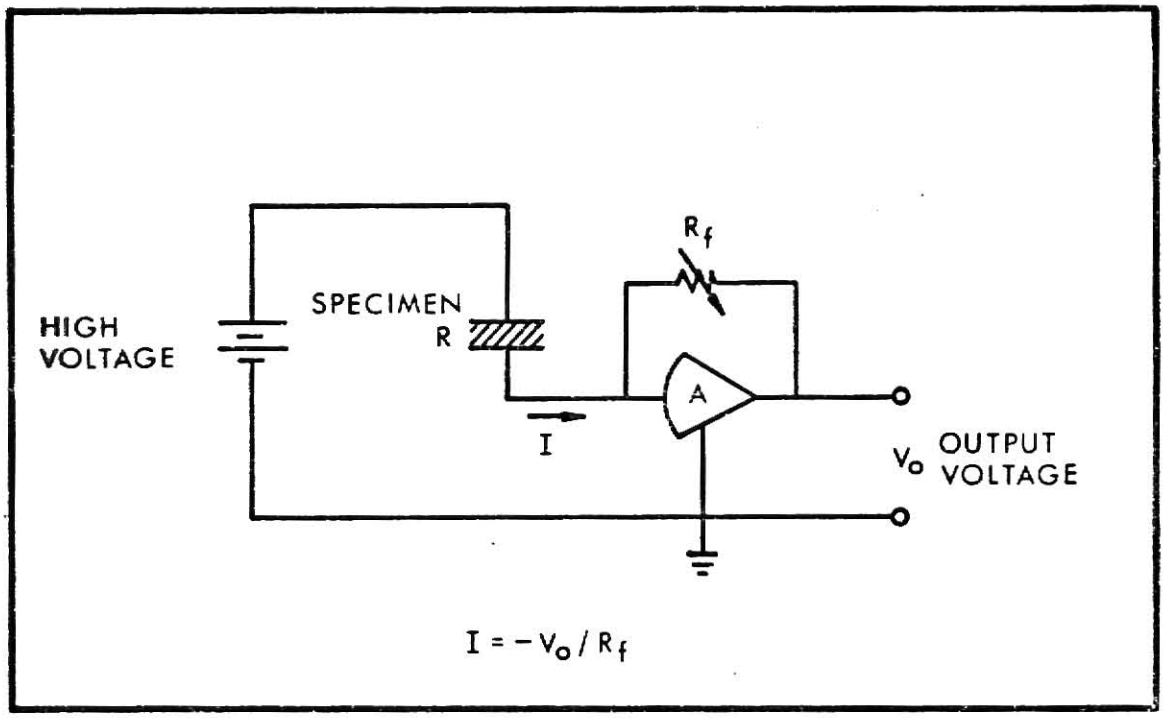

Fig. 3.1 Current measurement technique.

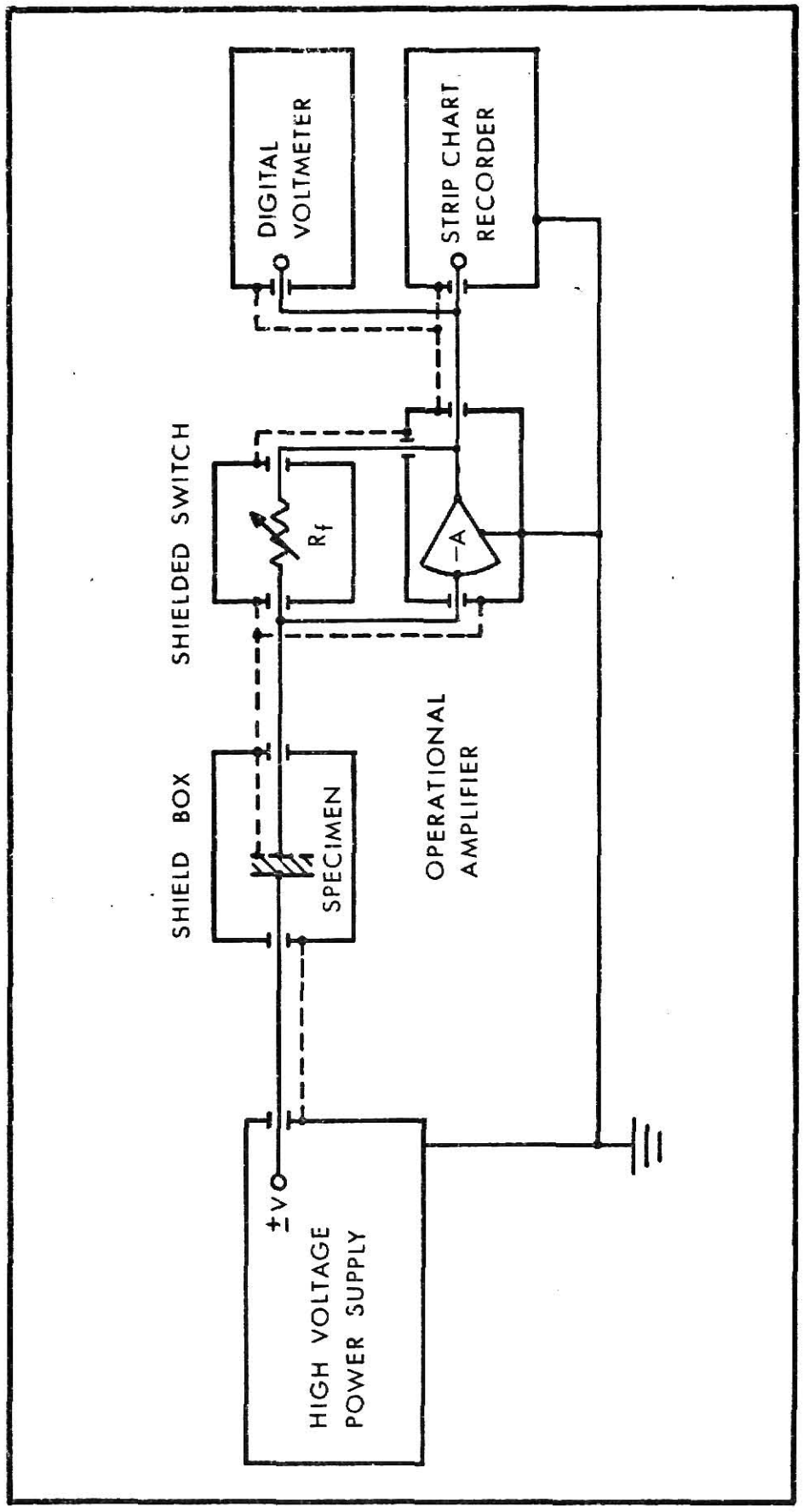

Fig. 3.2 Block diagram of current measurement apparatus. (Cable shielding is shown schematically as dashed lines.)

Table 3.1 Current Measurement Equipment

High Voltage Power Supply:	John Fluke Model 415B
Shielded Switch:	Keithley Model 3011
Feedback Resistors:	Keithley Precision Resistors--10^9, 10^{10}, 10^{11}, 10^{12}, and 10^{13} ohm
Electrometer:	Keithley Model 300
Electrometer DC Power Supply:	Keithley Model 3012
Digital Voltmeters:	Electronics Associates Inc. Model TDVM 5001 Eldorado Model 1820
Strip Chart Recorder:	Leeds and Northrup Model Speedomax X/L 680
Picoampere Source:	Keithley Model 261

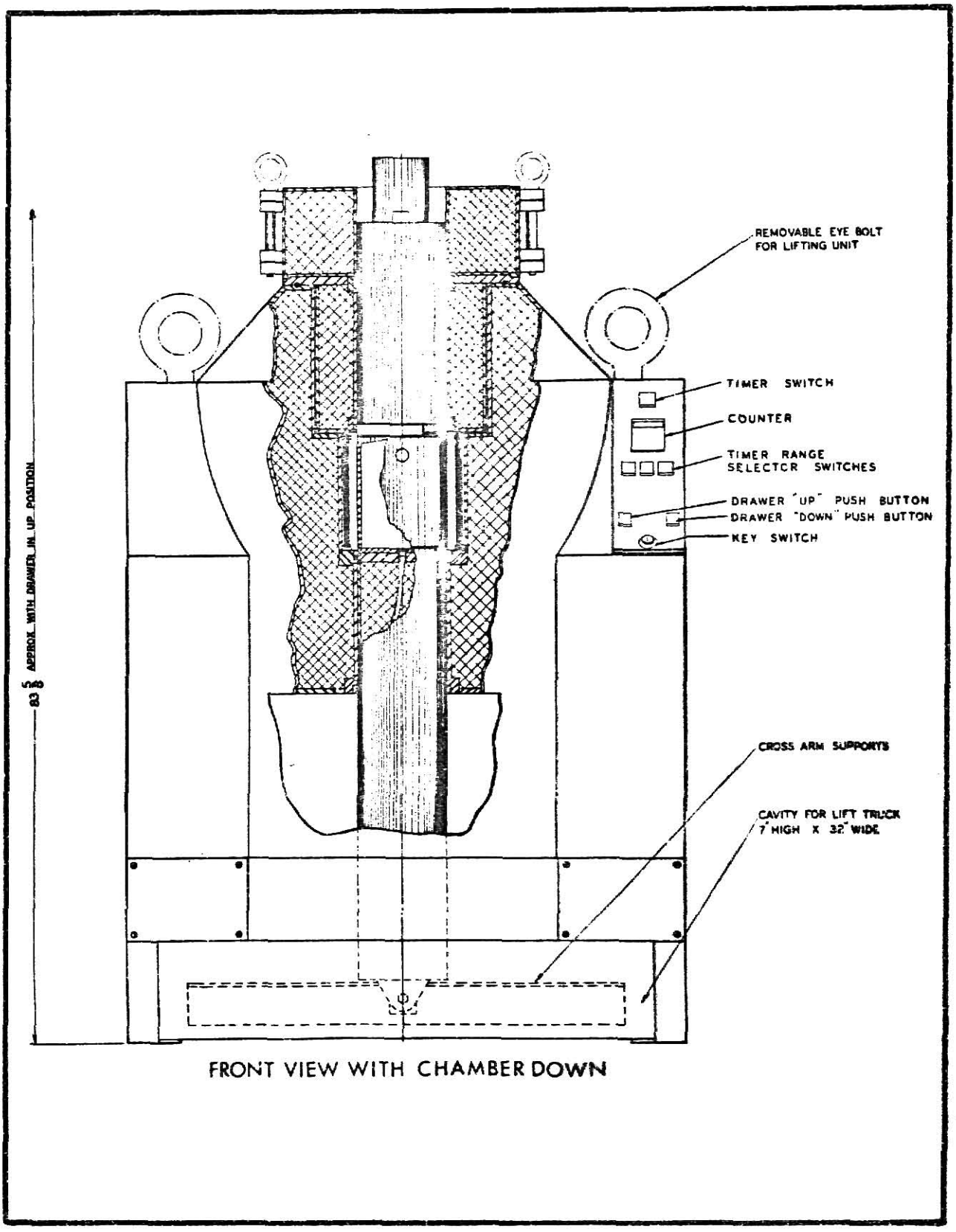

Fig. 3.3 AECL Model 220 Gammacell.

Four circular polyethylene specimens, cut from 0.1524 cm polyethylene sheet stock, were used during the gamma-irradiation work. The specimens have a nominal density of 0.953 g per cm^3 (16).

Plexiglass specimen holders of the type designed by Fellers (4) were used. Fellers' design was modified to give greater mechanical strength at the attachment points for the coaxial leads. Two specimens were designed for use with a guard ring, as in the work previously done by Fellers (4) and by Faw and Robinson (1). Two additional specimens were designed for use without a guard ring, since no fringing effects should occur under short-circuit conditions. One specimen of each type consisted of a single thickness of polyethylene, and the other specimen of each type consisted of a double thickness of polyethylene.

Machining problems during preparation of the copper electrodes resulted in a different electrode diameter for each specimen.

The two types of specimens and specimen holders are shown in Fig. 3.4 and Fig. 3.5, respectively. The specimen dimensions are given in Table 3.2.

Two coaxial leads 1 ft in length were connected to the electrodes by screws which penetrated the plexiglass specimen holders. The leads were Amphenol RG-58A/U cable with polyethylene insulation. The guard ring was connected to the braided shield of the low voltage lead.

An aluminum box designed by Fellers (4) provided electrical shielding of the specimens during the current measurements. The braided shields of both coaxial leads were connected to each other through the shield box.

Coaxial cables approximately 6 ft in length connected the specimen leads to the power supply and operational amplifier. The high voltage cable was Amphenol RG-62/U, while the signal cable was Amphenol RG-58A/U.

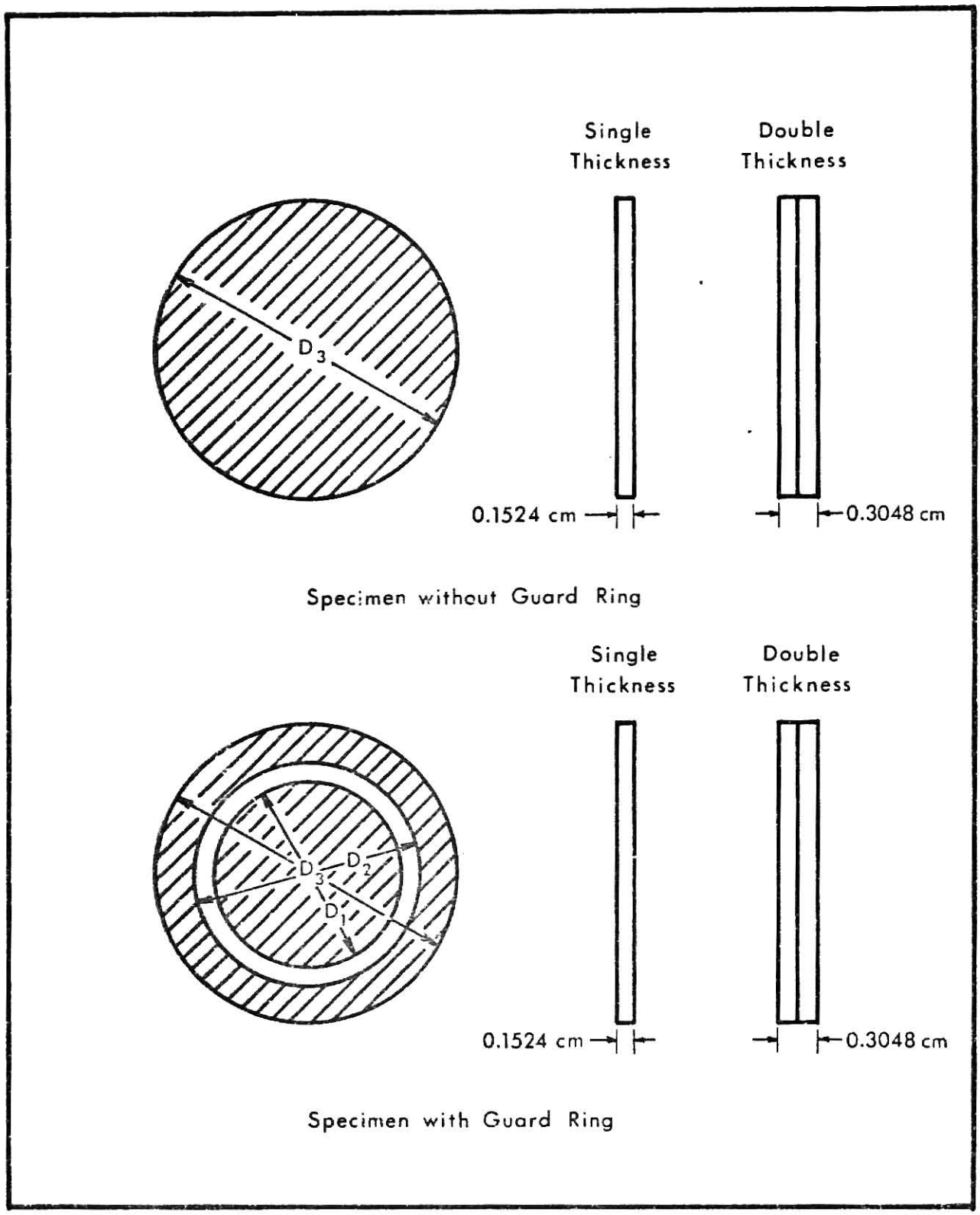

Fig. 3.4 Polyethylene specimens showing electrode positions.

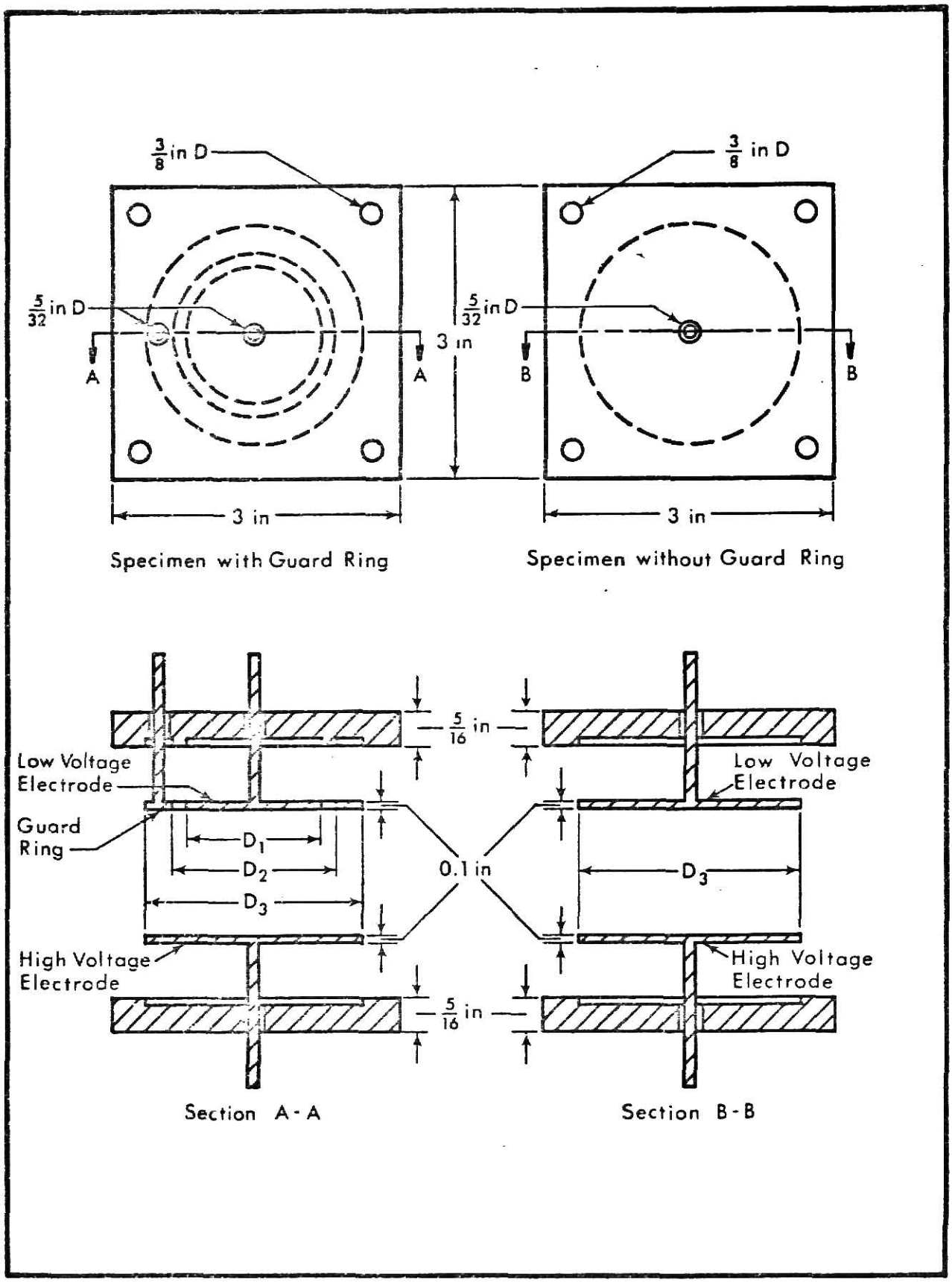

Fig. 3.5 Specimen holders and electrode systems.

Table 3.2 Specimen Dimensions

Dimensions (see Fig. 3.4):	D_1 {cm}	D_2 {cm}	D_3 {cm}
Specimens with Guard Ring			
Single Thickness	2.86	3.33	4.60
Double Thickness	2.86	3.25	4.76
Specimens w/o Guard Ring			
Single Thickness			4.37
Double Thickness			4.60

3.1.2 Experimental Procedure during Gamma Irradiation

Specimen preparation and cleaning are described in detail by Fellers (4) and followed ASTM standards (17). After cleaning with isopropyl alcohol and water, the specimens were dried at 50 (±2) °C for 4 hours, followed by conditioning at a relative humidity of 37 (±1)% for 40 hours. The specimens were then painted with silver conducting paint (E-KOTE, type 3030) at all points of contact with the electrodes and with each other in the case of double thickness specimens. Finally, the specimens were placed in the specimen holders between the electrodes, and potted with paraffin.

The current measuring equipment was allowed to warm up for at least 2 hours prior to taking any measurements to insure thermal stability of the measuring circuits. After the warmup period, the operational amplifier and strip chart recorder were zeroed and the recorder scales were checked using the high-voltage power supply and the digital voltmeter.

Following the equipment checkout, the specimen to be tested was placed in the gammacell irradiation chamber, connected to the measuring equipment, and allowed to rest under short-circuit conditions (zero applied voltage) for one-half hour to allow the decay of any residual space charge from previous tests.

Preliminary current measurements were taken on all 4 specimens both during and after irradiation for irradiation times of 30, 100, 500, and 1000 sec. Post-irradiation data were taken for 1020 sec in each case. During these preliminary tests, the low-voltage electrode of each specimen was connected to the operational amplifier. Two measurements during and after 100 sec irradiations were also taken on one specimen, using a coaxial cable shorting cap in place of the high-voltage power supply. The results of these tests confirmed that the high-voltage power supply, when set to 0 V, acted as a short circuit.

In addition, two tests during and after 1000 sec irradiations were run with a 5.1 MΩ resistor in series with the low-voltage lead. As the input impedance of the operational amplifier is approximately 5 MΩ, the test results should have been noticeably different if the amplifier input impedance affected the measurements. The test results using the additional resistance showed no significant deviation from the test results with no additional resistance, confirming that the amplifier input impedance had little or no effect on the current measurements (see Appendix 9.3).

Following the preliminary measurements, the currents flowing from the high-voltage electrodes and guard rings of all specimens were measured both during and after 1000 sec irradiations. Measurements were taken for two positions of each specimen within the gammacell chamber to determine the

effect of specimen orientation on the observed currents. In the "normal" position the high-voltage electrode faced the left side of the chamber when viewed from the front of the gammacell. In the "reversed" position the high-voltage electrode faced the right side of the chamber.

The test results for both specimens without guard rings seemed to yield no information; thus, testing of these specimens was abandoned.

Further tests for both specimens with guard rings were carried out using 1000 sec irradiations. The currents flowing from the high- and low-voltage electrodes and guard rings of each remaining specimen were measured at least three times in both the normal and reversed configurations. Post-irradiation currents were monitored for 1020 sec.

Finally, three measurements of the currents flowing from the low-voltage electrodes of both remaining specimens were taken during and after 1000 sec irradiations at ±500 V in the normal configuration to check against the results of Faw and Robinson (1).

3.1.3 Apparatus Used during Neutron Irradiation

The current measurement apparatus used during neutron irradiation was the same as that used during gamma irradiation.

The neutron source was the KSU Multi-Milligram ^{252}Cf Source (7), on loan from the U.S. Atomic Energy Commission. This source consisted of four SR-CF-100-Z sources containing $Cf_2(C_2O_4)_3$ encapsulated in zircaloy or stainless steel, with a nominal source strength of 6.0 curies each. A cross-sectional view of the KSU ^{252}Cf Facility is shown in Fig. 3.6. The four sources, totaling 34.9 mg of ^{252}Cf, were positioned in a source holder at the bottom of the well as shown in Fig. 3.6. The source holder is shown in Fig. 3.7, with the source positions as indicated.

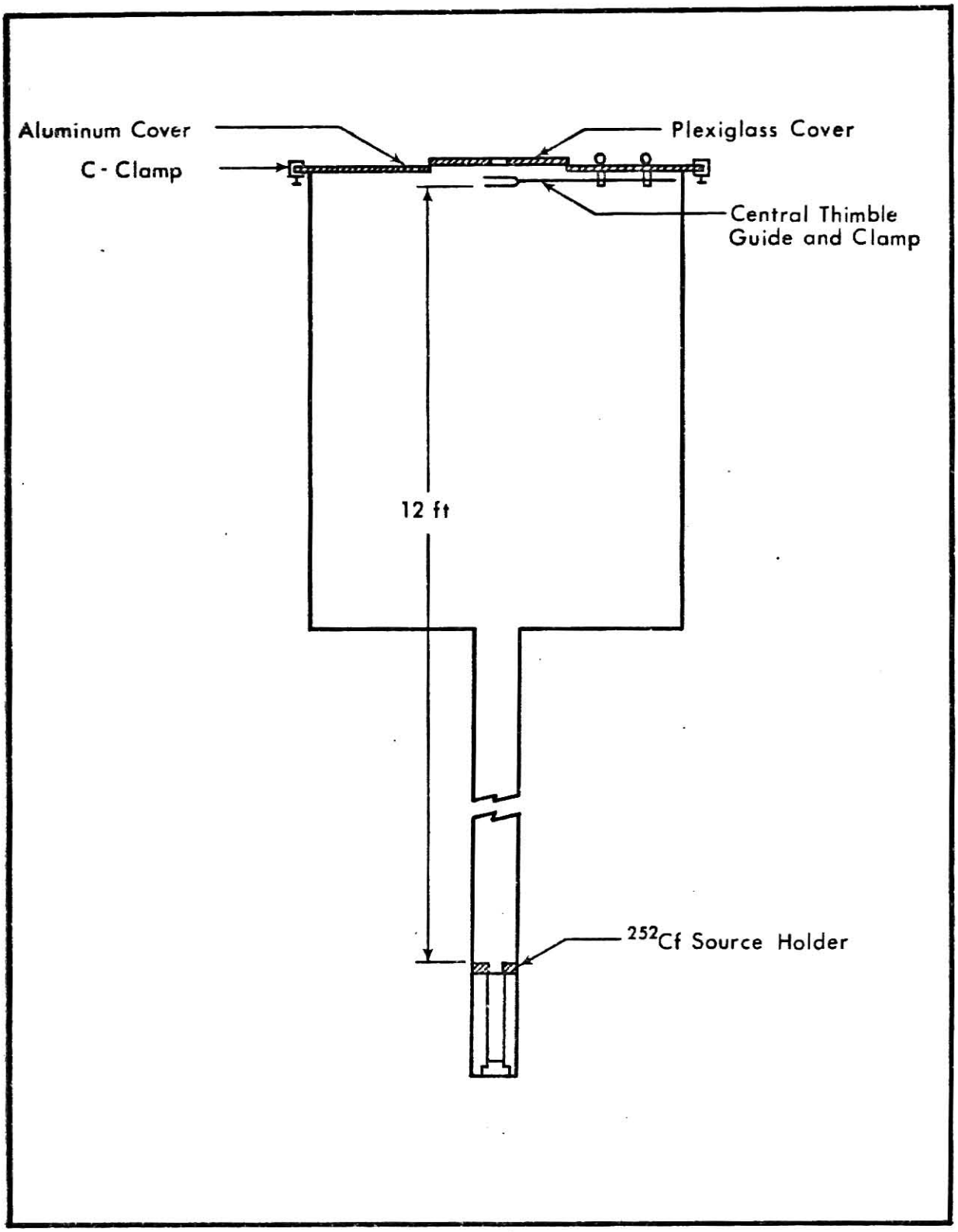

Fig. 3.6 KSU ^{252}Cf facility.

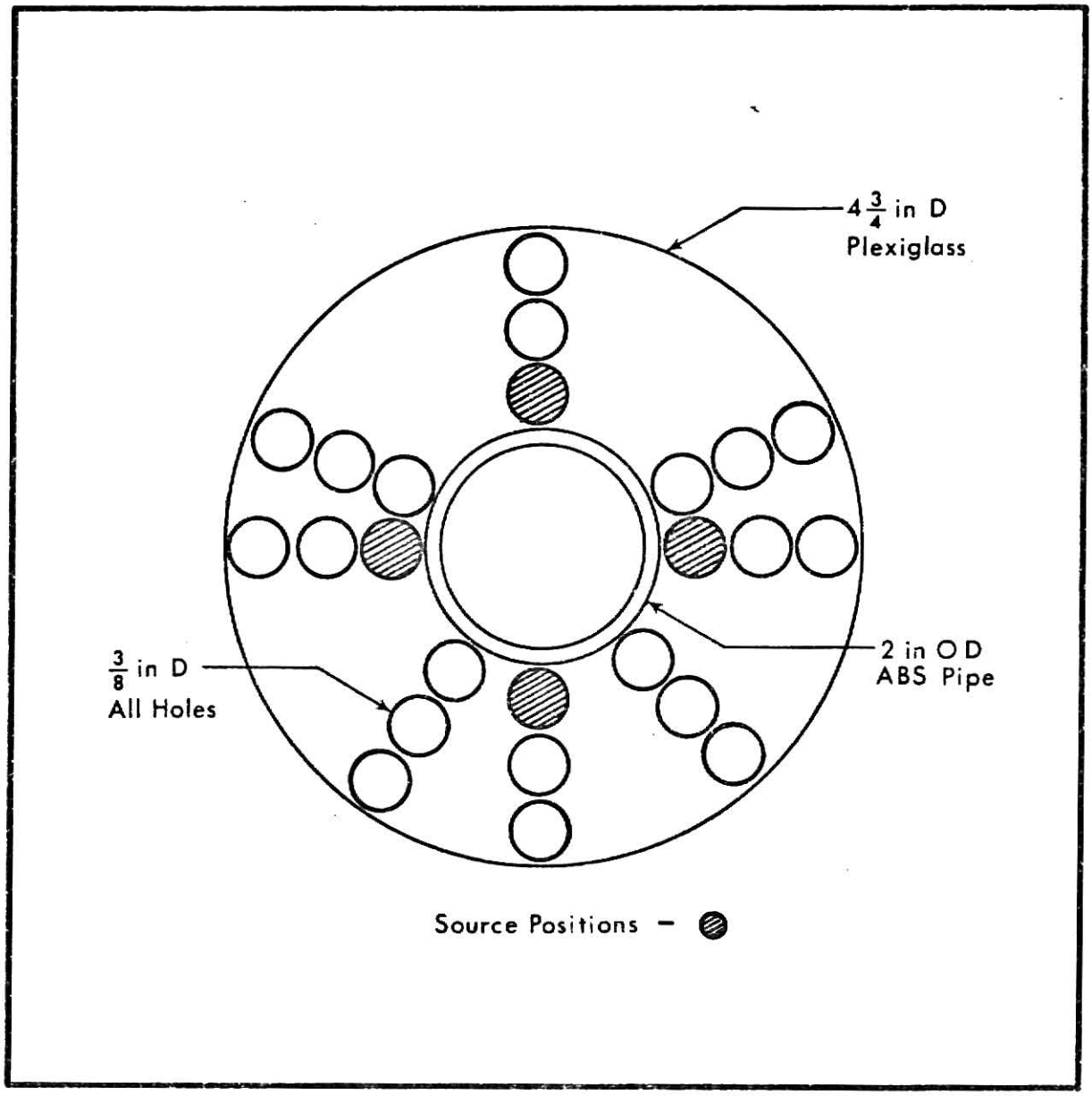

Fig. 3.7 ^{252}Cf source holder.

The plexiglass specimen holder is shown in Fig. 3.8. Aluminum electrodes were used during neutron irradiation since aluminum has a lower activation cross section than copper.

A watertight container, designed by Bailey and Villareal (18), surrounded the specimen holder to prevent water from contacting the specimen. This container is shown in Fig. 3.9. Attached to the top of this watertight container was 15 ft of ABS pipe through which the electrical connections were passed. A threaded section of plexiglass on the bottom of the container allowed connection of various lengths of ABS pipe to fix the different irradiation positions. A nipple which screwed on the bottom section of pipe rested in the central opening of the source holder.

The coaxial leads used during neutron irradiation were the same types used during gamma irradiation. A flexible steel sheath, connected to ground, was placed over both leads in an attempt to cut down the noise signal from the coaxial leads.

3.1.4 Experimental Procedure during Neutron Irradiation

Two specimens were dried at 50 (±2)°C for 4 hours and conditioned at a constant relative humidity of 37 (±1)% for 40 hours. The specimens were then painted with silver conducting paint (E-KOTE, type 3030), placed in the specimen holder between the electrodes, and potted in paraffin.

The specimen active dimensions, corrected for fringing effects (17), are 3.80 cm diameter by 0.305 cm thick. A specimen is shown in Fig. 3.10. Both specimens were double thicknesses of polyethylene sheet stock.

One specimen was inadvertently ruined by exposure to water when the specimen container was improperly sealed. All work reported here was carried out using the remaining specimen.

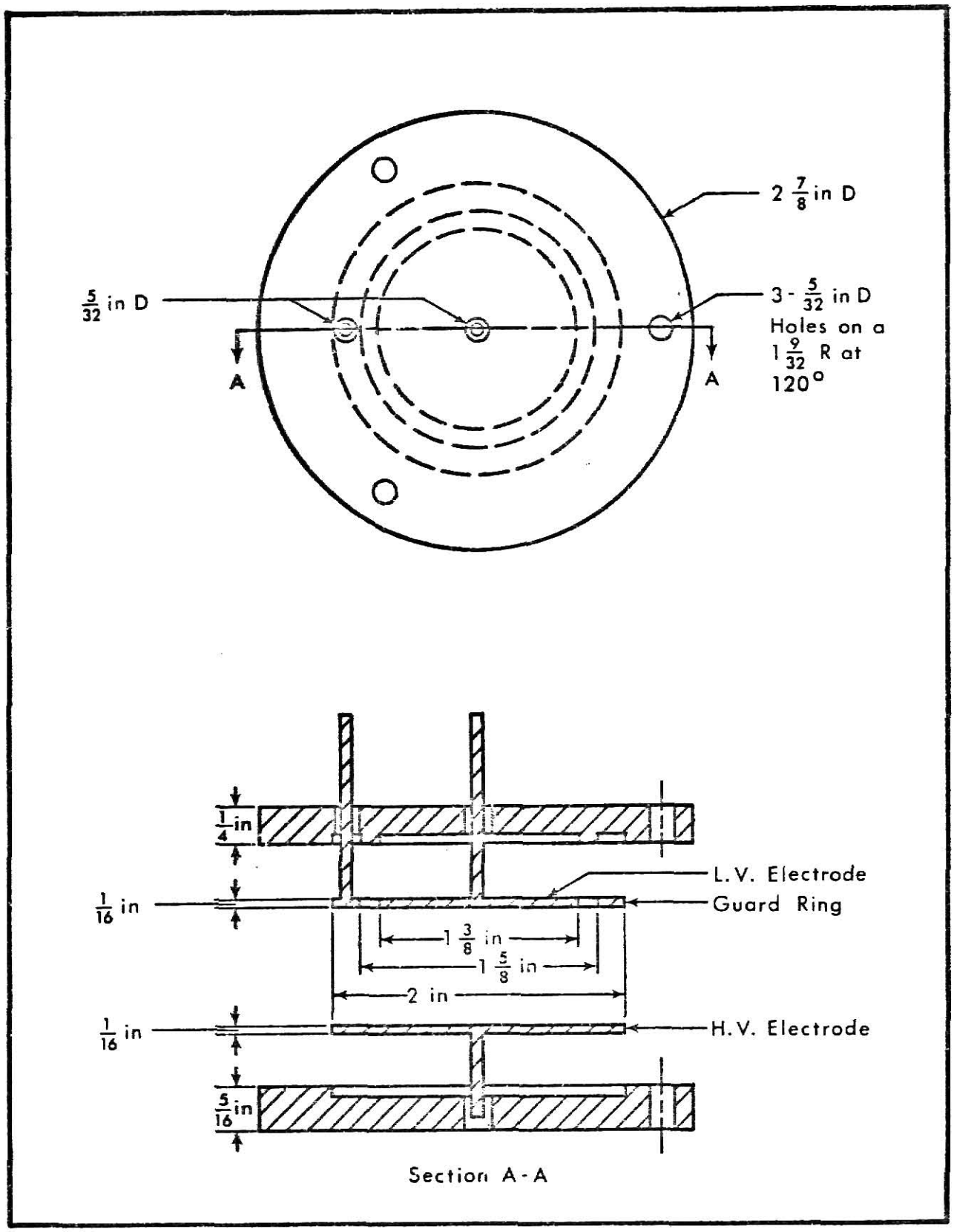

Fig. 3.8 Specimen holder and electrodes.

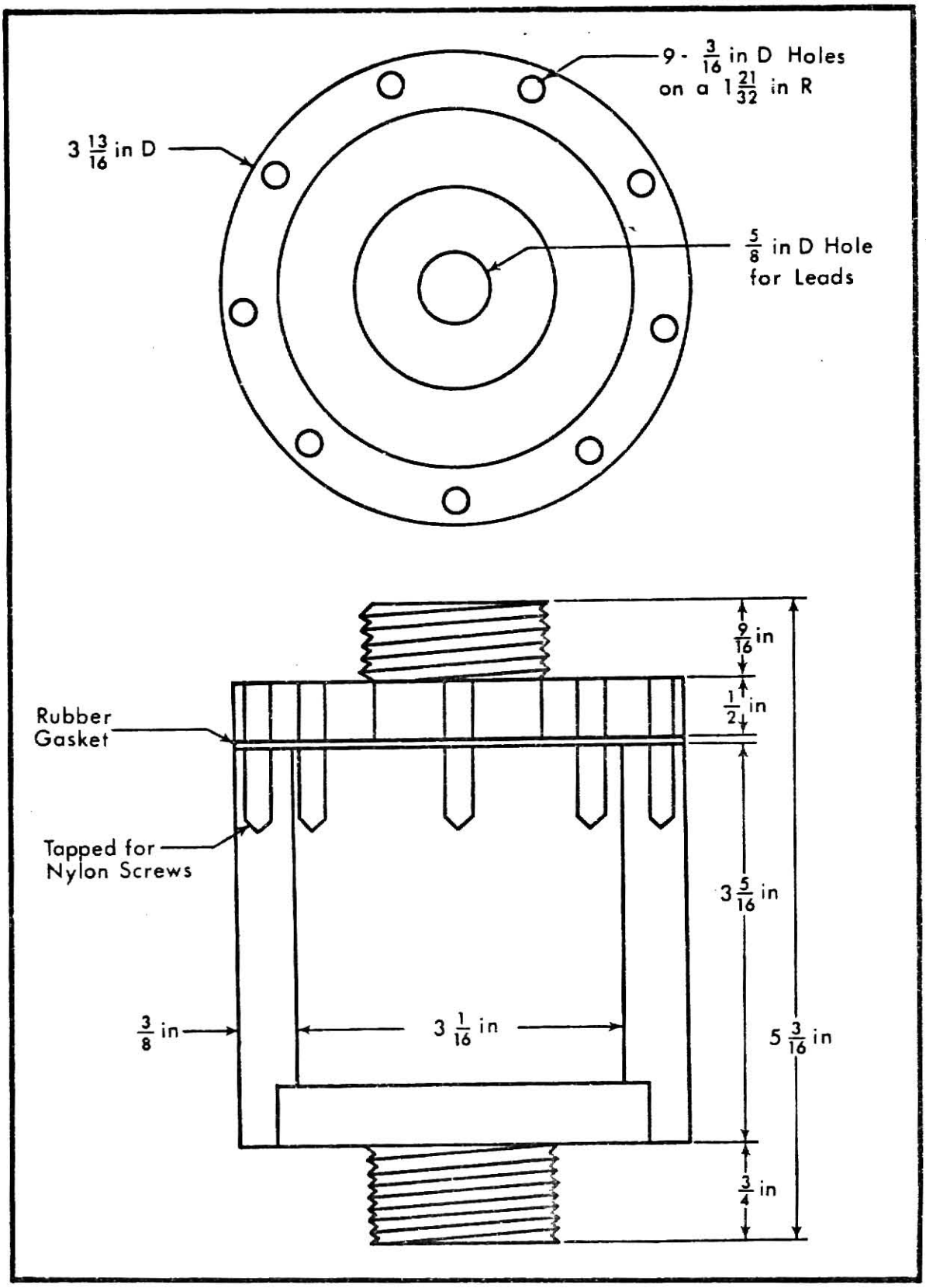

Fig. 3.9 Watertight container.

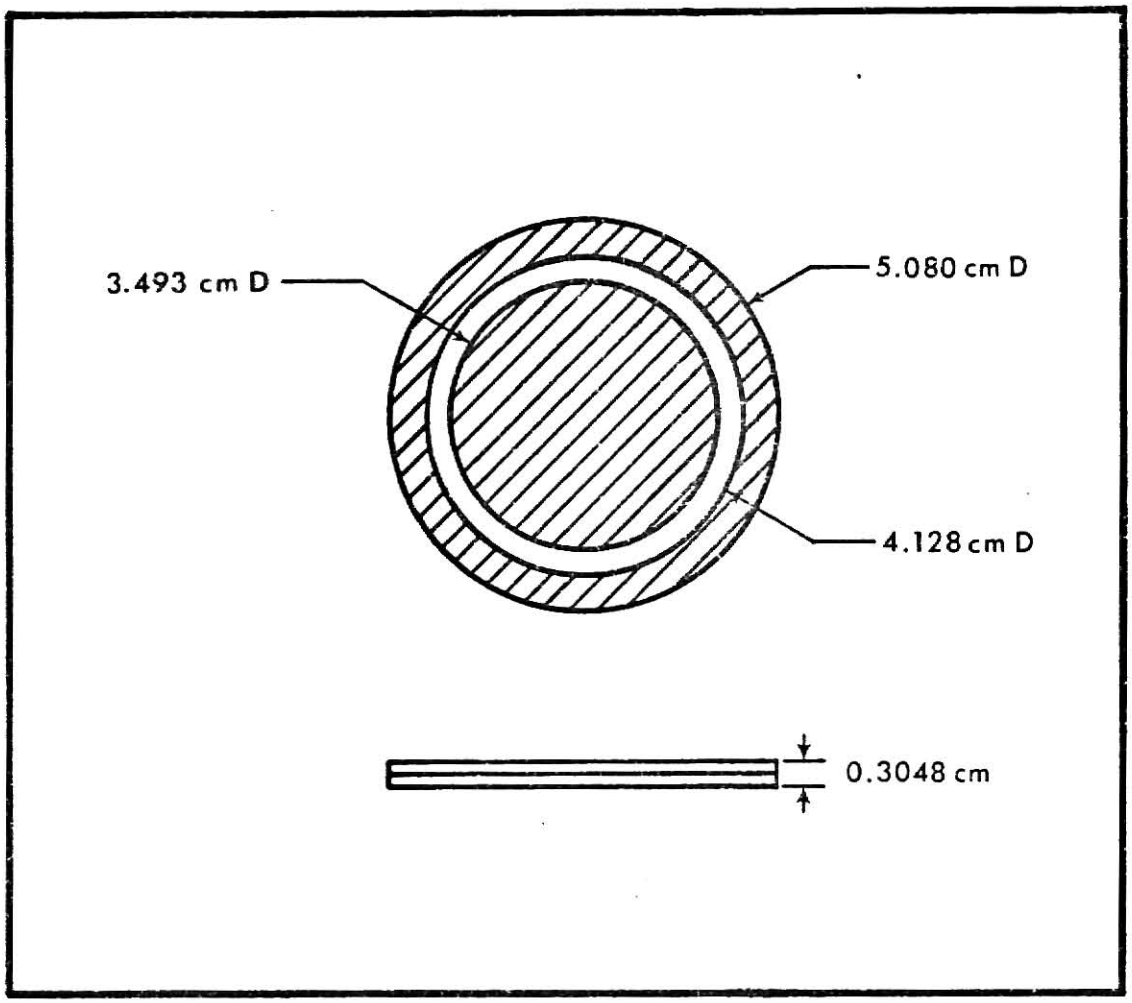

Fig. 3.10 Polyethylene specimen showing electrode positions.

The specimen was irradiated at four different positions near the source and current measurements were conducted at each position. Current measurements for use in the calculation of dark conductivity were taken prior to any irradiation.

The specimen, inside its watertight container, was lowered into position and allowed to rest for one-half hour before any current measurements were taken. Previous experience with gamma irradiation indicated this would be sufficient time for the specimen to reach a steady-state condition.

A common industrial technique (19) was used to measure the current as a function of applied voltage. A fixed increment of voltage ΔV was applied to the specimen. At a time interval Δt later the current I was measured, followed by an additional voltage increment, another current measurement Δt later, etc. Since the dielectric charging current depends on changes in voltage (1), the resistance of the specimen, after a few steps, is just $\Delta V/\Delta I$.

The beginning voltage for current measurements with no irradiation was 0 V. The voltage increment ΔV was 100 V. The time increment Δt was 5 min. The voltage was incremented to a maximum of +1000 V, decremented to a minimum of -1000 V, and incremented back to the initial voltage of 0 V. Examination of the data showed that this complete cycle of voltage was not necessary. Consequently, the initial voltage for all measurements during irradiation was chosen to be +1000 V. The voltage was then decremented to a final value of -1000 V using the same ΔV and Δt as before.

An attempt was made to study the buildup and decay of neutron-induced currents at voltages of ±500 V and during short-circuit conditions. The movement of the long coaxial cables induced a sizeable noise current which prevented study of current buildup. Further, the noise current present when

the leads were not shielded by the well wall of the ^{252}Cf tank prevented study of the decay currents. The only useable observation was that no current was induced during and after irradiation for 1000 sec under short-circuit conditions.

3.2 Neutron Flux Measurements

It was necessary to measure the neutron flux in order to establish the relationship between conductivity and dose rate (or flux). Ideally, the absolute fast neutron flux should have been measured.

However, the lack of suitable equipment and the length of time required for this type of measurement dictated that a simple measurement of the thermal neutron flux be used instead, as the time period of the ^{252}Cf loan agreement had almost expired. The approximation was then made that the ratio of fast flux to thermal flux was the same at each specimen location. The technique selected was activation of gold foils, which is described in detail by Price (20).

3.2.1 Apparatus

Thin gold foils on aluminum backing were used. The ^{252}Cf source and associated equipment are described in Section 3.1.3.

The foils were counted using two sets of counting equipment. A block diagram of equipment used for coincidence counting is shown in Fig. 3.11. A list of equipment, manufacturers, and model numbers is given in Table 3.3. The block diagram of equipment used for single detector counting is shown in Fig. 3.12, and the list of equipment is given in Table 3.4. A gamma spectroscopy reference source set, Model GSD.1, was used to determine the efficiency of the 3 in. by 3 in. NaI detector.

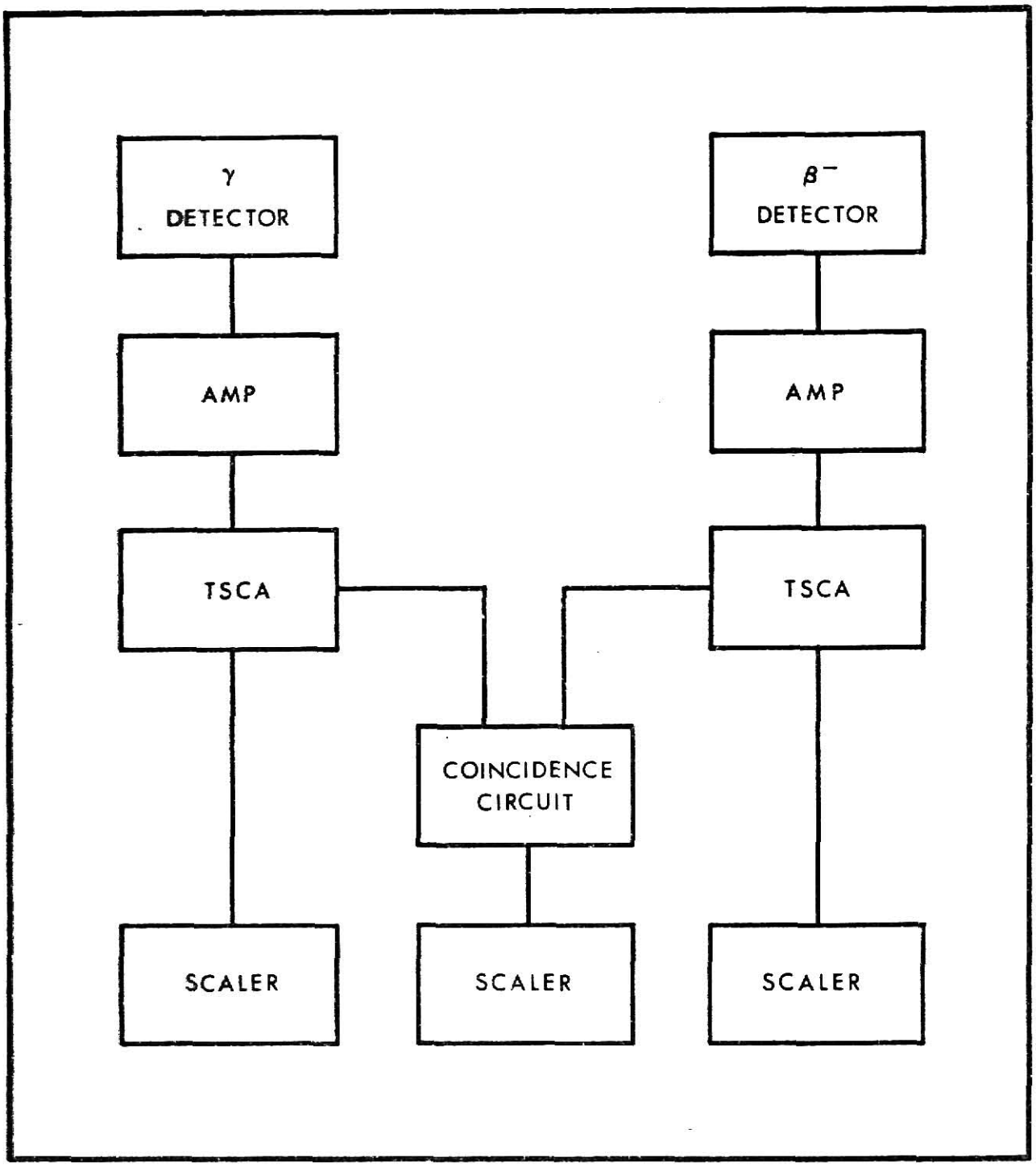

Fig. 3.11 Block diagram of coincidence counting equipment.

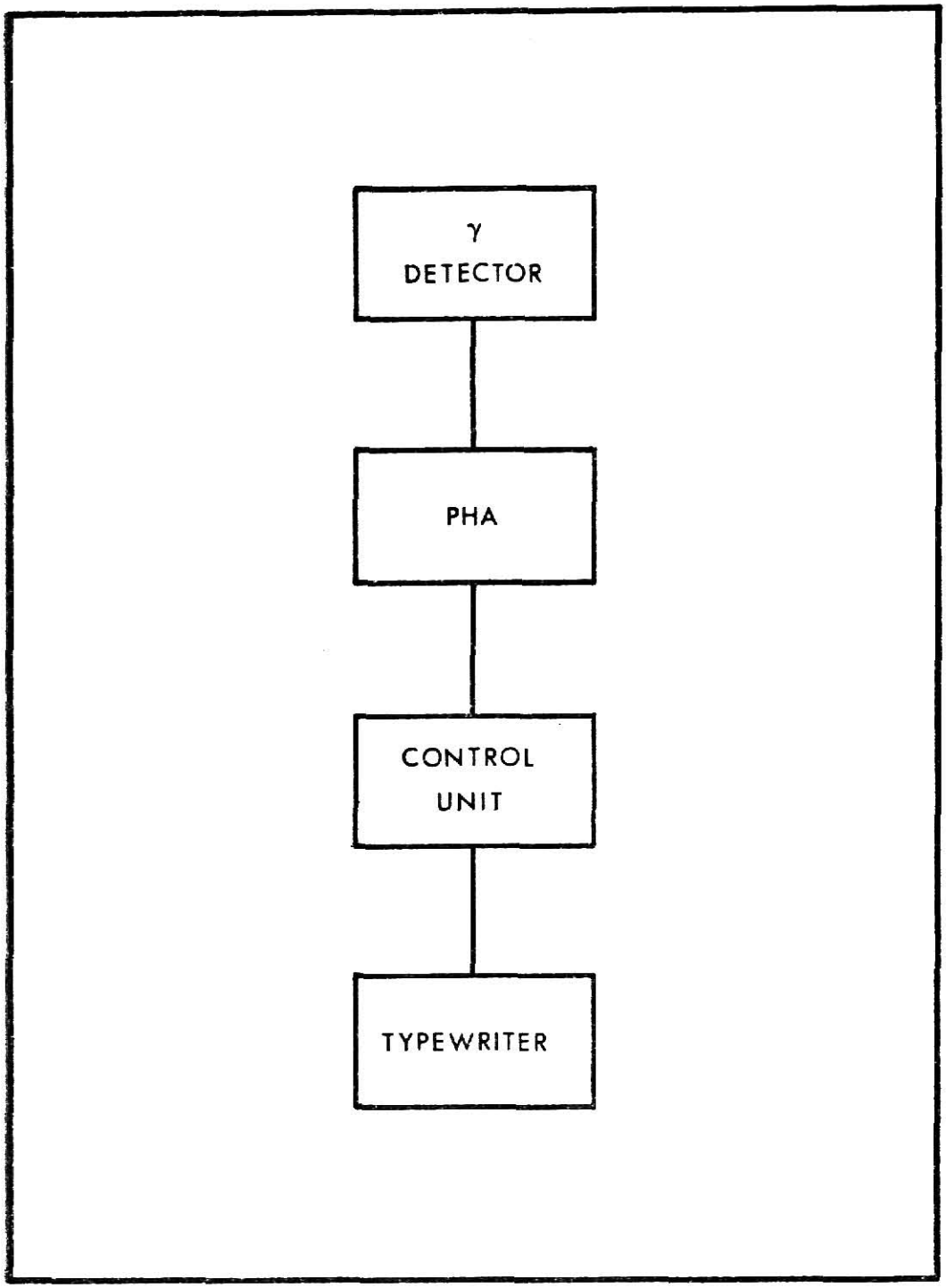

Fig. 3.12 Block diagram of single detector counting equipment.

Table 3.3 Equipment for Coincidence Counting

High voltage Power Supplies:	John Fluke Model 412A John Fluke Model 412B
NaI Detector for Gammas:	Technical Measurements Corporation Model DS-12
Plastic β^- Detector:	Constructed by Department of Nuclear Engineering Staff
Linear Amplifiers:	2 Ortec Model 410
Timing SCA's:	Ortec Model 455 Ortec Model 420A
Differential Discriminators:	2 EG&G Model TD101/N
Continuous Variable Delay Passive Network:	Ad-Yu Electronics Type 2011
Gate Generators:	2 EG&G Model GG200/N
Linear Gate:	Canberra Model 1451
Coincidence Circuits:	2 EG&G Model C104A/N
Scalers:	2 Nuclear Scaler Model 2005, Hamner Model NS-300
Timer:	Hamner Model NT-300

Table 3.4 Equipment for Single Detector Counting

High Voltage Power Supply:	John Fluke Model 412B
NaI Gamma Detector:	3 in. by 3 in. Harshaw Model 12S12
Pulse Height Analyzer:	Technical Measurements Corporation Model 402
Type-Punch-Read Control Unit:	Technical Measurements Corporation Model 520
Typewriter:	Technical Measurements Corporation IBM Model

3.2.2 Experimental Procedure

One bare and one cadmium-covered gold foil were activated at each position at which the current measurements were taken. The foils were placed inside a spare specimen holder so they would receive the same neutron flux as the specimen at each location. Since sealing the watertight container required a period of 24 hours drying time, the container was not sealed for the flux measurements as only one watertight container was available, and the time available for flux measurements was short. Irradiation times ranged from 4 min at the position nearest the source to 48 hours at the position farthest from the source.

After irradiation, the foils were removed from the specimen holder and allowed to decay for at least one-half day to eliminate measurement of gamma rays from the aluminum backings, which had been activated to a small extent.

The foils were then counted, using both a coincidence counting technique and a single 3 in. by 3 in. NaI detector. Two counts of each foil were made on each detector, except for the foils at the farthest position, which registered zero coincidence counts during the first run.

4. Analysis and Discussion of Experimental Data

4.1 Gamma-Irradiation Data

As described in Section 3.1.2, three current measurements were taken from each configuration of leads and specimen. Data points were read from the strip charts at intervals selected to match the time divisions on the charts. All data were then normalized to a base dose rate of 27.23 rad (H_2O) per sec, using the assumption of a linear dependence on dose rate:

$$I_{norm} = I_{meas} \left(\dot{\theta}^{\delta}_{base} / \dot{\theta}^{\delta}_{act}\right) \quad , \qquad \delta = 1.0 \ . \tag{4.1}$$

Numerical calculations showed that use of $\delta = 0.66$ as determined by Fellers (4) gave, in the worst case, a normalized current only 1.5% lower than the current calculated for $\delta = 1.0$. Thus, the assumption of linear dependence on dose rate should not significantly affect the analysis. The dose rate "seen" by the specimen was estimated from the isodose curves shown in Fig. 4.1 to be 90% of the dose rate at the central position of the gammacell chamber. The central position dose rate was measured with a Fricke dosimeter on March 16, 1965 and was found to be 90.83 rad (H_2O) per sec. The dose rate on any subsequent day is easily calculated from the radioactive decay law.

The normalized data were then averaged using a simple computer code. The averaged raw data under short-circuit conditions are presented in graphical form in Figs. 4.2 through 4.5, and in tabular form in Appendix 9.4. Averaged raw data with ±500 V applied voltage are given in Figs. 4.6 through 4.9 and in Appendix 9.5.

Three measurements of the current from the high-voltage electrode of the single-thickness specimen were thrown out because the post-irradiation

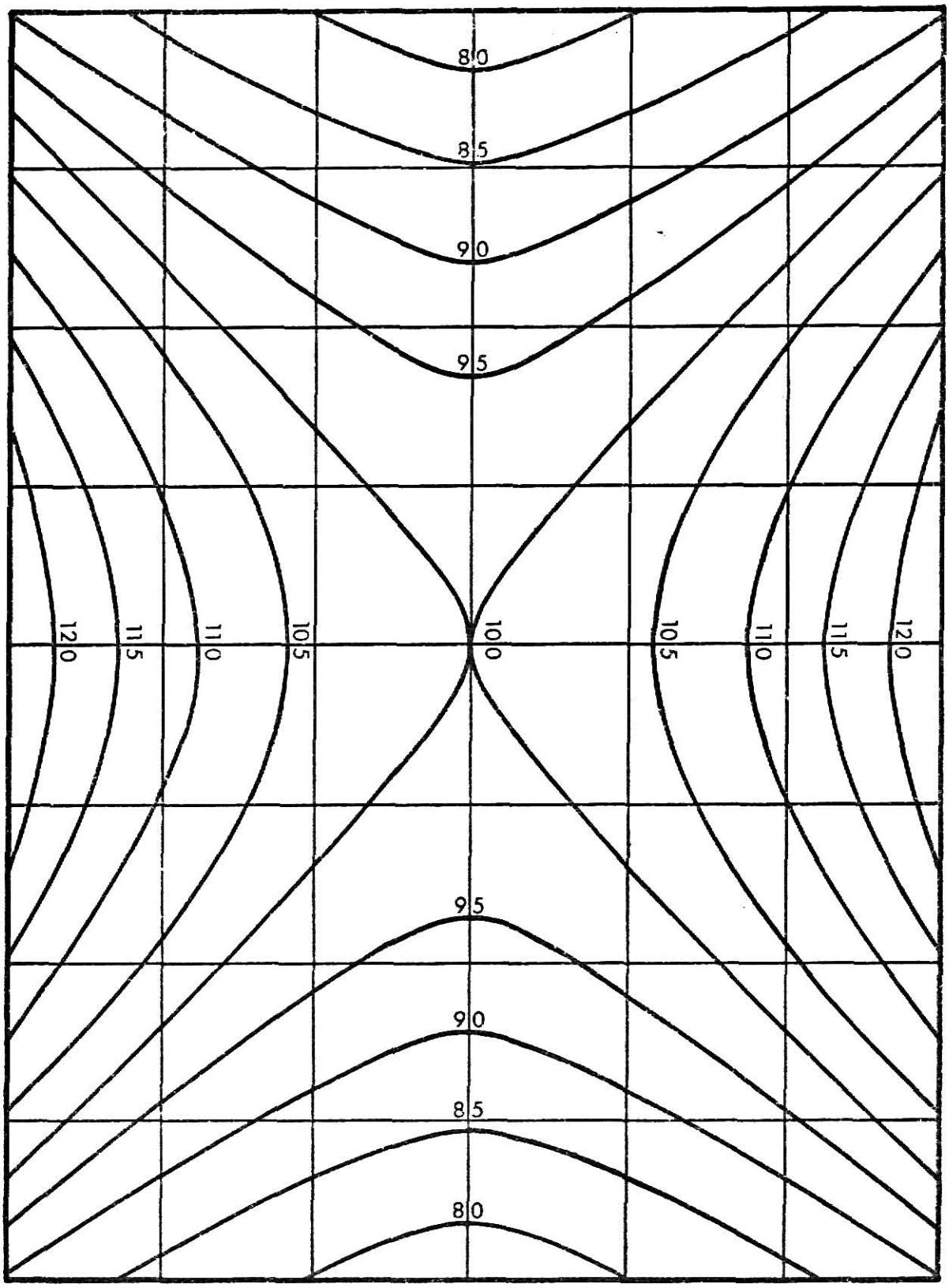

Fig. 4.1 Gammacell isodose curves.

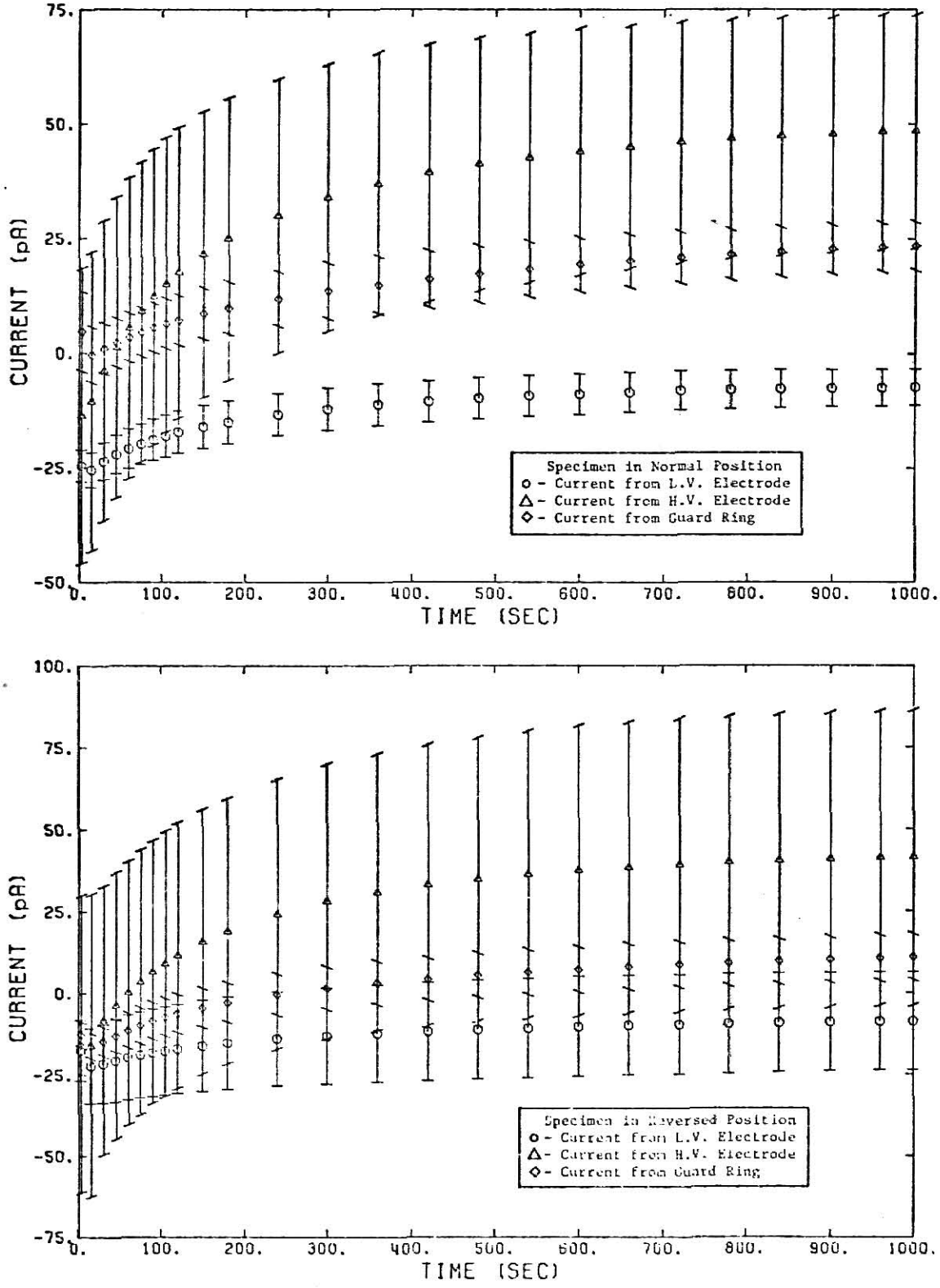

Fig. 4.2 Short-circuit currents during irradiation of double-thickness specimen.

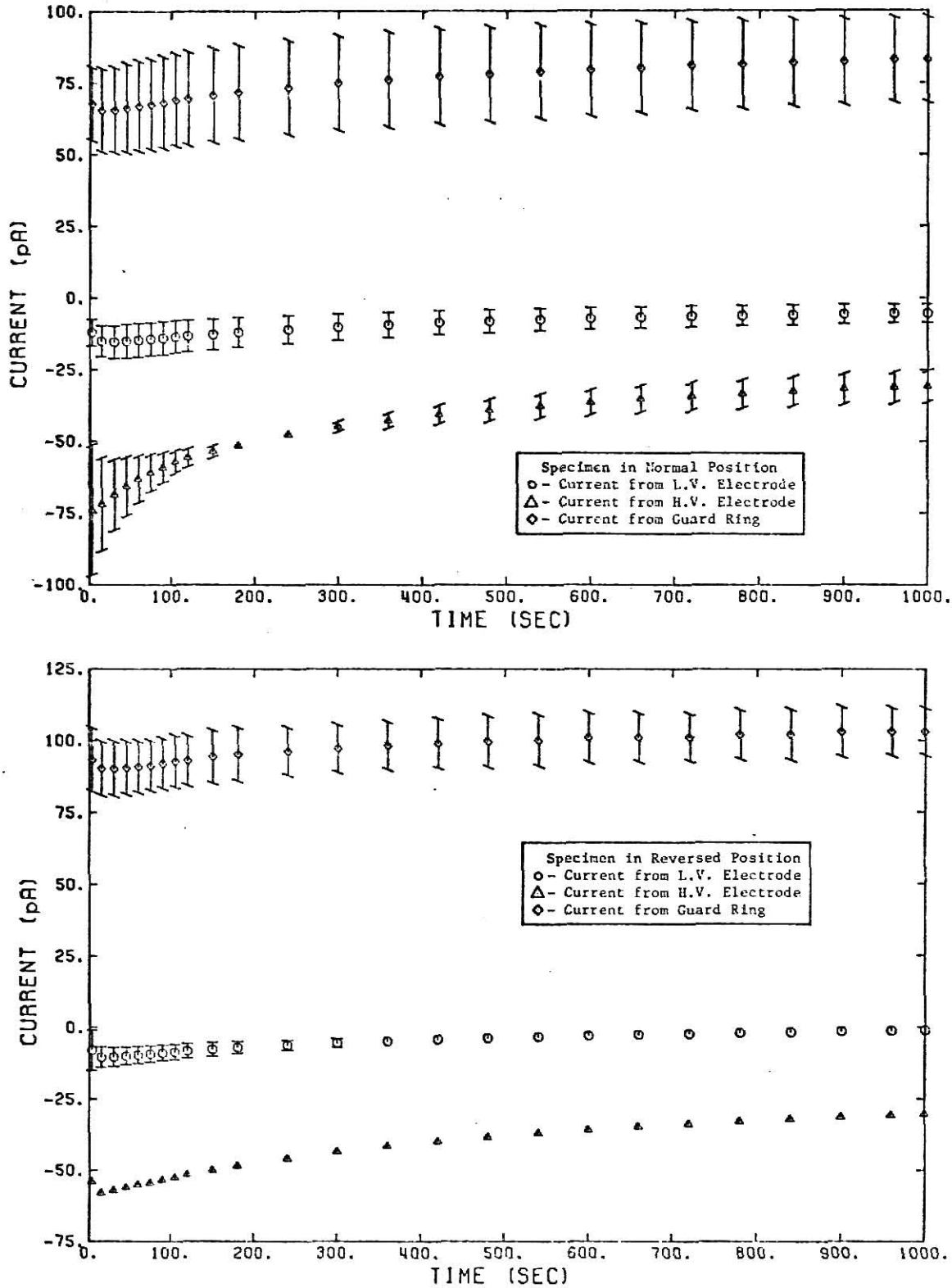

Fig. 4.3 Short-circuit currents during irradiation of single-thickness specimen.

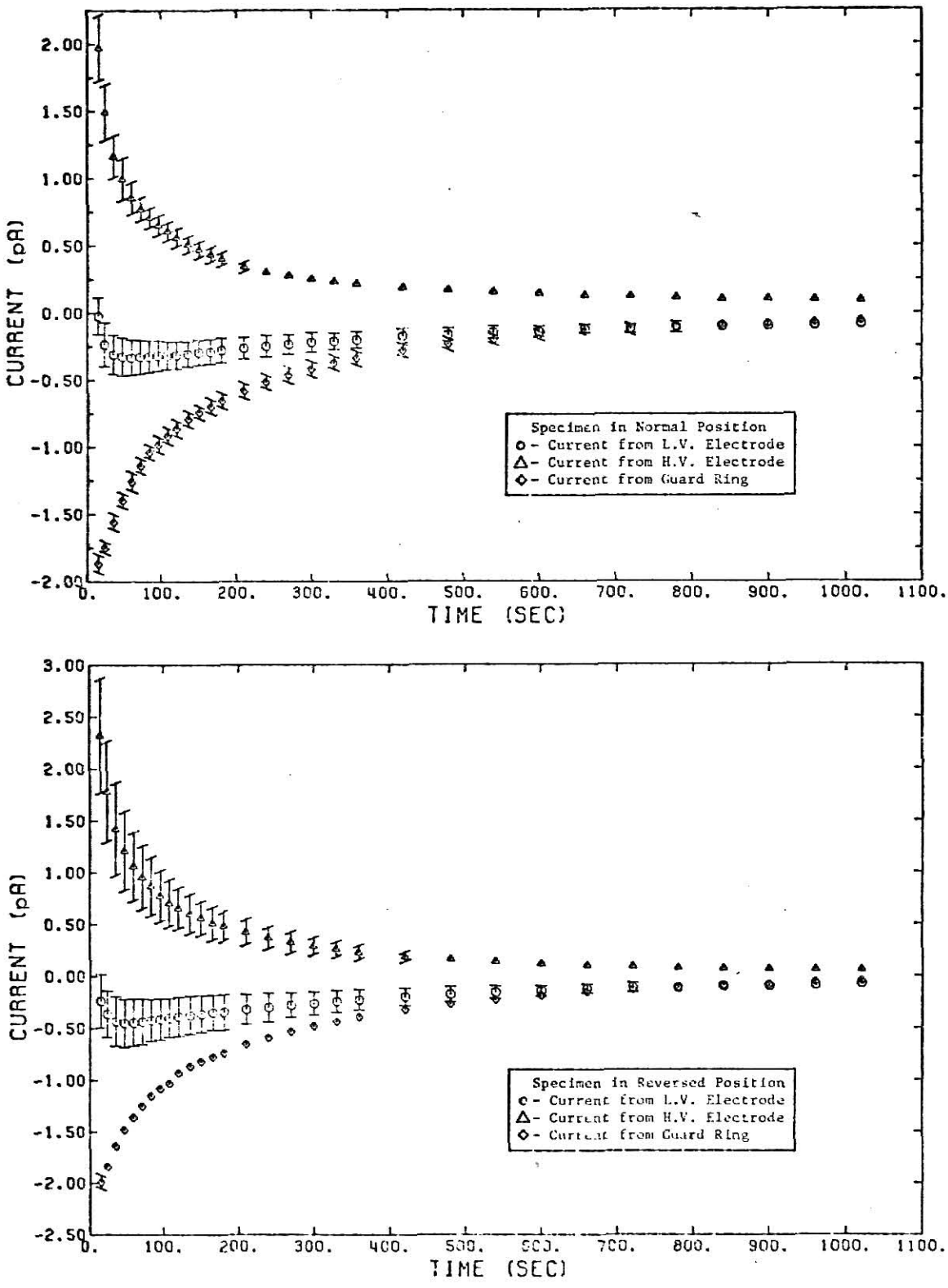

Fig. 4.4 Short-circuit currents after irradiation of double-thickness specimen.

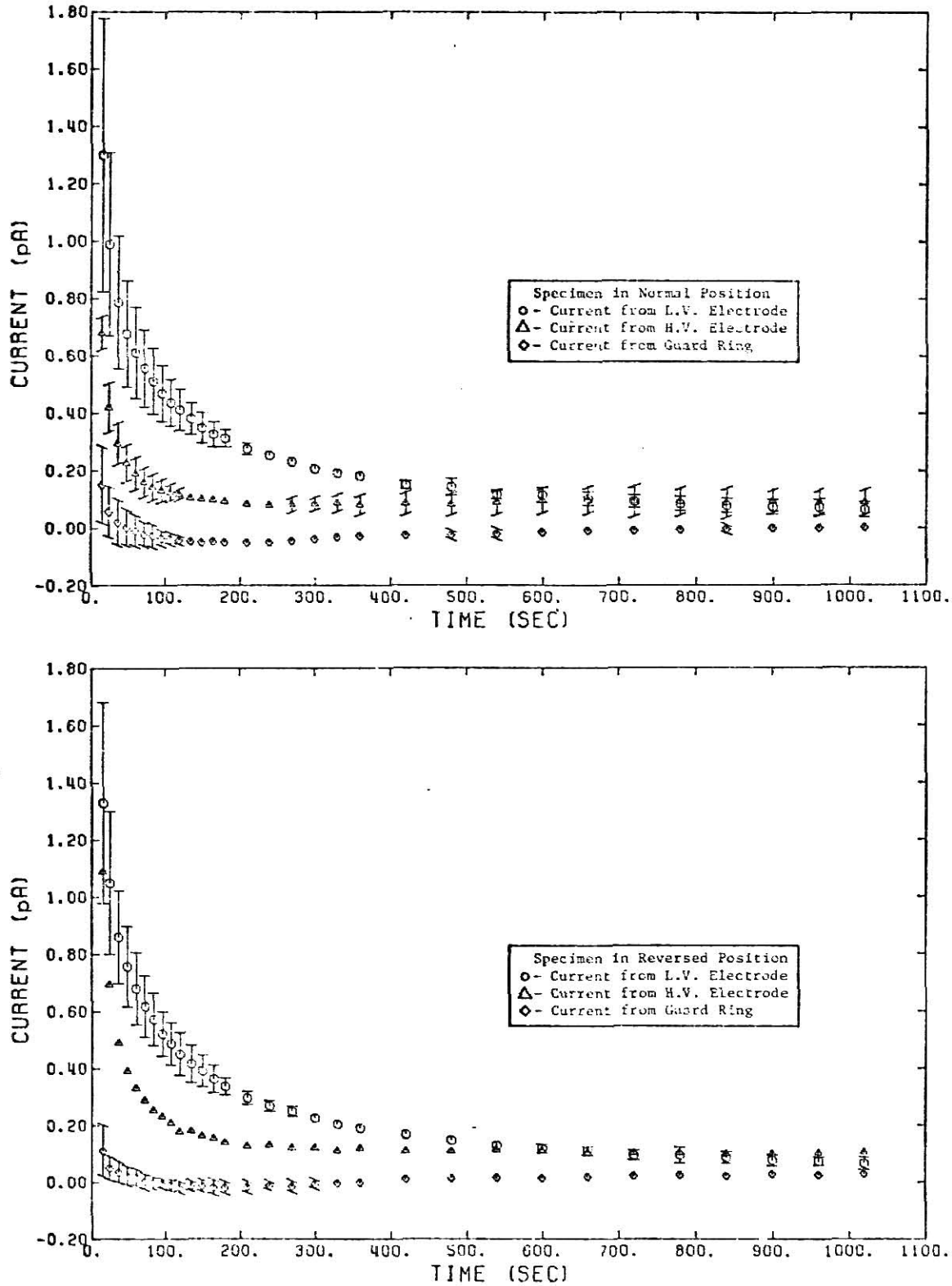

Fig. 4.5 Short-circuit currents after irradiation of single-thickness specimen.

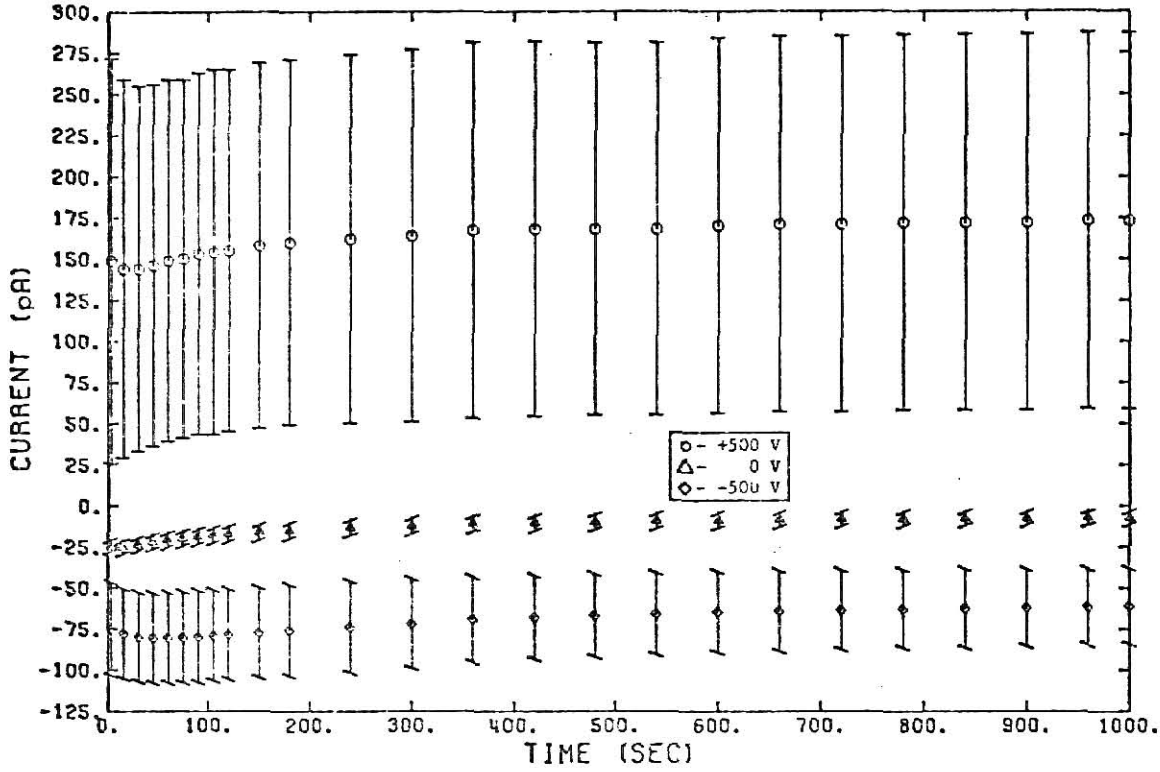

Fig. 4.6 Currents from double-thickness specimen during irradiation under applied voltage.

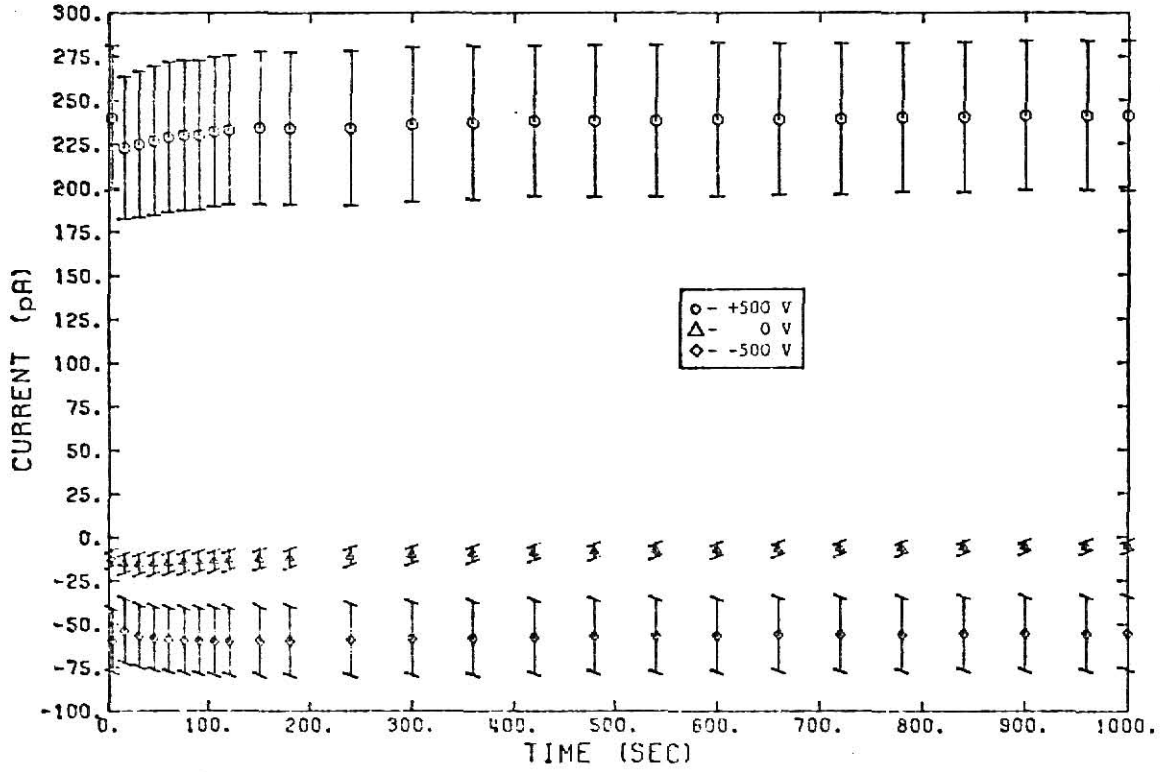

Fig. 4.7 Currents from single-thickness specimen during irradiation under applied voltage.

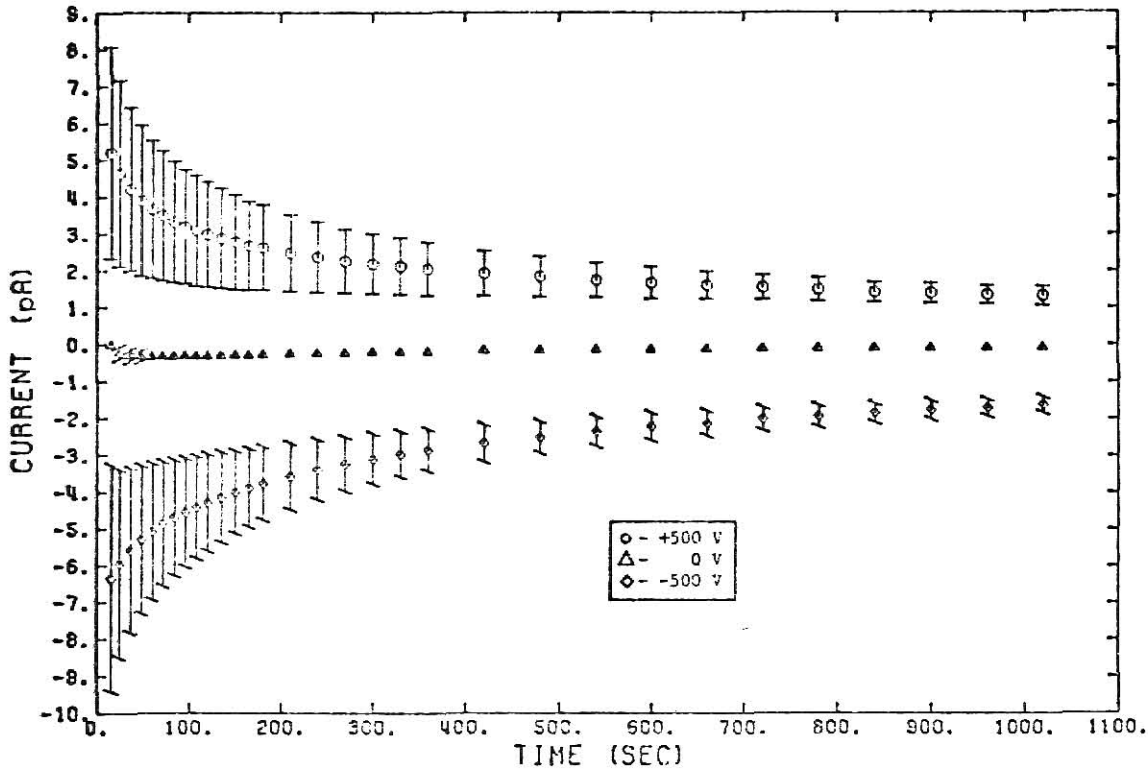

Fig. 4.8 Currents from double-thickness specimen after irradiation under applied voltage.

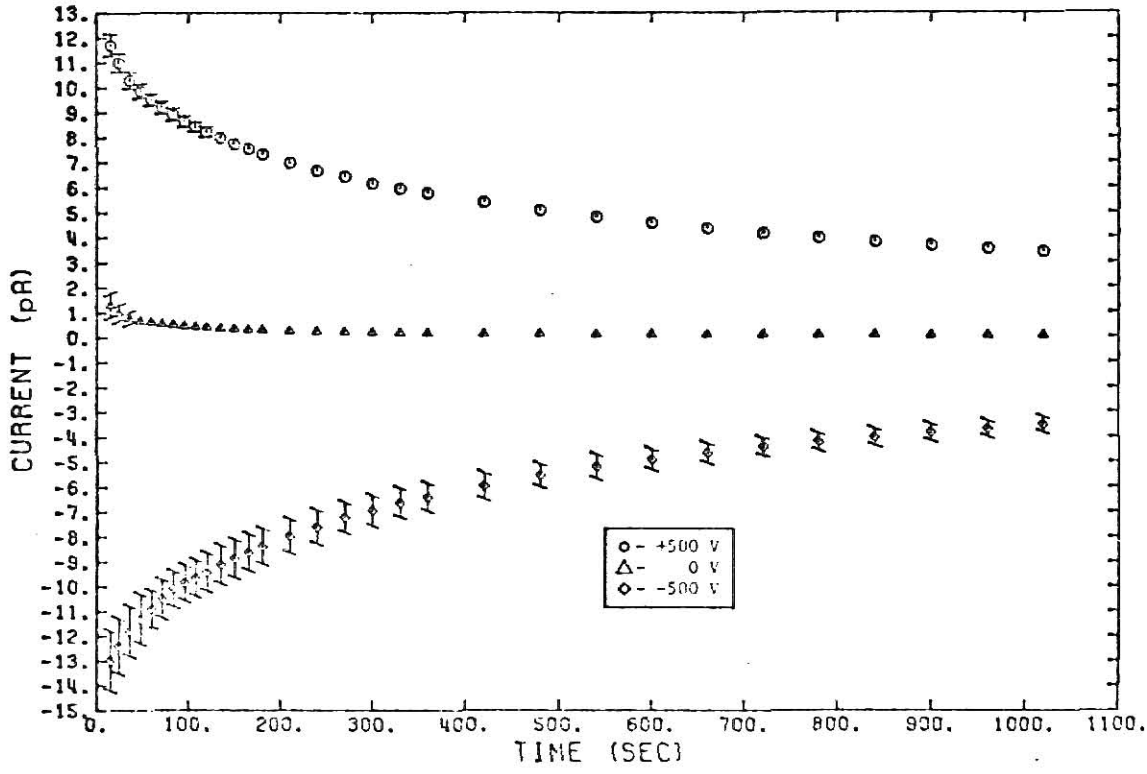

Fig. 4.9 Currents from single-thickness specimen after irradiation under applied voltage.

currents had the opposite sign of the currents which were normally observed in that configuration. Examination of the specimen holder revealed that the high-voltage lead was broken, and it is believed that the broken lead was responsible for the strange behavior of the measured currents. Thus, the data for the currents from the high-voltage electrode of the single-thickness specimen consisted of two measurements in the normal specimen position, and only one measurement in the reversed specimen position.

An attempt was made to model the externally observed currents in terms of fictitious current generators located within the specimen and coaxial leads. Circuit diagrams of the model used are shown in Figs. 4.10 through 4.12. The notation for the model is as follows:

I_{LH} = current generated between low- and high-voltage electrodes

I_{GH} = current generated between guard ring and high-voltage electrode

I_C = current generated in coaxial cable

I_L = measured current from low-voltage electrode

I_H = measured current from high-voltage electrode

I_G = measured current from guard ring

R_V = output resistance of power supply

R_M = input resistance of measuring circuit

R_C = shunt resistance of coaxial cable

R_H = resistance between high-voltage electrode and central plane of double-thickness specimen

R_L = resistance between low-voltage electrode and central plane of double-thickness specimen

R_{LH} = resistance between low- and high-voltage electrodes of single-thickness specimen

R_{GH} = resistance between guard ring and high-voltage electrode of single-thickness specimen.

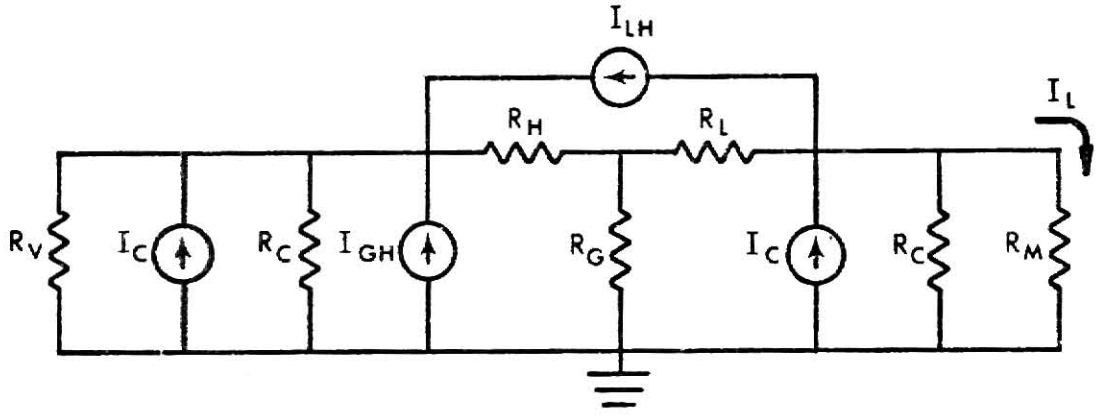

Double-thickness Specimen

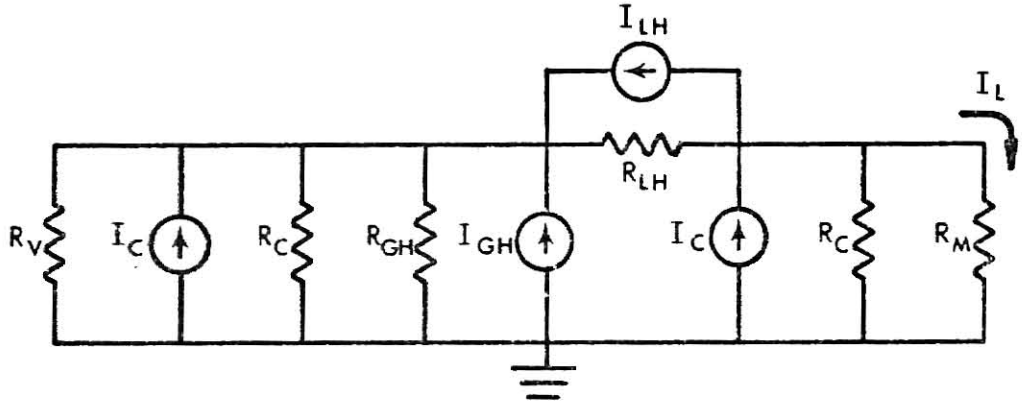

Single-thickness Specimen

Fig. 4.10 Circuit models during measurement of currents from the low-voltage electrodes.

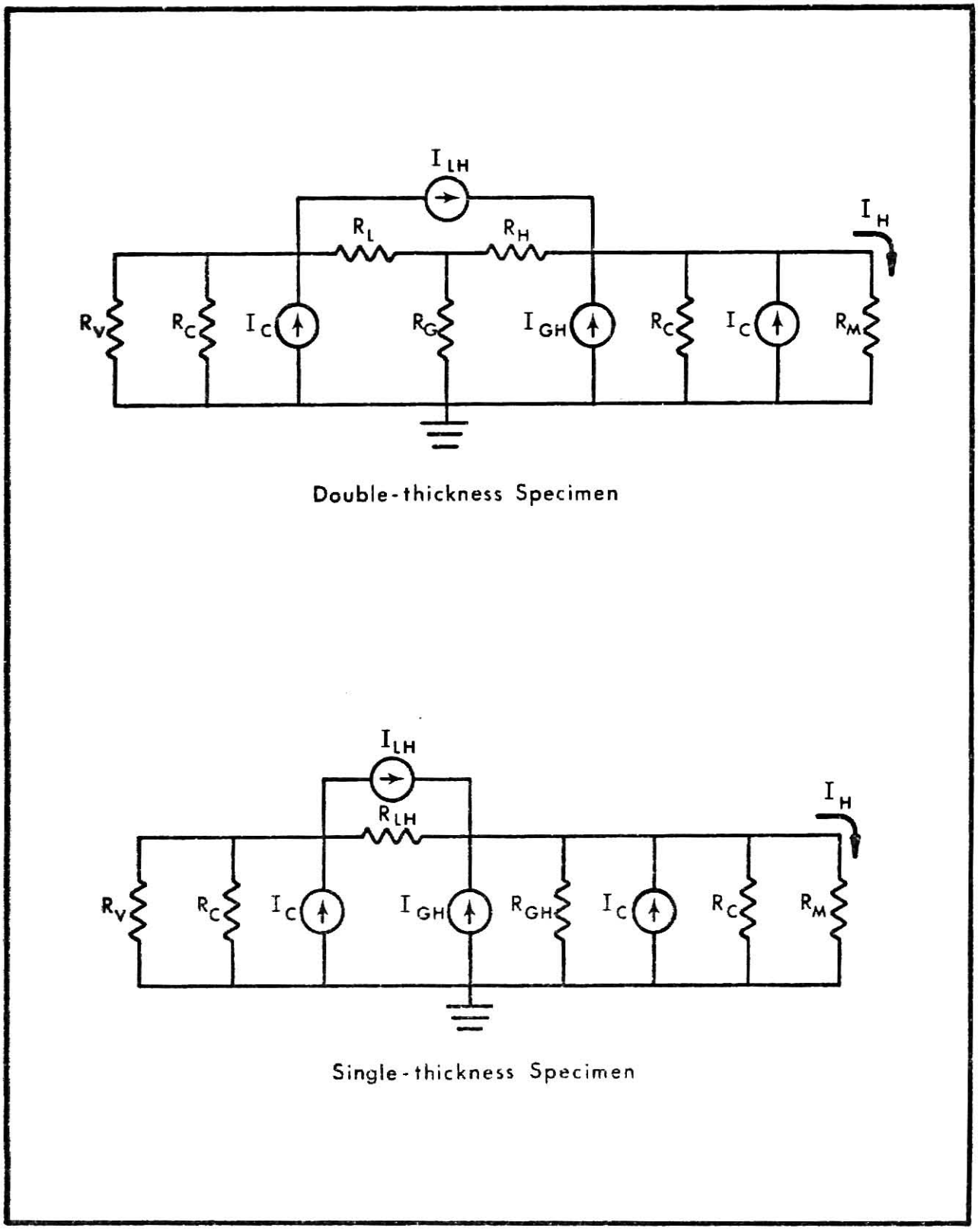

Fig. 4.11 Circuit models during measurement of currents from the high-voltage electrodes.

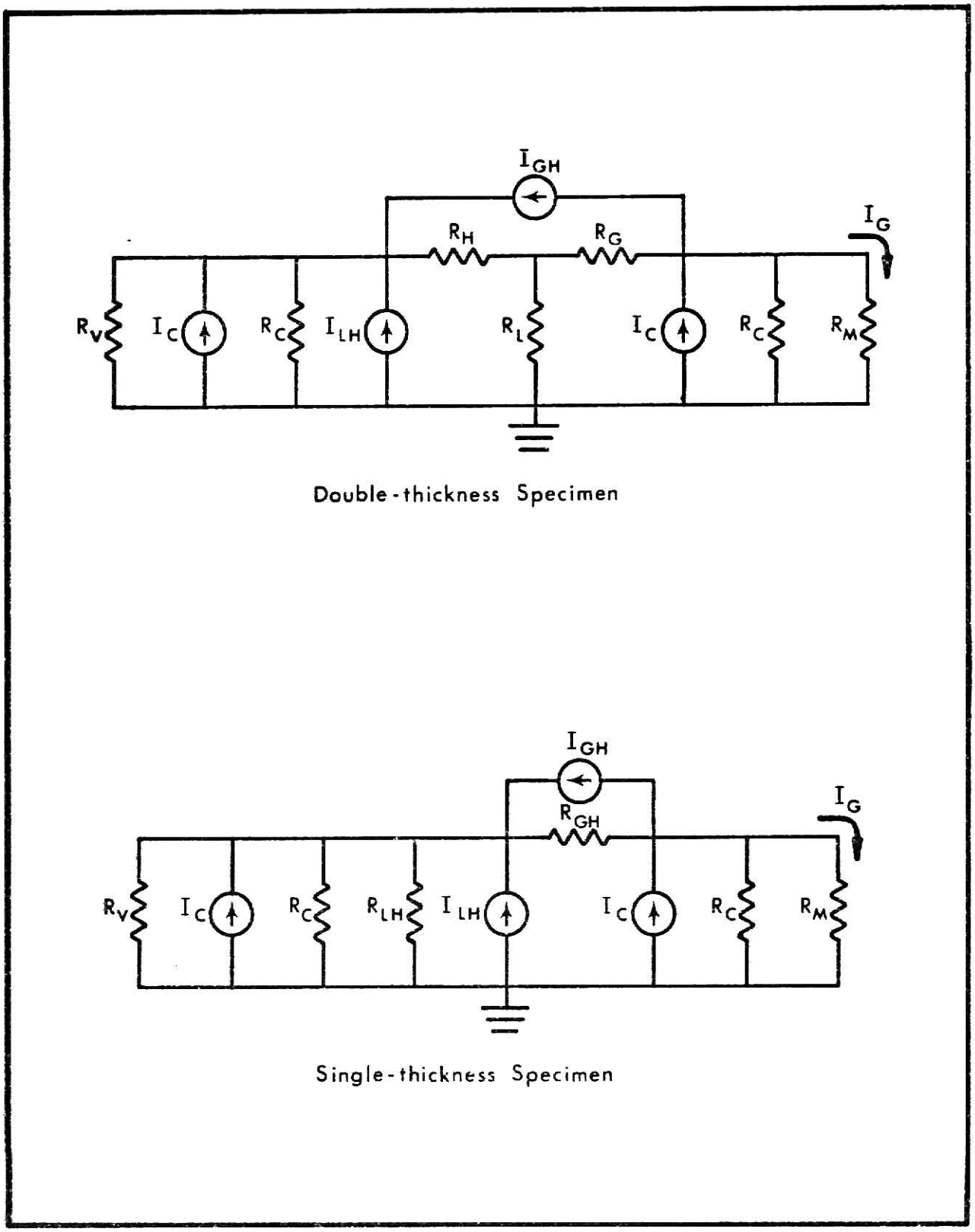

Fig. 4.12 Circuit models during measurement of currents from the guard rings.

Only direct currents are considered, so there is no need to show the capacitance between components. When the power supply is set to 0 V, the output resistance R_V is essentially a short circuit. Using the results of Fellers investigation (4), the resistances within the specimens and cables were calculated to lie in the range 10^{10} Ω to 10^{12} Ω. Since the input resistance of the operational amplifier is ∿5 MΩ the measured currents may be described solely in terms of the currents from the current generators, as the currents flowing in the various shunt resistances will be negligible. The equations for the measured currents in either specimen are

$$I_C - I_{LH} = I_L \ , \tag{4.2}$$

$$I_C + I_{LH} + I_{GH} = I_H \ , \tag{4.3}$$

and

$$I_C - I_{GH} = I_G \ . \tag{4.4}$$

The solution to this set of linear equations is easily shown to be

$$I_C = (I_L + I_H + I_G)/3 \ , \tag{4.5}$$

$$I_{LH} = (-2I_L + I_H + I_G)/3 \ , \tag{4.6}$$

and

$$I_{GH} = (I_L + I_H - 2I_G)/3 \ . \tag{4.7}$$

The values of the currents produced by the current generators were calculated both during and after irradiation using the equations shown above. The results are shown in Figs. 4.13 through 4.16 and are also given in tabular form in Appendix 9.6.

To compare results from the present investigation with those of Faw and Robinson (1), the short-circuit currents during post-irradiation recovery were subtracted from the post-irradiation currents at ±500 V. Faw and

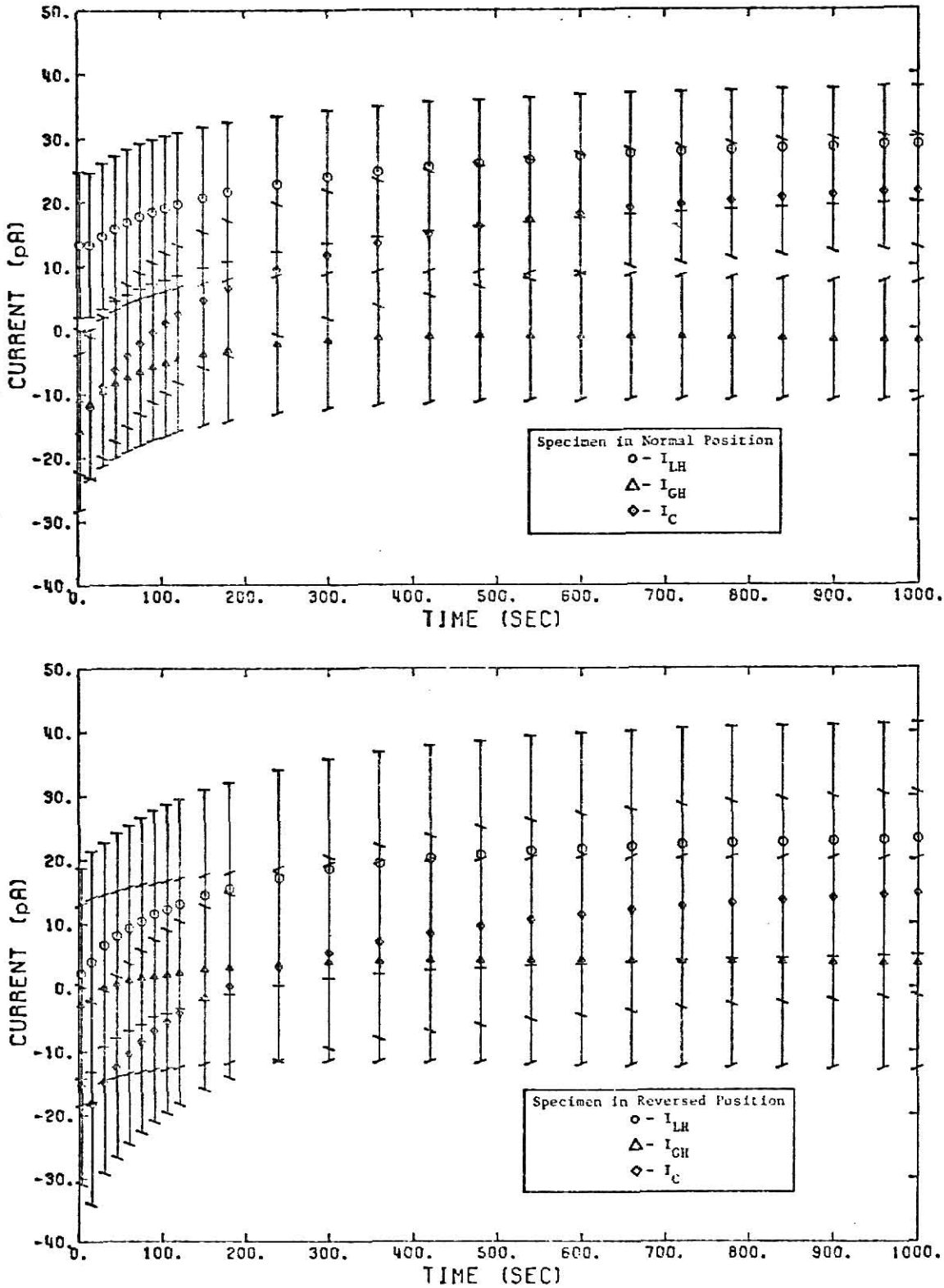

Fig. 4.13 Current generator strengths during irradiation of double-thickness specimen.

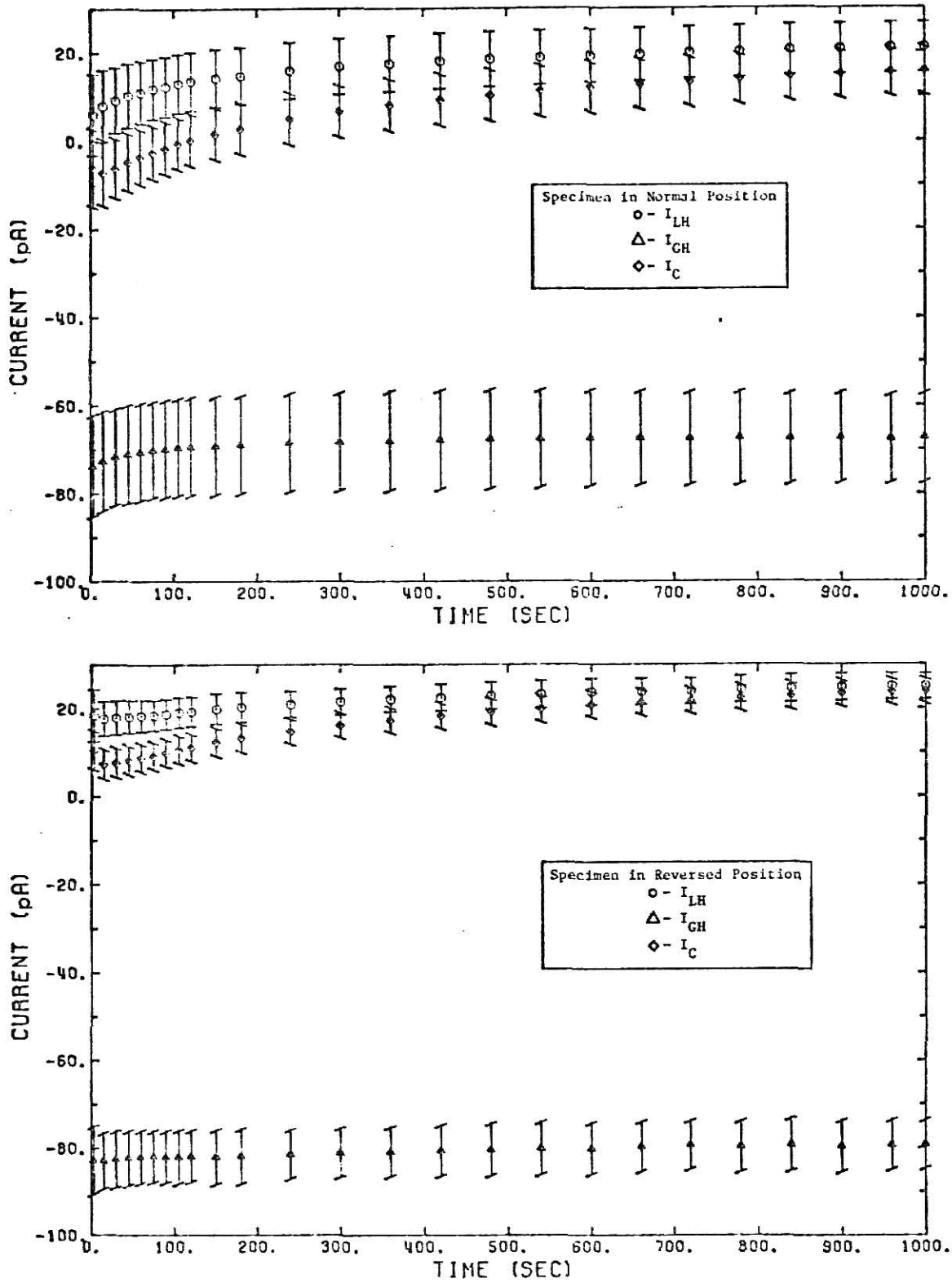

Fig. 4.14 Current generator strengths during irradiation of single-thickness specimen.

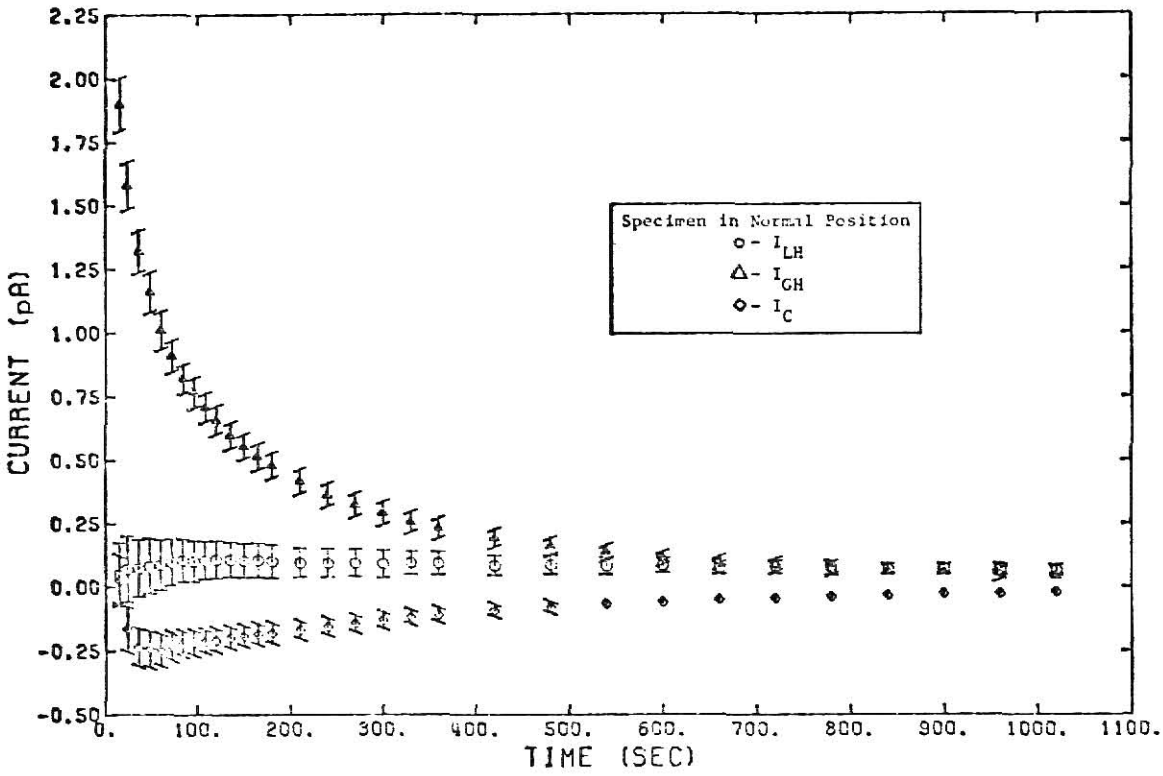

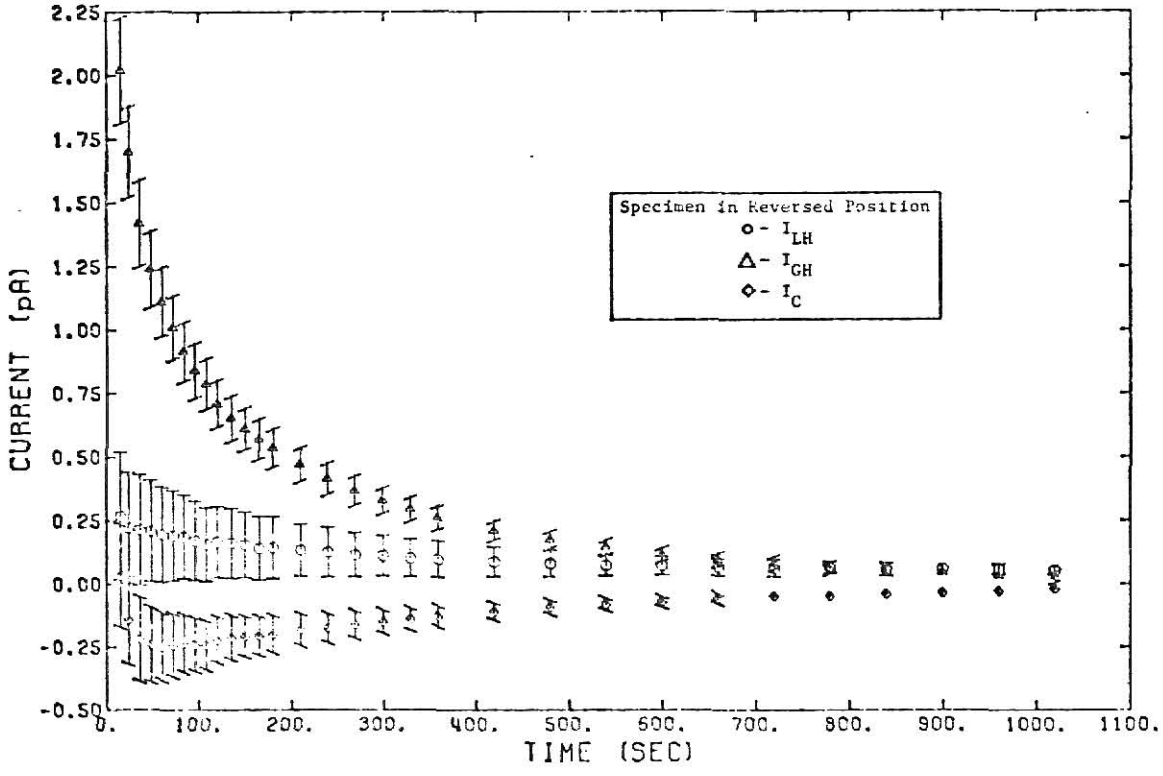

Fig. 4.15 Current generator strengths after irradiation of double-thickness specimen.

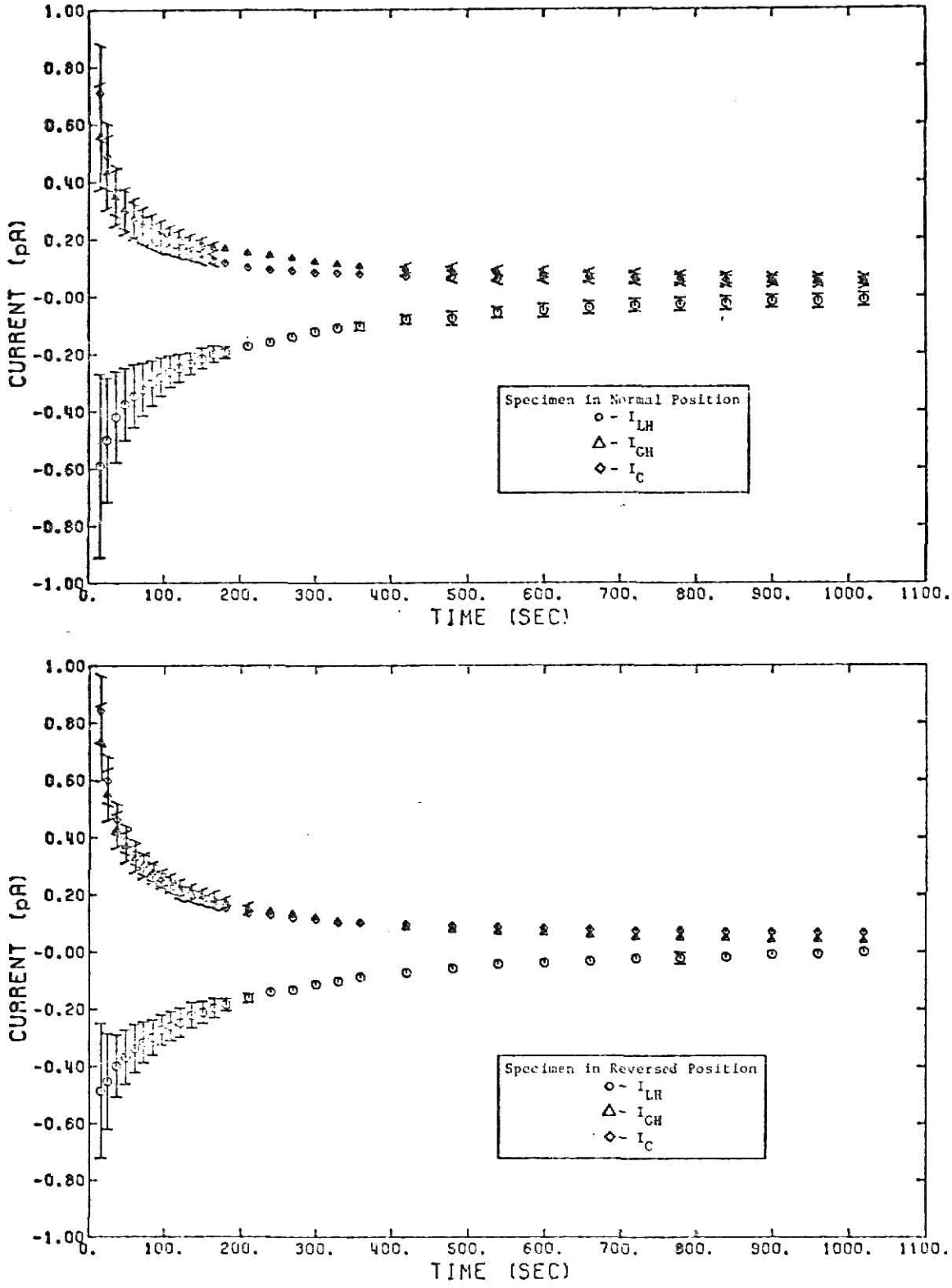

Fig. 4.16 Current generator strengths after irradiation of single-thickness specimen.

Robinson found that when this was done, the absolute values of the corrected currents became the same. The corrected values of the currents are shown in Figs. 4.17 and 4.18.

To determine if the absolute values of the corrected currents were really the same, a t-test for the difference between two means was performed on each pair of corrected current values. The null hypothesis of the t-test was that the absolute values of the two currents at any specified time were the same. The currents and t-values are found in Appendix 9.7. The results of the tests indicated no significant difference between the values of the currents in the case of the double-thickness specimen. However, in the case of the single-thickness specimen, the difference between the currents was found to be significant. The null hypothesis could be rejected at the 95% confidence level for the majority of the current values tested.

4.2 Neutron-Irradiation Data

The current data as a function of applied voltage are presented in Figs. 4.19 through 4.23 and in Appendix 9.8. The specimen resistance at each irradiation position was calculated using a non-weighted linear least squares fit to the I-V data. Once the resistances were known, the conductivity at each position was calculated from the formula

$$\sigma = \frac{L}{AR} \tag{4.8}$$

where L is the specimen thickness, A is the effective specimen area, and R is the specimen resistance. The effective specimen area, corrected for fringing effects, was calculated using ASTM procedures (17), and was found to be 11.32 cm^2. The conductivity as a function of distance from the ^{252}Cf source is presented in Table 4.1.

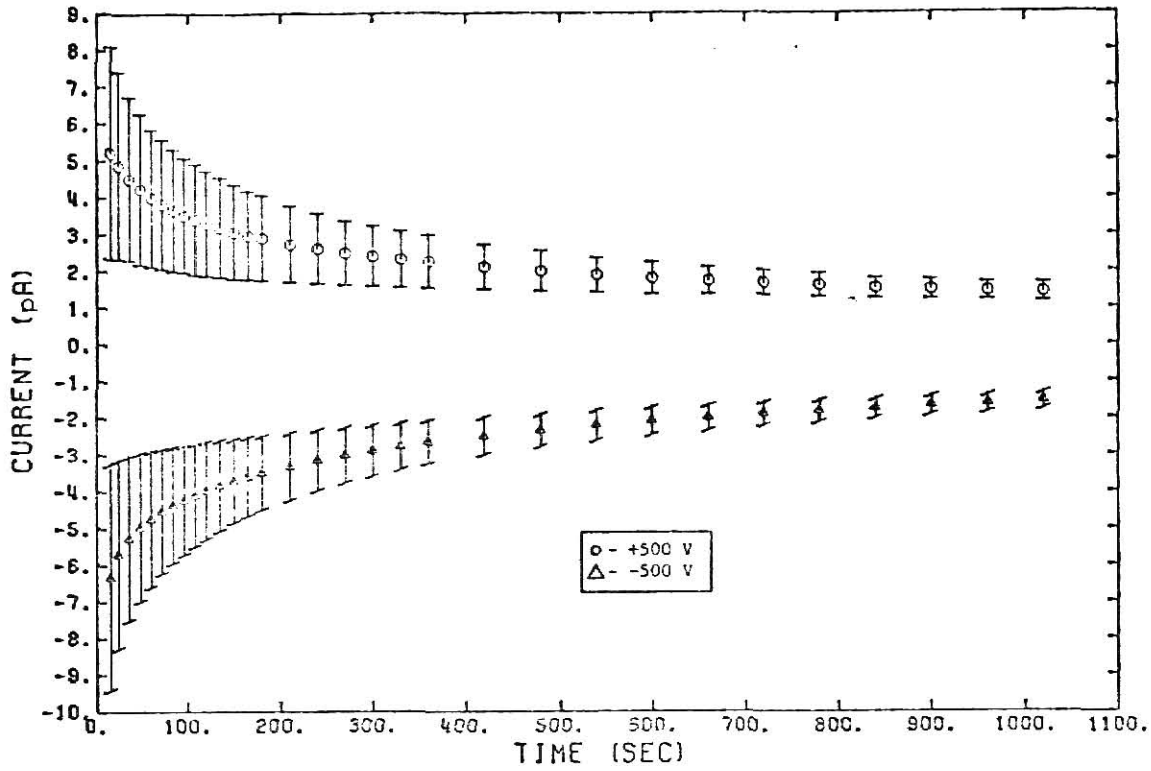

Fig. 4.17 Corrected current values during post-irradiation recovery of double-thickness specimen.

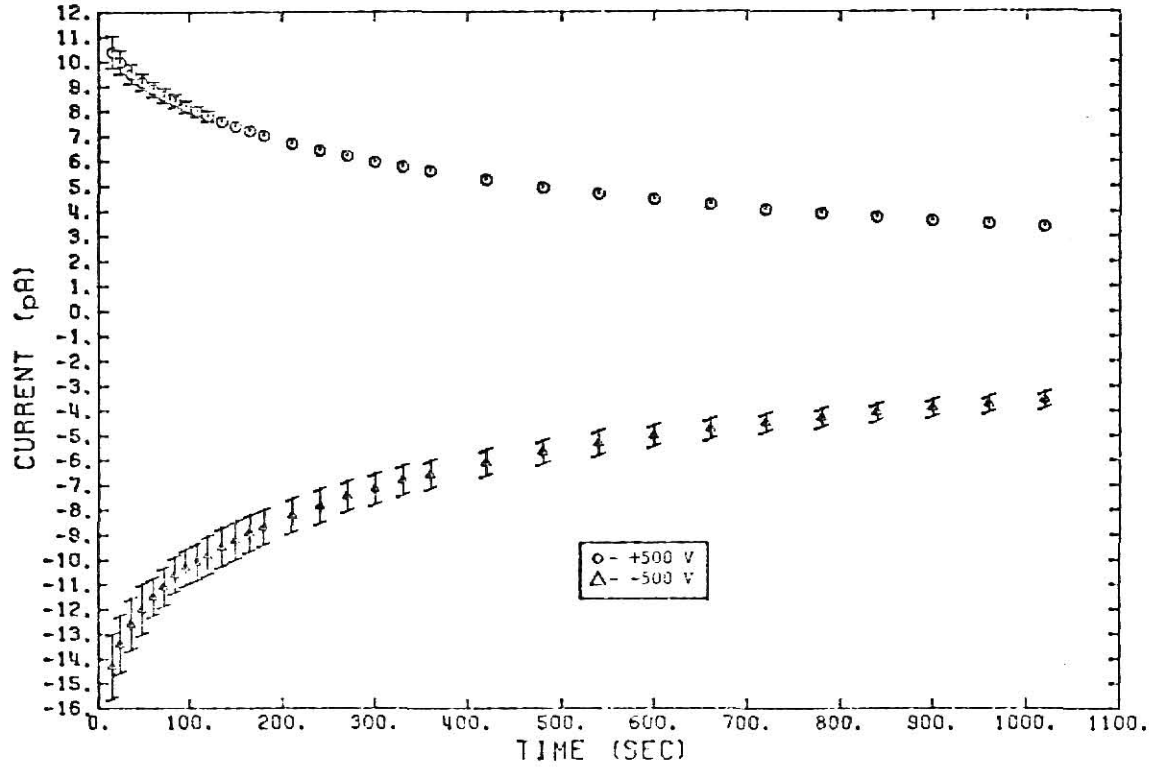

Fig. 4.18 Corrected current values during post-irradiation recovery of single-thickness specimen.

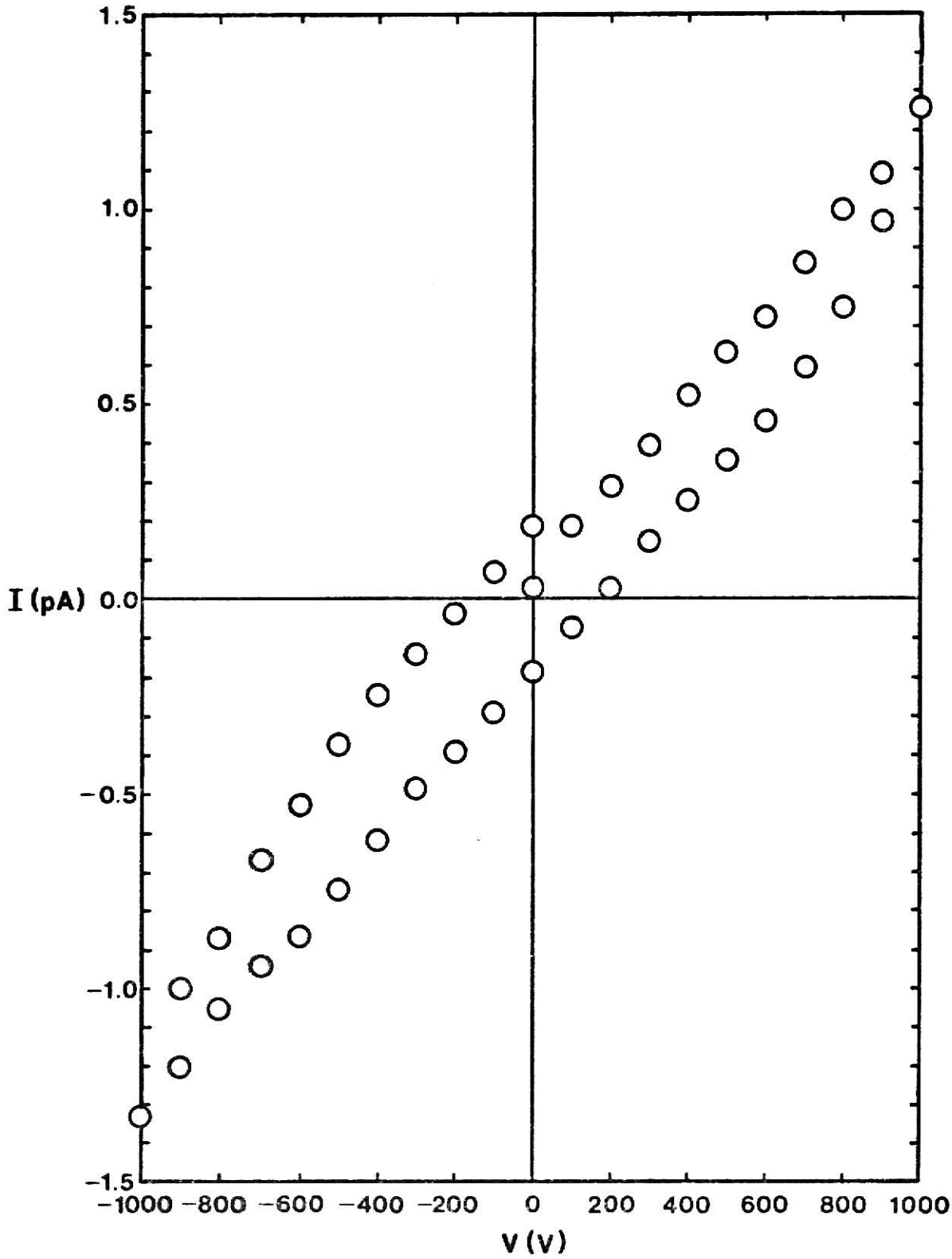

Fig. 4.19 I-V characteristics for dark conductivity calculation.

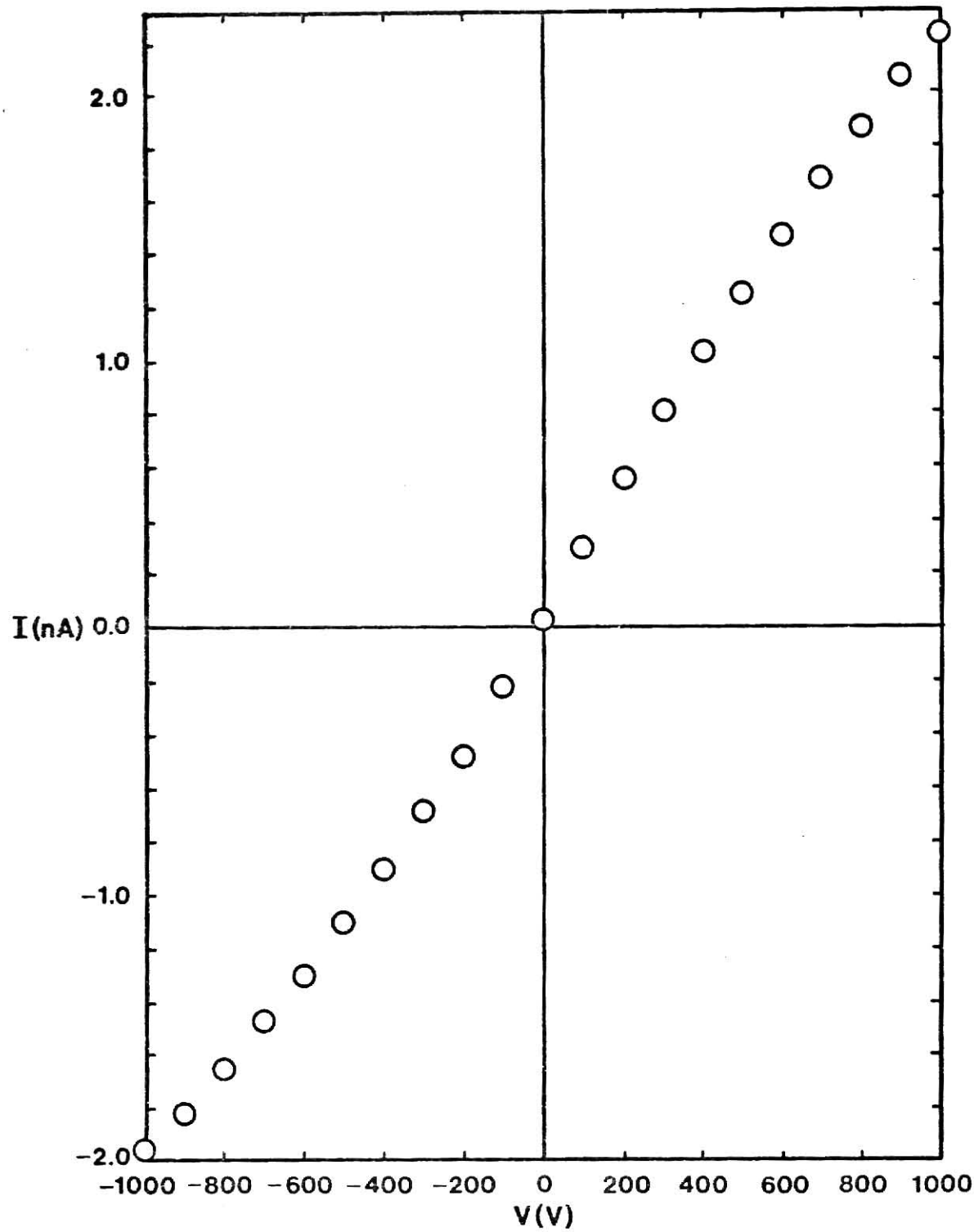

Fig. 4.20 I-V characteristics at position 1.

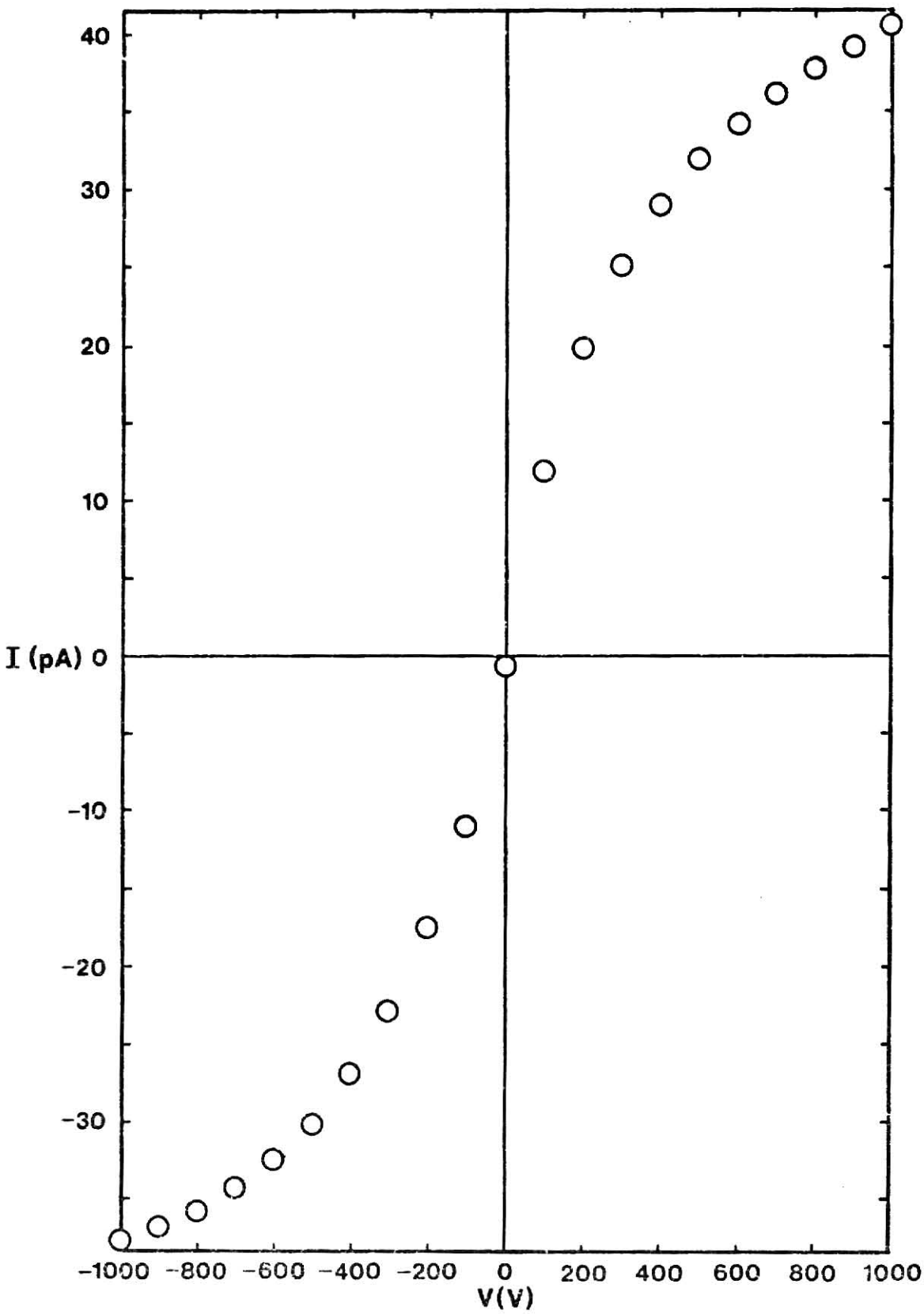

Fig. 4.21 I-V characteristics at position 2.

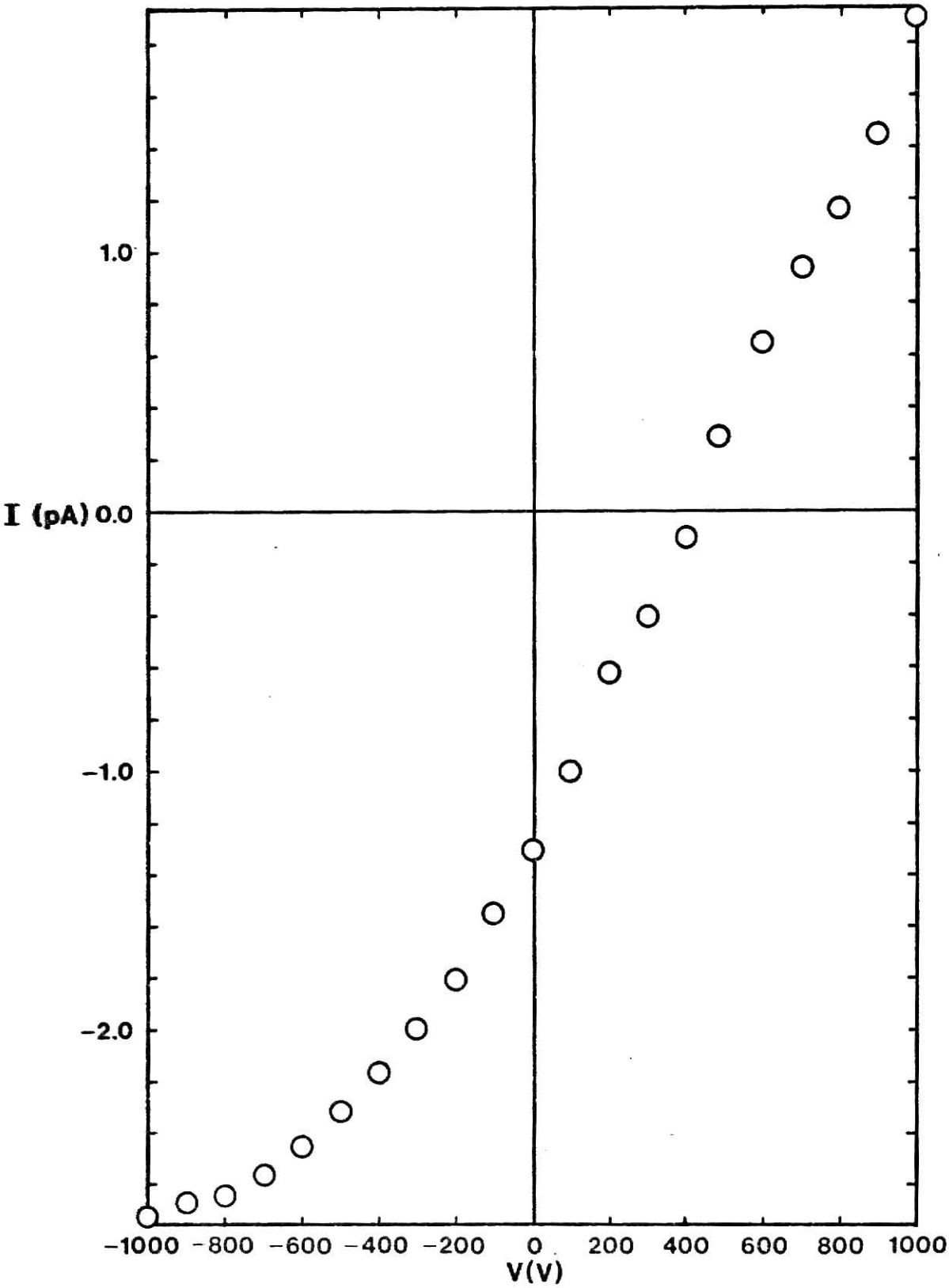

Fig. 4.22 I-V characteristics at position 3.

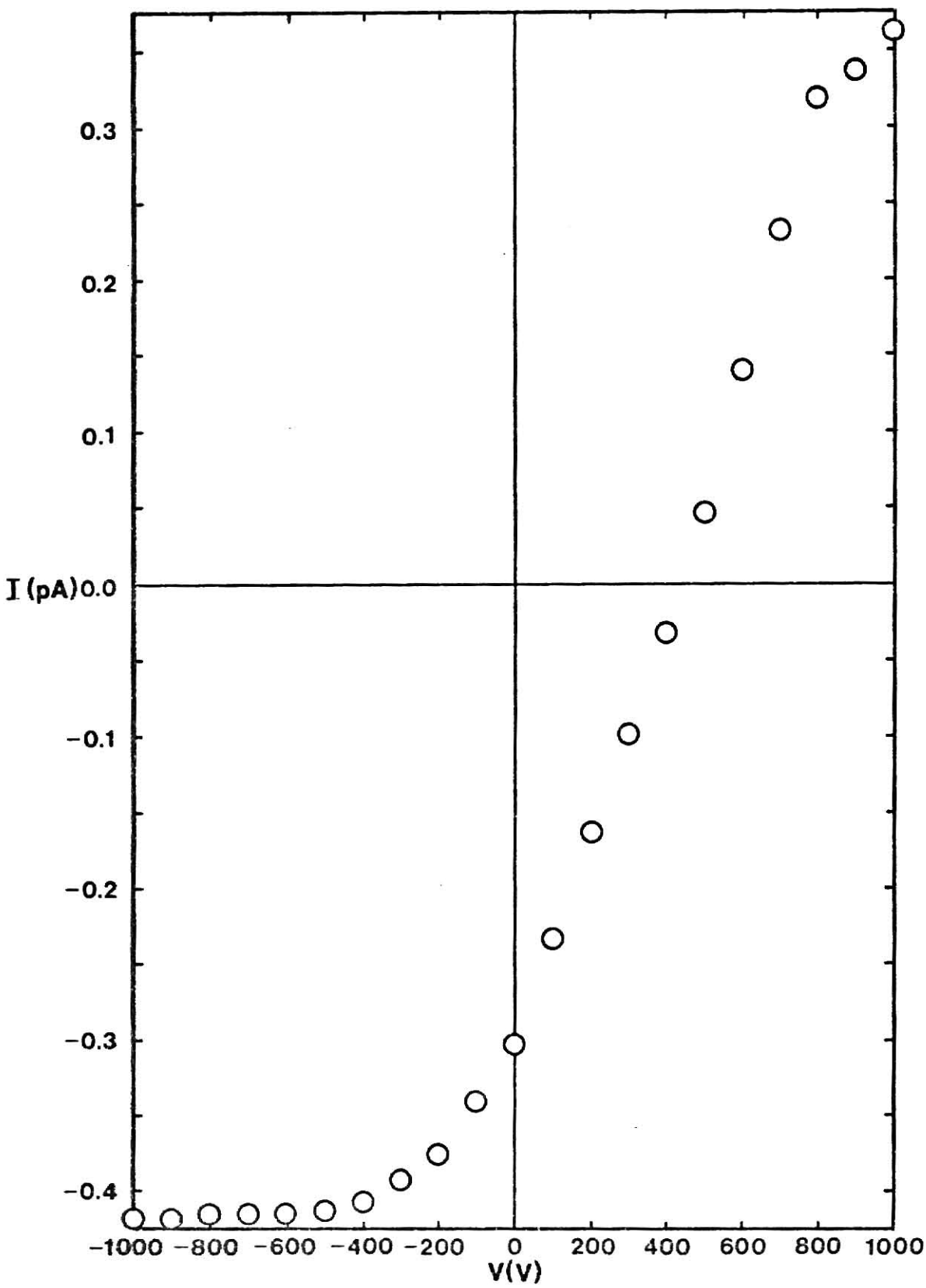

Fig. 4.23 I-V characteristics at position 4.

The reference source spectra necessary to calculate the efficiency of the 3 in. by 3 in. NaI detector can be found in an earlier report by this author (21). Reference source data are presented in Appendix 9.9. Gamma ray data for the reference sources and gold foils are from references (22) and (23).

Calculation of efficiency as a function of gamma energy for the 3 in. by 3 in. NaI detector is presented in Appendix 9.10. The efficiency for the 0.4118 MeV gamma from ^{198}Au was estimated to be 21.7 percent.

The gold foil irradiation and counting data are given in Appendices 9.11 and 9.12, respectively. The gold foil spectra may be found in reference (21).

Calculations of foil activities and thermal neutron flux levels are presented in Appendices 9.13 through 9.15. The calculated values of thermal neutron flux, using data from each counting technique, are presented in Table 4.2. The ratio of the calculated flux values should be the same at every position. It is seen, however, that this ratio is not a constant. Evaluation of the two counting techniques employed leads to the conclusion that there is a greater chance for error in the coincidence technique, since the circuitry is more complex, and the gate widths, etc. must be set very precisely. Therefore, it is believed that the flux calculations using the data from the single NaI detector are the better of the two. Further calculations are carried out, however, using both sets of flux data, for comparison.

The ratio of fast flux to thermal flux is assumed to be the same at each position, so that the calculated values of conductivity should bear the following relationship to the measured values of thermal flux:

Table 4.1 Conductivity vs. Distance from Source

σ $\{\Omega^{-1}\ cm^{-1}\}$	Position	Distance {cm}
5.97×10^{-14}	1	7.45
1.37×10^{-15}	2	42.20
6.75×10^{-17}	3	73.00
1.34×10^{-17}	4	102.45
3.20×10^{-17}	(Dark Conductivity)	∞

Table 4.2 Thermal Flux vs. Distance from Source

ϕ_{th} $\{cm^{-2}\ sec^{-1}\}$ (Single Detector)	ϕ_{th} $\{cm^{-2}\ sec^{-1}\}$ (Coincidence Detector)	Position
1.35×10^{8}	1.93×10^{8}	1
2.50×10^{5}	3.73×10^{5}	2
4.76×10^{4}	3.44×10^{4}	3
~ 0	~ 0	4

$$(\sigma - \sigma_o) = K \phi_{th}^{\delta} \tag{4.9}$$

where σ is the conductivity during irradiation, σ_o is the dark conductivity, K is a proportionality constant, ϕ_{th} is the thermal neutron flux, and $0.5 \leq \delta \leq 1.0$.

The values of $(\sigma - \sigma_o)$ and ϕ_{th} are summarized in Table 4.3. It is seen that $(\sigma - \sigma_o)$ is negative for position 4. This may be due to the fact that I-V data for σ_o were taken with much shorter leads than those used for the measurements during irradiation.

Table 4.3 Thermal Flux vs. $(\sigma - \sigma_o)$

ϕ_{th} $\{cm^{-2}\ sec^{-1}\}$ (Single Detector)	ϕ_{th} $\{cm^{-2}\ sec^{-1}\}$ (Coincidence Detector)	$(\sigma - \sigma_o)$ $\{\Omega^{-1}\ cm^{-1}\}$	Position
1.35×10^{8}	1.93×10^{8}	5.97×10^{-14}	1
2.50×10^{5}	3.73×10^{5}	1.34×10^{-15}	2
4.76×10^{4}	3.44×10^{4}	3.56×10^{-17}	3
~ 0	~ 0	-1.87×10^{-17}	4

If the logarithms are taken of both sides of Eq. (4.9), the result is

$$\ln(\sigma - \sigma_o) = \ln K + \delta \ln \phi_{th} . \tag{4.10}$$

The values of $(\sigma - \sigma_o)$ vs. ϕ_{th} for positions 1 through 3 were fitted to Eq. (4.10) using a linear least squares technique. The resulting slope of the line is the value of δ. Using the single detector data,

$$\delta = 0.71 \pm 0.03 . \tag{4.11}$$

Using the coincidence detector data,

$$\delta = 0.81 \pm 0.05 . \tag{4.12}$$

5. Conclusions

5.1 Gamma-Irradiation Study

It may be noted from Figs. 4.1 through 4.8 that the short-circuit currents represent a reproducible phenomenon. Further, it is seen that the reproducibility is much better, in general, during post-irradiation recovery. It is believed that the larger standard deviations of current values observed during irradiation are due to variations in coaxial cable position from measurement to measurement. The coaxial cables ran through slots in the electrical shielding box, and then up the walls of the gammacell chamber and out the top. It may be seen from the isodose curves of Fig. 4.1 that the dose rate varies rapidly with position near the walls of the chamber. Hence, a relatively small change in cable position could result in a noticeably different value of Compton injection current in the cable.

It is also obvious from the averaged raw data that there is no significant difference in currents due to specimen orientation within the gammacell chamber.

The current generator model seems to give consistent results during irradiation of the specimens. The current generator strengths calculated for the coaxial cables of both the double- and single-thickness specimens have the same behavior with time and have nearly the same magnitude at any specified time. The calculated strengths of the current generators within the specimens have the same sign in each of the two specimens, but different magnitudes. The difference in magnitudes is not surprising, since the specimens have neither the same thickness nor cross-sectional area.

The calculated strengths of the current generators during post-irradiation recovery are not consistent at all, however. The current

THE FOLLOWING

DOCUMENT(S)

IS/ARE ILLEGIBLE DUE TO INK BLEED THROUGH

generators in the cables have opposite signs in the two specimens. Since the coaxial cables are the same for both specimens, and since there is no interaction between the cable insulator and the specimen, the behavior should be the same for both cables.

A possible explanation for this discrepancy is as follows. During irradiation, the injection current is probably the larger component of the total current. Considering injection current only, the two current generators postulated in the specimen are the only ones necessary because of the electrode geometry. No electrons can be injected into the specimen from the guard ring towards the low-voltage electrode, or vice versa. During post-irradiation recovery, however, the space-charge controlled current is the only component of the current. This current may well have a radial component which would require the addition of a current generator between the guard ring and low-voltage electrode. The addition of another unknown to the model would obviously change the calculated values of the current generators. Since there are only three measured currents, a current generator model with four unknowns would not have a unique solution. There appears to be no way to experimentally measure any other current, so that the use of a model with four current generators is inconsistent with the present experimental setup.

As indicated in the discussion of the current generator model, the short-circuit currents are believed to have two components. One component present only during irradiation would be an injection current due to scattered Compton electrons. The second component is a conduction current controlled by a time-dependent spatially non-uniform charge distribution within the specimen. This belief is supported by the fact that no short-circuit currents were observed during neutron irradiation. Neutron bombardment would cause relatively little charge injection, and should give rise to a spatially

uniform charge distribution. Ionization occurs as a result of the displacement and movement of primary knock-on atoms. Since the displacement of these atoms will occur uniformly throughout a thin specimen, and since their path lengths are relatively short, the resulting charge distribution should be uniform.

The space-charge-controlled current density is described by the governing equations of Section 2.1. No attempt was made to obtain numerical solutions to the governing equations or to correlate solutions to the experimentally measured currents. The source functions for electron and hole generation are unknown, as are the injection current densities. Solution of a combined gamma ray and electron transport problem would be necessary to find these source functions and injection current densities. Also, the pertinent material properties of polyethylene, such as trapping coefficients and energy distribution of traps, are known only approximately. Monteith and Hauser (10) solved the governing equations in one dimension for polyethylene terephthalate, in the absence of recombination, and for monodirectional electron irradiation. They found correlation of calculated results to experimental data to be impractical because of the large number of material parameters involved. Thus, it appears that more investigation of material properties is needed before correlation of theoretical and experimental results may be successfully attempted.

The behavior of post-irradiation current in the double-thickness specimen with an applied voltage is consistent with that observed by Faw and Robinson (1), who also used a double-thickness specimen. Subtraction of the short-circuit current from those observed at ±500 V gives corrected current values which show no statistically significant difference in magnitude. The post-irradiation currents in the single-thickness specimen do not show this

behavior. It is possible that the layer of conductive paint in the middle of the double-thickness specimen may have an effect on the post-irradiation current behavior, since this layer can carry an induced charge.

At present, there is no way to predict the post-irradiation behavior of short-circuit currents for either specimen, since the governing equations are nonlinear, and no analytical solutions have been found.

In summary, the following conclusions seem justified. First, the short-circuit currents observed during and after irradiation of organic insulators represent a reproducible physical phenomenon. The basic mechanisms for the production of these currents are probably a Compton electron injection current and a space-charge-controlled conduction current. These current components can be described by a mathematical model as presented in Section 2.1. Finally, in the case of the double-thickness specimen, subtraction of the post-irradiation short-circuit currents from the post-irradiation currents observed at ±500 V results in corrected currents which have the same behavior as those observed by Faw and Robinson (1).

5.2 Neutron-Irradiation Study

The calculated values of δ (0.71 and 0.81) lie within the range predicted by Rose (12): $0.5 \leq \delta \leq 1.0$. The only value available for comparison is that found by Harrison et al. (2) for polystyrene. They found δ to be 0.97 during the "transient equilibrium" period of a combined gamma ray and neutron pulse from the Sandia Pulsed Reactor. The investigation of neutron-induced conductivity by Frankovsky and Shatzkes (3) did not use the Rose model.

It should be noted that the dose rate due to gamma irradiation from ^{252}Cf has been neglected in the calculations. Other work done with the KSU ^{252}Cf source (24) indicates that the gamma contribution to the total dose rate is less than 10% at locations close to the source.

The effect of total neutron dose received by the specimen is negligible. Permanent damage to organic solids such as polyethylene generally requires a total integrated flux in excess of 10^{16} to 10^{18} neutrons per cm^2. The total exposure time of the specimen was approximately 4 hours. Multiplication of this time by the flux at each position gives a total integrated flux of approximately 3×10^{12} neutrons per cm^2, well below the threshold of measureable permanent damage.

In conclusion, the experimentally determined relationship of steady-state neutron-induced conductivity to neutron flux level was found to agree with that predicted by the Rose model (15).

6. Suggestions for Future Work

Further study, both theoretical and experimental, of radiation-induced short-circuit currents is needed. First, the experimental determination of trap energy distributions and trapping kinetics parameters for polyethylene should be done. When these parameters are known, numerical solutions of the governing equations may be obtained. Additional measurements of short-circuit currents should be conducted using specimens with a different type of signal lead, to eliminate the current contribution from the coaxial cable. Then, correlation of the theoretical and experimental results should be attempted.

There is a great deal of work yet to be done in the investigation of neutron-induced conductivity. More correlations of steady-state conductivity to neutron dose rate need to be done. In particular, the absolute fast neutron flux should be measured in order to calculate the total dose rate seen by the specimen. A wider range of dose rates and the effect of total dose need to be studied.

Data are needed for the study of buildup and decay of conductivity during and after irradiation in a neutron environment.

Other possible studies include the variation of specimen geometry and the effects of temperature and humidity.

In short, the possibilities for further study of neutron-induced conductivity are many and challenging.

7. Literature Cited

1. Faw, R. E. and M. J. Robinson, "Radiation-Induced Electrical Conductivity in Polyethylene, Progress Report: Task: 1.3.5, Radiation Effects in Amorphous Insulators, Contract: N00014-68-A-0504, Office of Naval Research," Department of Nuclear Engineering, Kansas State University, 1971.

2. Harrison, S. E., F. N. Coppage, and A. W. Snyder, "Gamma-Ray and Neutron-Induced Conductivity in Insulating Materials," IEEE Trans. on Nucl. Sci., 10, No. 5, 118-130 (1963).

3. Frankovsky, F. A. and M. Shatzkes, "Reactor and Linear Accelerator Induced Effects in Dielectrics," IEEE Trans. on Nucl. Sci., 13, No. 5, 8-21 (1966).

4. Fellers, S. G., "Radiation-Induced Conductivity in Polyethylene," M.S. Thesis, Department of Nuclear Engineering, Kansas State University, 1971.

5. Yahagi, K. and A. Danno, "Gamma-Ray Induced Conductivity in Polyethylene and Teflon under Radiation at High Dose Rates," J. Appl. Phys., 34, No. 4, 804-809 (1963).

6. Mizutani, T., Y. Takai, and M. Ieda, "Ultraviolet Transient Photocurrents in Polyethylene with Zero External Field," Jap. J. Appl. Phys., 12, No. 10, 1553-1557 (1973).

7. Roberts, T. C., "An Evaluation of the KSU Multi-Milligram ^{252}Cf Facility," M.S. Thesis, Department of Nuclear Engineering, Kansas State University, 1972.

8. Lindmayer, J., "Current Transients in Insulators," J. Appl. Phys., 36, No. 1, 196-201 (1965).

9. Gross, B. and M. M. Perlman, "Short-Circuit Currents in Charged Dielectrics and Motion of Zero-Field Planes," J. Appl. Phys., 43, No. 3, 853-855 (1972).

10. Monteith, L. K. and J. R. Hauser, "Space-Charge Effects in Insulators Resulting from Electron Irradiation," J. Appl. Phys., 38, No. 13, 5355-5365 (1967).

11. Murphy, P. V. and B. Gross, "Polarization of Dielectrics by Nuclear Radiation. II. Gamma-Ray-Induced Polarization," J. Appl. Phys., 35, No. 1, 171-174 (1964).

12. Rose, A., "An Outline of Some Photoconductive Processes," R.C.A. Review, 12, 362-414 (1951).

13. Billington, D. S. and J. H. Crawford, Jr., Radiation Damage in Solids, Princeton University Press, 1961.

14. Rose, A., "Recombination Processes in Insulators and Semiconductors," Phys. Rev., 97, 322-333 (1955).

15. Rose, A., Concepts in Photoconductivity and Allied Problems, Interscience Publishers, 1963.

16. Cadillac Plastic and Chemical Company, Plastic Catalog and Price Sheet (March 1, 1963).

17. 1969 Book of ASTM Standards with Related Material, Part 29: Electrical Insulating Materials, ASTM Designation D257, ASTM, 1969.

18. Bailey, J. A. and J. F. Villareal, "Radiation-Induced Conductivity in Polyethylene," Lab Report for Radioisotope Applications Engineering, Kansas State University, 1972.

19. Tagg, G. F., The Practical Measurement of Insulation Resistance, Newnes Books, 1968.

20. Price, W. J., Nuclear Radiation Detection, McGraw-Hill, 1964.

21. Ryman, J. C., "Fast-Neutron Induced Electrical Conductivity in Polyethylene, Final Report, Task II.1(b).(2) & (3), Contract: AEC No. AT(38-1)-612, ^{252}Cf Loan Agreement," Department of Nuclear Engineering, Kansas State University, 1973.

22. Radiological Health Handbook, U.S. Dept. of H.E.W., U.S. Government Printing Office, 1970.

23. Health, R. L., "Scintillation Spectrometry Gamma-Ray Spectrum Catalogue," USAEC Report IDO-16880-1, TID-4500, Vol. 2, 1964.

24. Kan, C., "The Response of CaF_2:Mn Thermoluminescent Dosimeters to Neutrons from a ^{252}Cf source," M.S. Thesis, Department of Nuclear Engineering, Kansas State University, 1973.

25. Volk, W., Applied Statistics for Engineers, McGraw-Hill, 1958.

8. Acknowledgements

The author wishes to express his sincere appreciation to Dr. R. E. Faw for his help and guidance throughout the course of this investigation. A special thanks goes to Dr. M. S. Krick for his help in carrying out the foil activation measurements. The technical assistance provided by Messrs. George Abshire, Bill Starr, Oscar Mulhern, and Michael McEwan was invaluable. The assistance of Mr. Roger Lanksbury in the preparation of foil counting data was greatly appreciated. Special thanks are also due to Drs. J. F. Merklin, H. J. Donnert, and G. L. Johnson for their helpful discussions.

The author also wishes to thank the Atomic Energy Commission for providing financial support in the form of an A.E.C. Special Fellowship in Nuclear Science and Engineering and the K.S.U. Department of Nuclear Engineering for financial support through a graduate assistantship. The support of this research by the U.S. Department of Defense (Office of Naval Research) through project THEMIS is gratefully acknowledged.

Finally, the author wishes to thank his parents, Mr. and Mrs. Royal Ryman, for their continued encouragement throughout his many years of study.

9. Appendices

Appendix 9.1

Continuity Equation for Trapped Electrons

It is assumed that all hole traps below the electron Fermi level E_{fn} are filled, and that all traps between the conduction band and the Fermi level are vacant, i.e.,

$$n_t(x,r,t,E) = 0 \quad , \quad 0 \leq E \leq E_{fn} \ ,$$

and

$$n_t(x,r,t,E) = n_T(E) \quad , \quad E_{fn} < E \leq E_g \ . \tag{9.1.1}$$

With the additional assumption that the free hole concentration is negligible, the continuity equation for trapped electrons reduces to

$$\frac{\partial n_t(x,r,t)}{\partial t} = \langle \alpha_n \rangle \, n(x,r,t) \int_0^{E_{fn}} n_T(E)dE - \langle \nu_n \rangle \int_{E_{fn}}^{E_g} n_T(E) e^{-E/kT} dE \ . \tag{9.1.2}$$

The electron trap distribution is assumed to vary exponentially with energy:

$$n_T(E) = \frac{B}{kT_c} e^{-E/kT_c} \tag{9.1.3}$$

where B and T_c are empirical constants governing the energy distribution. The total trap density is just

$$n_T = \int_0^{E_g} n_T(E)dE = \int_0^{E_g} \frac{B}{kT_c} e^{-E/kT_c} dE$$

$$= B(1 - e^{-E_g/kT_c}) \ . \tag{9.1.4}$$

Since $E_g >> kT_c$ for most insulators, $n_T \simeq B$. The first integral of Eq. (9.1.2) is

$$\int_0^{E_{fn}} n_T(E)dE = n_T\left(1 - e^{-E_{fn}/kT_c}\right) = n_T - n_t(x,r,t) \ . \tag{9.1.5}$$

The second integral of Eq. (9.1.2) is

$$\int_{E_{fn}}^{E_g} \frac{n_T}{kT_c} \exp\left[-\frac{E}{K}\left(\frac{1}{T}+\frac{1}{T_c}\right)\right] dE$$

$$= n_T\left(1+\frac{T_c}{T}\right)^{-1}\left\{\exp\left[-\frac{E_{fn}}{kT_c}\left(1+\frac{T_c}{T}\right)\right] - \exp\left[-\frac{E_g}{kT_c}\left(1+\frac{T_c}{T}\right)\right]\right\}$$

$$\simeq n_T\left(1+\frac{T_c}{T}\right)^{-1} \exp\left[-\frac{E_{fn}}{kT_c}\left(1+\frac{T_c}{T}\right)\right] . \qquad (9.1.6)$$

From Eq. (9.1.5), it follows that

$$\frac{n_t(x,r,t)}{n_T} = e^{-E_{fn}/kT_c} . \qquad (9.1.7)$$

Then,

$$\int_{E_{fn}}^{E_g} n_T(E) e^{-E/kT}\, dE = n_T\left(1+\frac{T_c}{T}\right)^{-1}\left[\frac{n_t(x,r,t)}{n_T}\right]^{(1+T_c/T)} , \qquad (9.1.8)$$

and the reduced form of the continuity equation is

$$\frac{\partial n_t(x,r,t)}{\partial t} = \langle \alpha_n \rangle\, n(x,r,t)\,[n_T - n_t(x,r,t)]$$

$$- \langle \nu_n \rangle\, n_T\left[1+\frac{T_c}{T}\right]^{-1}\left[\frac{n_t(x,r,t)}{n_T}\right]^{(1+T_c/T)} . \qquad (9.1.9)$$

Appendix 9.2

Relation of Currents to Zero-Field Surfaces

9.2.1 Case of Plane-Parallel Geometry

Poisson's equation for plane-parallel geometry is

$$\varepsilon \frac{\partial E(x,t)}{\partial x} = \rho(x,t) \ , \tag{9.2.1}$$

with the boundary condition

$$\int_0^L E(x,t)dx = V = \text{constant} \ . \tag{9.2.2}$$

Integration of Eq. (9.2.1) gives

$$\varepsilon \ E(x,t) - \varepsilon \ E(0,t) = \int_0^x \rho(x',t)dx' \ . \tag{9.2.3}$$

Integration again from x = 0 to x = L, and rearrangement results in

$$\varepsilon \ E(0,t) = \frac{\varepsilon V}{L} - \frac{1}{L}\int_0^L dx \int_0^x \rho(x',t)dx' \tag{9.2.4}$$

so that

$$\begin{aligned} \varepsilon \ E(x,t) &= \int_0^x \rho(x',t)dx' + \frac{\varepsilon V}{L} - \frac{1}{L}\int_0^L \rho(x',t)dx' \int_{x'}^L dx \\ &= \int_0^x \rho(x',t)dx' + \frac{\varepsilon V}{L} \int_0^L \rho(x',t)\left(1 - \frac{x'}{L}\right)dx' \ , \end{aligned} \tag{9.2.5}$$

where the order of integration has been interchanged in the second integral.

If one or more zero-field planes exist, their locations are defined by

$$E(x_i,t) = 0 \quad , \qquad i = 1,2,... \tag{9.2.6}$$

Then, at any x_i,

$$\int_0^{x_i} \rho(x',t)dx' = \int_0^L \rho(x',t)\left(1 - \frac{x'}{L}\right)dx' - \frac{\varepsilon V}{L} \ . \tag{9.2.7}$$

Differentiation of Eq. (9.2.7) with respect to time gives

$$\rho[x_i(t),t]\,\frac{dx_i}{dt} + \int_0^{x_i(t)} \frac{\partial\rho(x,t)}{\partial t}dx = \int_0^L \frac{\partial\rho(x,t)}{\partial t}\left(1 - \frac{x}{L}\right)dx \ . \qquad (9.2.8)$$

Continuity requires that

$$\frac{\partial\rho(x,t)}{\partial t} = -\frac{\partial J_c(x,t)}{\partial x} \ . \qquad (9.2.9)$$

Then,

$$\rho[x_i(t),t]\,\frac{dx_i}{dt} - \int_0^{x_i(t)} \frac{\partial J_c(x,t)}{\partial x}\,dx = -\int_0^L \frac{\partial J_c(x,t)}{\partial x}\left(1 - \frac{x}{L}\right)dx \qquad (9.2.10)$$

and

$$J_c[x_i(t),t] = \rho[x_i(t),t]\,\frac{dx_i}{dt} + \frac{1}{L}\int_0^L J_c(x,t)dx \ . \qquad (9.2.11)$$

The total current density J(t) at any point is just

$$J(t) = \varepsilon\,\frac{\partial E(x,t)}{\partial t} + J_c(x,t) \ . \qquad (9.2.12)$$

Integration of Eq. (9.2.12) yields

$$J(t) = \frac{1}{L}\int_0^L J_c(x,t)dx \ . \qquad (9.2.13)$$

Then, from Eq. (9.2.11),

$$J(t) = -\rho[x_i(t),t]\,\frac{dx_i}{dt} + J_g[x_i(t),t] \qquad (9.2.14)$$

since the conduction current density at any zero-field plane consists only of the injection current density $J_g[x_i(t),t]$.

9.2.2 Case of Cylindrical Geometry

Poisson's equation for cylindrical geometry is

$$\frac{\varepsilon}{r}\frac{\partial}{\partial r}\,[r\,E(r,t)] = \rho(r,t) \ , \qquad (9.2.15)$$

with the boundary condition

$$\int_{R_I}^{R_o} E(r,t)dr = V = \text{constant} . \tag{9.2.16}$$

Integration of Eq. (9.2.15) gives

$$\varepsilon r\, E(r,t) - \varepsilon R_I\, E(R_I,t) = \int_{R_I}^{r} r'\rho(r',t)dr' . \tag{9.2.17}$$

Division of Eq. (9.2.17) by r, integration from $r = R_I$ to $r = R_o$, and rearrangement yields

$$\varepsilon R_I\, E(R_I,t) = \varepsilon V - \frac{1}{\ell n(R_o/R_I)} \int_{R_I}^{R_o} \frac{dr}{r} \int_{R_I}^{r} r'\rho(r',t)dr' \tag{9.2.18}$$

so that

$$\begin{aligned} \varepsilon E(r,t) &= \frac{1}{r}\int_{R_I}^{r} r'\rho(r',t)dr' + \frac{\varepsilon V}{r} - \frac{1}{r\ell n(R_o/R_I)} \int_{R_I}^{R_o} r'\rho(r',t)dr' \int_{r'}^{R_o} \frac{dr}{r} \\ &= \frac{1}{r}\int_{R_I}^{r} r'\rho(r',t)dr' + \frac{\varepsilon V}{r} - \frac{1}{r}\int_{R_I}^{R_o} r'\rho(r',t) \frac{\ell n(R_o/r')}{\ell n(R_o/R_I)} dr' \end{aligned} \tag{9.2.19}$$

where the order of integration has been interchanged in the second integral.

If one or more zero-field cylinders exist, their locations are defined by

$$E(r_i,t) = 0 \quad , \qquad i = 1,2,\ldots \tag{9.2.20}$$

Then, at any r_i,

$$\int_{R_I}^{r_i} r'\rho(r',t)dr' + \varepsilon V = \int_{R_I}^{R_o} r'\rho(r',t) \frac{\ell n(R_o/r')}{\ell n(R_o/R_I)} dr' . \tag{9.2.21}$$

Differentiation of Eq. (9.2.21) with respect to time gives

$$r_i(t)\rho[r_i(t),t]\frac{dr_i}{dt} + \int_{R_I}^{r_i(t)} r' \frac{\partial\rho(r't)}{\partial t}\,dr' = \int_{R_I}^{R_o} r' \frac{\partial\rho(r',t)}{\partial t}\frac{\ell n(R_o/r')}{\ell n(R_o/R_I)}\,dr' . \tag{9.2.22}$$

Continuity requires that

$$\frac{1}{r}\frac{\partial}{\partial r}[r\,J_c(r,t)] = -\frac{\partial\rho(r,t)}{\partial t} . \tag{9.2.23}$$

Then,

$$r_i(t)\rho[r_i(t),t]\frac{dr_i}{dt} = \int_{R_I}^{r_i(t)} \frac{\partial}{\partial r}[r\,J_c(r,t)]dr - \int_{R_I}^{R_o} \frac{\partial}{\partial r}[r\,J_c(r,t)]\frac{\ell n(R_o/r)}{\ell n(R_o/R_I)}\,dr . \tag{9.2.24}$$

Integration by parts of Eq. (9.2.24) and rearrangement gives

$$\rho[r_i(t),t]\frac{dr_i}{dt} = J_c[r_i(t),t] - \frac{1}{r_i(t)\ \ell n(R_o/R_I)}\int_{R_I}^{R_o} J_c(r,t)dr . \tag{9.2.25}$$

The total current density J(t) at any point is given by

$$J(t) = \varepsilon\frac{\partial E(r,t)}{\partial t} + J_c(r,t) . \tag{9.2.26}$$

Integration of Eq. (9.2.26) yields

$$(R_o - R_I)J(t) = \int_{R_I}^{R_o} J_c(r,t)dr . \tag{9.2.27}$$

Then, from Eq. (9.2.25),

$$J(t) = \frac{r_i(t)\ \ell n(R_o/R_I)}{(R_o - R_I)}\left\{-\rho[r_i(t),t]\frac{dr_i}{dt} + J_g[r_i(t),t]\right\} \tag{9.2.28}$$

since the conduction current density at any zero-field cylinder consists only of the injection component.

Appendix 9.3

Test Results with and without a 5.1 MΩ Resistor in Series with Low-Voltage Lead

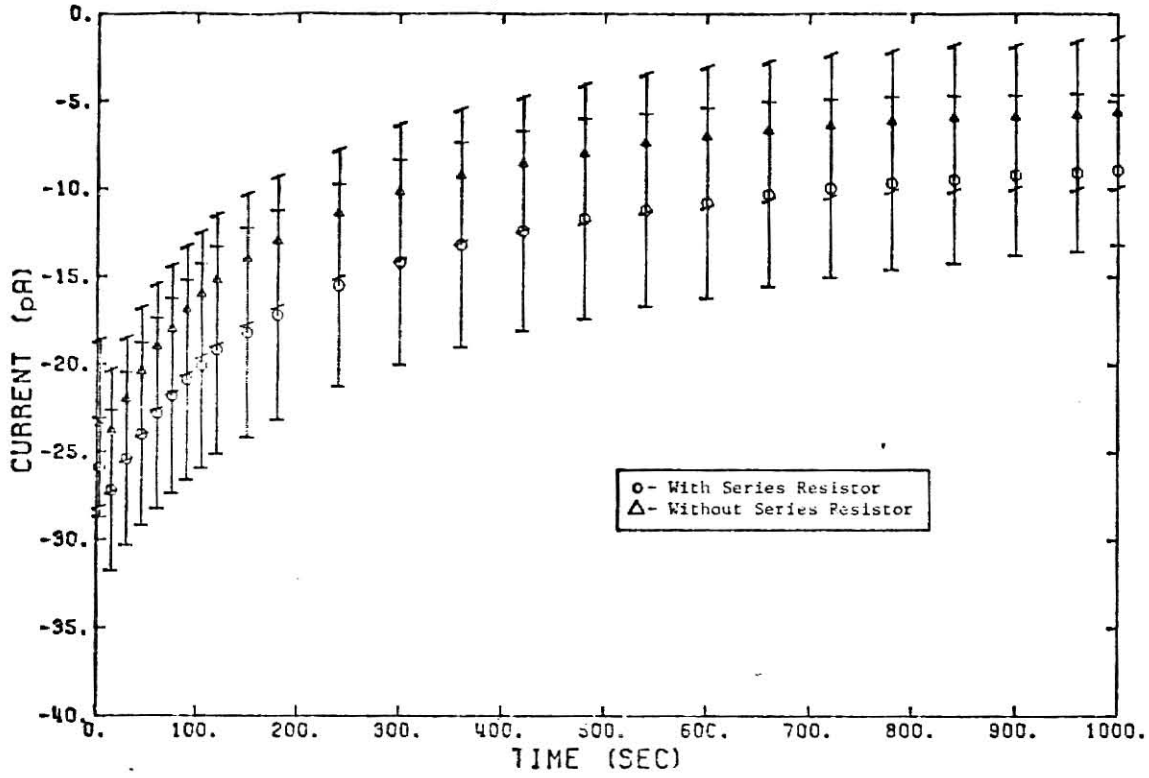

Fig. 9.3.1 Short-circuit currents during irradiation with and without 5.1 MΩ series resistor. (Currents from L.V. electrode of double-thickness specimen with guard ring.)

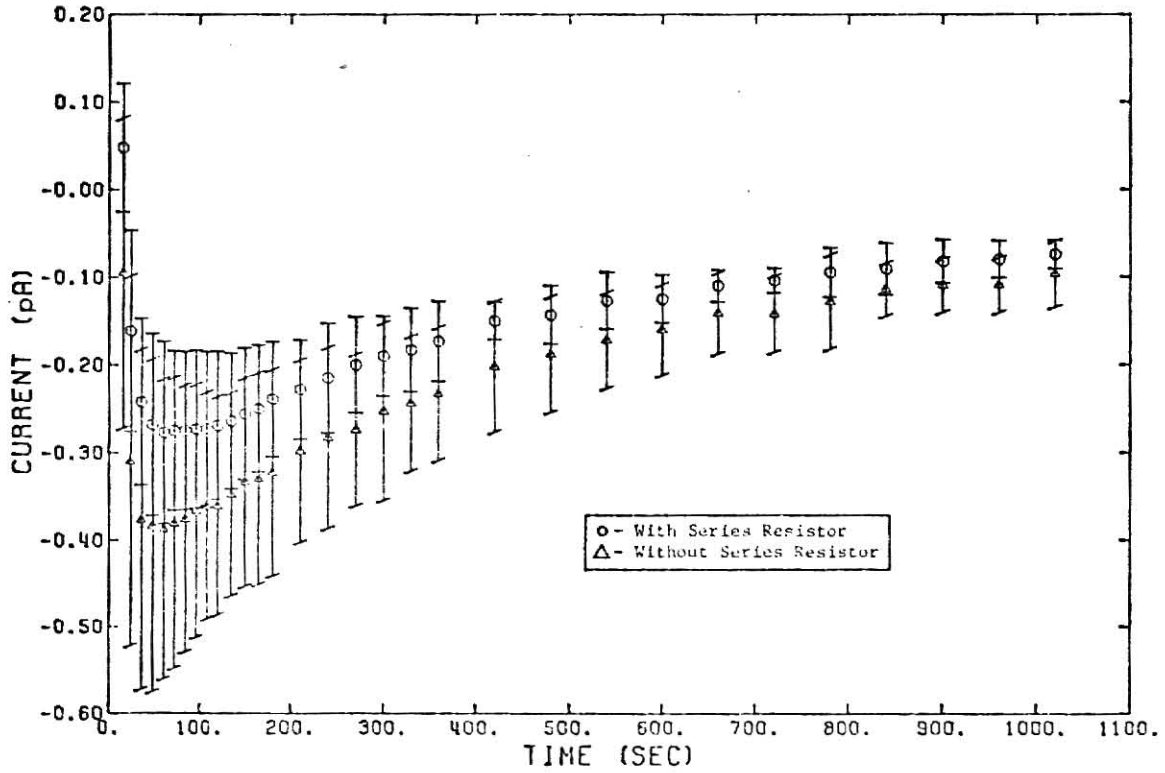

Fig. 9.3.2 Short-circuit currents after irradiation with and without 5.1 MΩ series resistor. (Currents from L.V. electrode of double-thickness specimen with guard ring.)

Appendix 9.4

Averaged Short-Circuit Current Data

TABLE 9.4.1 IRRADIATION CURRENTS FOR DOUBLE-THICKNESS SPECIMEN IN NORMAL POSITION

FROM LOW-VOLTAGE ELECTRODE			FROM HIGH-VOLTAGE ELECTRODE			FROM GUARD RING		
TIME (SEC)	CURRENT (A)	STD DEV (A)	TIME (SEC)	CURRENT (A)	STD DEV (A)	TIME (SEC)	CURRENT (A)	STD DEV (A)
3.	-2.46E-11	3.52E-12	3.	-1.37E-11	3.22E-11	3.	4.70E-12	8.69E-12
15.	-2.55E-11	3.87E-12	15.	-1.06E-11	3.26E-11	15.	-4.23E-13	6.05E-12
30.	-2.37E-11	4.02E-12	30.	-3.95E-12	3.27E-11	30.	7.74E-13	5.45E-12
45.	-2.22E-11	4.24E-12	45.	1.10E-12	3.28E-11	45.	2.09E-12	5.28E-12
60.	-2.09E-11	4.34E-12	60.	5.42E-12	3.28E-11	60.	3.38E-12	5.23E-12
75.	-1.99E-11	4.43E-12	75.	9.01E-12	3.27E-11	75.	4.46E-12	5.23E-12
90.	-1.89E-11	4.55E-12	90.	1.22E-11	3.23E-11	90.	5.44E-12	5.33E-12
105.	-1.81E-11	4.60E-12	105.	1.49E-11	3.21E-11	105.	6.31E-12	5.39E-12
120.	-1.72E-11	4.66E-12	120.	1.75E-11	3.17E-11	120.	7.09E-12	5.41E-12
150.	-1.61E-11	4.73E-12	150.	2.15E-11	3.12E-11	150.	8.51E-12	5.53E-12
180.	-1.51E-11	4.73E-12	180.	2.49E-11	3.08E-11	180.	9.70E-12	5.68E-12
240.	-1.34E-11	4.60E-12	240.	2.99E-11	2.94E-11	240.	1.17E-11	5.93E-12
300.	-1.22E-11	4.66E-12	300.	3.39E-11	2.91E-11	300.	1.35E-11	6.04E-12
360.	-1.12E-11	4.62E-12	360.	3.69E-11	2.86E-11	360.	1.48E-11	6.23E-12
420.	-1.05E-11	4.54E-12	420.	3.93E-11	2.81E-11	420.	1.61E-11	6.18E-12
480.	-9.65E-12	4.55E-12	480.	4.12E-11	2.76E-11	480.	1.72E-11	6.15E-12
540.	-9.28E-12	4.49E-12	540.	4.26E-11	2.72E-11	540.	1.83E-11	6.02E-12
600.	-8.93E-12	4.47E-12	600.	4.40E-11	2.69E-11	600.	1.93E-11	5.85E-12
660.	-8.50E-12	4.35E-12	660.	4.50E-11	2.65E-11	660.	2.01E-11	5.81E-12
720.	-8.18E-12	4.29E-12	720.	4.60E-11	2.63E-11	720.	2.09E-11	5.63E-12
780.	-7.90E-12	4.20E-12	780.	4.68E-11	2.60E-11	780.	2.15E-11	5.50E-12
840.	-7.70E-12	4.19E-12	840.	4.74E-11	2.59E-11	840.	2.21E-11	5.42E-12
900.	-7.55E-12	4.03E-12	900.	4.78E-11	2.56E-11	900.	2.27E-11	5.39E-12
960.	-7.43E-12	4.04E-12	960.	4.84E-11	2.56E-11	960.	2.31E-11	5.32E-12
1000.	-7.28E-12	3.99E-12	1000.	4.85E-11	2.54E-11	1000.	2.34E-11	5.27E-12

TABLE 9.4.2 IRRADIATION CURRENTS FOR DOUBLE-THICKNESS SPECIMEN IN REVERSED POSITION

FROM LOW-VOLTAGE ELECTRODE			FROM HIGH-VOLTAGE ELECTRODE			FROM GUARD RING		
TIME (SEC)	CURRENT (A)	STD DEV (A)	TIME (SEC)	CURRENT (A)	STD DEV (A)	TIME (SEC)	CURRENT (A)	STD DEV (A)
3.	-1.76E-11	9.30E-12	3.	-1.57E-11	4.56E-11	3.	-1.27E-11	3.91E-12
15.	-2.23E-11	1.15E-11	15.	-1.61E-11	4.64E-11	15.	-1.62E-11	3.81E-12
30.	-2.16E-11	1.21E-11	30.	-8.33E-12	4.11E-11	30.	-1.49E-11	4.44E-12
45.	-2.07E-11	1.27E-11	45.	-3.91E-12	4.07E-11	45.	-1.31E-11	5.02E-12
60.	-1.97E-11	1.31E-11	60.	1.45E-13	4.03E-11	60.	-1.15E-11	5.29E-12
75.	-1.89E-11	1.32E-11	75.	3.40E-12	4.05E-11	75.	-9.97E-12	5.56E-12
90.	-1.83E-11	1.35E-11	90.	6.53E-12	4.02E-11	90.	-8.47E-12	5.60E-12
105.	-1.77E-11	1.36E-11	105.	8.99E-12	4.06E-11	105.	-7.34E-12	5.75E-12
120.	-1.71E-11	1.37E-11	120.	1.15E-11	4.06E-11	120.	-6.23E-12	5.88E-12
150.	-1.61E-11	1.40E-11	150.	1.57E-11	4.04E-11	150.	-4.50E-12	5.98E-12
180.	-1.53E-11	1.42E-11	180.	1.89E-11	4.05E-11	180.	-2.90E-12	5.98E-12
240.	-1.40E-11	1.45E-11	240.	2.40E-11	4.12E-11	240.	-4.73E-13	6.27E-12
300.	-1.32E-11	1.48E-11	300.	2.80E-11	4.19E-11	300.	1.45E-12	6.48E-12
360.	-1.24E-11	1.49E-11	360.	3.07E-11	4.23E-11	360.	3.03E-12	6.64E-12
420.	-1.18E-11	1.51E-11	420.	3.30E-11	4.29E-11	420.	4.16E-12	6.49E-12
480.	-1.12E-11	1.52E-11	480.	3.47E-11	4.33E-11	480.	5.40E-12	6.76E-12
540.	-1.08E-11	1.53E-11	540.	3.62E-11	4.38E-11	540.	6.32E-12	6.87E-12
600.	-1.03E-11	1.53E-11	600.	3.74E-11	4.43E-11	600.	7.11E-12	6.87E-12
660.	-9.94E-12	1.52E-11	660.	3.83E-11	4.44E-11	660.	7.95E-12	6.90E-12
720.	-9.69E-12	1.53E-11	720.	3.91E-11	4.47E-11	720.	8.60E-12	6.95E-12
780.	-9.45E-12	1.53E-11	780.	3.99E-11	4.48E-11	780.	9.11E-12	6.94E-12
840.	-9.13E-12	1.51E-11	840.	4.03E-11	4.49E-11	840.	9.62E-12	6.87E-12
900.	-8.90E-12	1.50E-11	900.	4.07E-11	4.53E-11	900.	1.01E-11	6.90E-12
960.	-8.73E-12	1.50E-11	960.	4.12E-11	4.50E-11	960.	1.06E-11	6.99E-12
1000.	-8.64E-12	1.50E-11	1000.	4.14E-11	4.51E-11	1000.	1.09E-11	6.97E-12

TABLE 9.4.3 POST-IRRADIATION CURRENTS FOR DOUBLE-THICKNESS SPECIMEN IN NORMAL POSITION

FROM LOW-VOLTAGE ELECTRODE			FROM HIGH-VOLTAGE ELECTRODE			FROM GUARD RING		
TIME (SEC)	CURRENT (A)	STD DEV (A)	TIME (SEC)	CURRENT (A)	STD DEV (A)	TIME (SEC)	CURRENT (A)	STD DEV (A)
15.	-2.36E-14	1.38E-13	15.	1.97E-12	2.44E-13	15.	-1.87E-12	6.59E-14
18.	-1.21E-13	1.58E-13	18.	1.76E-12	2.35E-13	18.	-1.84E-12	5.15E-14
21.	-1.92E-13	1.64E-13	21.	1.63E-12	2.32E-13	21.	-1.80E-12	4.11E-14
24.	-2.35E-13	1.64E-13	24.	1.49E-12	2.08E-13	24.	-1.75E-12	4.13E-14
27.	-2.64E-13	1.58E-13	27.	1.38E-12	2.07E-13	27.	-1.70E-12	2.67E-14
30.	-2.84E-13	1.54E-13	30.	1.30E-12	1.90E-13	30.	-1.66E-12	4.29E-14
36.	-3.09E-13	1.47E-13	36.	1.16E-12	1.59E-13	36.	-1.56E-12	5.70E-14
42.	-3.24E-13	1.44E-13	42.	1.07E-12	1.57E-13	42.	-1.47E-12	5.50E-14
48.	-3.26E-13	1.42E-13	48.	9.93E-13	1.53E-13	48.	-1.40E-12	5.09E-14
54.	-3.31E-13	1.36E-13	54.	9.15E-13	1.34E-13	54.	-1.33E-12	5.64E-14
60.	-3.32E-13	1.33E-13	60.	8.54E-13	1.15E-13	60.	-1.26E-12	5.71E-14
66.	-3.28E-13	1.30E-13	66.	8.11E-13	9.58E-14	66.	-1.20E-12	6.62E-14
72.	-3.28E-13	1.26E-13	72.	7.71E-13	8.25E-14	72.	-1.14E-12	5.25E-14
78.	-3.26E-13	1.22E-13	78.	7.38E-13	7.33E-14	78.	-1.11E-12	6.97E-14
84.	-3.26E-13	1.18E-13	84.	7.07E-13	6.96E-14	84.	-1.04E-12	4.70E-14
90.	-3.22E-13	1.13E-13	90.	6.76E-13	7.32E-14	90.	-1.02E-12	5.64E-14
96.	-3.20E-13	1.13E-13	96.	6.51E-13	6.93E-14	96.	-9.84E-13	5.61E-14
102.	-3.18E-13	1.09E-13	102.	6.27E-13	6.57E-14	102.	-9.43E-13	5.50E-14
108.	-3.17E-13	1.04E-13	108.	6.04E-13	6.38E-14	108.	-9.20E-13	5.50E-14
114.	-3.16E-13	1.03E-13	114.	5.79E-13	6.03E-14	114.	-8.93E-13	6.67E-14
120.	-3.15E-13	1.02E-13	120.	5.58E-13	6.43E-14	120.	-8.65E-13	5.76E-14
135.	-3.06E-13	9.38E-14	135.	5.08E-13	5.67E-14	135.	-7.95E-13	5.28E-14
150.	-2.95E-13	9.22E-14	150.	4.68E-13	5.61E-14	150.	-7.45E-13	4.58E-14
165.	-2.90E-13	9.38E-14	165.	4.34E-13	5.15E-14	165.	-6.99E-13	5.33E-14
180.	-2.81E-13	9.22E-14	180.	3.99E-13	4.69E-14	180.	-6.59E-13	5.33E-14
210.	-2.63E-13	7.84E-14	210.	3.44E-13	3.45E-14	210.	-5.84E-13	5.69E-14
240.	-2.49E-13	8.01E-14	240.	3.03E-13	3.06E-14	240.	-5.18E-13	5.00E-14
270.	-2.37E-13	7.27E-14	270.	2.76E-13	2.77E-14	270.	-4.67E-13	5.50E-14
300.	-2.21E-13	7.34E-14	300.	2.52E-13	2.55E-14	300.	-4.21E-13	5.47E-14
330.	-2.14E-13	6.27E-14	330.	2.31E-13	2.24E-14	330.	-3.75E-13	4.95E-14
360.	-2.03E-13	6.14E-14	360.	2.13E-13	2.16E-14	360.	-3.41E-13	5.15E-14
420.	-1.76E-13	5.40E-14	420.	1.84E-13	1.27E-14	420.	-2.84E-13	4.55E-14
480.	-1.66E-13	4.99E-14	480.	1.66E-13	1.04E-14	480.	-2.38E-13	4.29E-14
540.	-1.49E-13	4.51E-14	540.	1.52E-13	1.13E-14	540.	-2.03E-13	3.60E-14
600.	-1.43E-13	3.99E-14	600.	1.40E-13	1.14E-14	600.	-1.72E-13	3.12E-14
660.	-1.25E-13	3.40E-14	660.	1.23E-13	1.14E-14	660.	-1.48E-13	2.62E-14
720.	-1.23E-13	3.44E-14	720.	1.19E-13	1.31E-14	720.	-1.30E-13	3.43E-14
780.	-1.11E-13	4.00E-14	780.	1.10E-13	8.51E-15	780.	-1.10E-13	2.72E-14
840.	-1.03E-13	2.81E-14	840.	9.83E-14	1.07E-14	840.	-9.43E-14	2.56E-14
900.	-9.63E-14	2.79E-14	900.	1.01E-13	9.22E-15	900.	-8.33E-14	2.57E-14
960.	-9.43E-14	2.75E-14	960.	9.33E-14	1.39E-14	960.	-7.68E-14	2.81E-14
1020.	-8.53E-14	2.68E-14	1020.	9.11E-14	1.11E-14	1020.	-6.13E-14	2.50E-14

TABLE 9.4.4 POST-IRRADIATION CURRENTS FOR DOUBLE-THICKNESS SPECIMEN IN REVERSED POSITION

FROM LOW-VOLTAGE ELECTRODE			FROM HIGH-VOLTAGE ELECTRODE			FROM GUARD RING		
TIME (SEC)	CURRENT (A)	STD DEV (A)	TIME (SEC)	CURRENT (A)	STD DEV (A)	TIME (SEC)	CURRENT (A)	STD DEV (A)
15.	-2.37E-13	2.59E-13	15.	2.32E-12	5.48E-13	15.	-1.99E-12	6.53E-14
18.	-2.81E-13	2.21E-13	18.	2.09E-12	5.67E-13	18.	-1.94E-12	5.47E-14
21.	-3.26E-13	2.25E-13	21.	1.93E-12	5.41E-13	21.	-1.89E-12	4.01E-14
24.	-3.63E-13	2.25E-13	24.	1.78E-12	4.80E-13	24.	-1.84E-12	2.62E-14
27.	-3.91E-13	2.23E-13	27.	1.67E-12	4.36E-13	27.	-1.78E-12	2.61E-14
30.	-4.12E-13	2.26E-13	30.	1.57E-12	4.63E-13	30.	-1.72E-12	2.85E-14
36.	-4.33E-13	2.37E-13	36.	1.42E-12	4.44E-13	36.	-1.64E-12	3.49E-14
42.	-4.50E-13	2.38E-13	42.	1.31E-12	4.14E-13	42.	-1.55E-12	3.44E-14
48.	-4.51E-13	2.32E-13	48.	1.21E-12	3.81E-13	48.	-1.49E-12	1.50E-14
54.	-4.52E-13	2.30E-13	54.	1.13E-12	3.51E-13	54.	-1.41E-12	5.69E-15
60.	-4.44E-13	2.26E-13	60.	1.06E-12	3.30E-13	60.	-1.36E-12	2.89E-14
66.	-4.43E-13	2.19E-13	66.	1.00E-12	3.19E-13	66.	-1.29E-12	1.00E-14
72.	-4.35E-13	2.20E-13	72.	9.55E-13	3.05E-13	72.	-1.25E-12	5.99E-15
78.	-4.27E-13	2.11E-13	78.	9.02E-13	2.93E-13	78.	-1.20E-12	9.99E-15
84.	-4.23E-13	2.03E-13	84.	8.67E-13	2.80E-13	84.	-1.15E-12	1.51E-14
90.	-4.18E-13	1.98E-13	90.	8.19E-13	2.74E-13	90.	-1.11E-12	1.02E-14
96.	-4.13E-13	1.99E-13	96.	7.72E-13	2.45E-13	96.	-1.08E-12	2.51E-14
102.	-4.08E-13	1.90E-13	102.	7.35E-13	2.31E-13	102.	-1.06E-12	2.52E-14
108.	-3.99E-13	1.85E-13	108.	7.04E-13	2.25E-13	108.	-1.03E-12	2.51E-14
114.	-3.93E-13	1.87E-13	114.	6.79E-13	2.11E-13	114.	-9.64E-13	1.90E-14
120.	-3.88E-13	1.87E-13	120.	6.55E-13	1.96E-13	120.	-9.31E-13	1.82E-14
135.	-3.74E-13	1.84E-13	135.	6.01E-13	1.87E-13	135.	-8.64E-13	2.04E-14
150.	-3.63E-13	1.78E-13	150.	5.59E-13	1.59E-13	150.	-8.17E-13	2.10E-14
165.	-3.48E-13	1.69E-13	165.	5.09E-13	1.58E-13	165.	-7.75E-13	2.19E-14
180.	-3.44E-13	1.70E-13	180.	4.82E-13	1.40E-13	180.	-7.34E-13	2.04E-14
210.	-3.17E-13	1.42E-13	210.	4.26E-13	1.22E-13	210.	-6.52E-13	2.94E-14
240.	-3.01E-13	1.36E-13	240.	3.67E-13	1.02E-13	240.	-5.89E-13	3.19E-14
270.	-2.77E-13	1.19E-13	270.	3.24E-13	1.01E-13	270.	-5.29E-13	3.34E-14
300.	-2.62E-13	1.12E-13	300.	2.90E-13	7.83E-14	300.	-4.78E-13	2.90E-14
330.	-2.43E-13	1.05E-13	330.	2.59E-13	6.99E-14	330.	-4.35E-13	3.02E-14
360.	-2.27E-13	9.91E-14	360.	2.28E-13	6.59E-14	360.	-3.89E-13	3.34E-14
420.	-1.98E-13	8.58E-14	420.	1.80E-13	4.37E-14	420.	-3.20E-13	2.59E-14
480.	-1.74E-13	7.46E-14	480.	1.62E-13	3.06E-14	480.	-2.67E-13	2.89E-14
540.	-1.55E-13	5.93E-14	540.	1.39E-13	2.61E-14	540.	-2.26E-13	2.73E-14
600.	-1.43E-13	5.12E-14	600.	1.17E-13	2.24E-14	600.	-1.87E-13	2.86E-14
660.	-1.25E-13	4.41E-14	660.	1.03E-13	3.16E-14	660.	-1.55E-13	2.74E-14
720.	-1.12E-13	4.58E-14	720.	9.30E-14	2.53E-14	720.	-1.32E-13	2.90E-14
780.	-1.12E-13	3.13E-14	780.	7.64E-14	2.12E-14	780.	-1.10E-13	2.63E-14
840.	-9.71E-14	3.36E-14	840.	7.24E-14	2.36E-14	840.	-9.47E-14	2.14E-14
900.	-9.51E-14	2.16E-14	900.	6.75E-14	2.41E-14	900.	-8.21E-14	2.17E-14
960.	-8.72E-14	2.06E-14	960.	5.98E-14	2.00E-14	960.	-6.00E-14	2.23E-14
1020.	-7.28E-14	2.06E-14	1020.	6.08E-14	2.10E-14	1020.	-4.80E-14	2.62E-14

TABLE 9.4.5 IRRADIATION CURRENTS FOR SINGLE-THICKNESS SPECIMEN IN NORMAL POSITION

FROM LOW-VOLTAGE ELECTRODE			FROM HIGH-VOLTAGE ELECTRODE			FROM GUARD RING		
TIME (SEC)	CURRENT (A)	STD DEV (A)	TIME (SEC)	CURRENT (A)	STD DEV (A)	TIME (SEC)	CURRENT (A)	STD DEV (A)
3.	-1.21E-11	4.70E-12	3.	-7.40E-11	2.26E-11	3.	6.77E-11	1.28E-11
15.	-1.51E-11	5.47E-12	15.	-7.20E-11	1.62E-11	15.	6.55E-11	1.46E-11
30.	-1.54E-11	5.69E-12	30.	-6.87E-11	1.23E-11	30.	6.55E-11	1.49E-11
45.	-1.51E-11	5.40E-12	45.	-6.57E-11	1.02E-11	45.	6.62E-11	1.55E-11
60.	-1.47E-11	5.90E-12	60.	-6.32E-11	8.10E-12	60.	6.69E-11	1.57E-11
75.	-1.44E-11	5.79E-12	75.	-6.10E-11	6.33E-12	75.	6.75E-11	1.58E-11
90.	-1.40E-11	5.79E-12	90.	-5.92E-11	5.27E-12	90.	6.82E-11	1.60E-11
105.	-1.36E-11	5.69E-12	105.	-5.72E-11	3.86E-12	105.	6.89E-11	1.61E-11
120.	-1.33E-11	5.55E-12	120.	-5.57E-11	3.15E-12	120.	6.96E-11	1.63E-11
150.	-1.27E-11	5.37E-12	150.	-5.35E-11	2.09E-12	150.	7.07E-11	1.64E-11
180.	-1.20E-11	5.19E-12	180.	-5.15E-11	6.30E-13	180.	7.17E-11	1.64E-11
240.	-1.10E-11	4.91E-12	240.	-4.76E-11	9.44E-13	240.	7.34E-11	1.65E-11
300.	-1.02E-11	4.66E-12	300.	-4.48E-11	1.79E-12	300.	7.49E-11	1.65E-11
360.	-9.39E-12	4.39E-12	360.	-4.27E-11	2.57E-12	360.	7.61E-11	1.66E-11
420.	-8.76E-12	4.26E-12	420.	-4.07E-11	3.20E-12	420.	7.71E-11	1.66E-11
480.	-8.17E-12	4.09E-12	480.	-3.91E-11	3.77E-12	480.	7.79E-11	1.65E-11
540.	-7.62E-12	3.86E-12	540.	-3.77E-11	4.12E-12	540.	7.88E-11	1.63E-11
600.	-7.22E-12	3.73E-12	600.	-3.64E-11	4.33E-12	600.	7.94E-11	1.60E-11
660.	-6.86E-12	3.63E-12	660.	-3.52E-11	4.61E-12	660.	8.01E-11	1.57E-11
720.	-6.58E-12	3.69E-12	720.	-3.44E-11	4.90E-12	720.	8.08E-11	1.54E-11
780.	-6.24E-12	3.51E-12	780.	-3.35E-11	4.97E-12	780.	8.13E-11	1.54E-11
840.	-5.99E-12	3.46E-12	840.	-3.25E-11	5.04E-12	840.	8.20E-11	1.51E-11
900.	-5.70E-12	3.36E-12	900.	-3.17E-11	5.32E-12	900.	8.23E-11	1.49E-11
960.	-5.46E-12	3.23E-12	960.	-3.12E-11	5.39E-12	960.	8.30E-11	1.47E-11
1000.	-5.34E-12	3.23E-12	1000.	-3.07E-11	5.46E-12	1000.	8.31E-11	1.48E-11

TABLE 9.4.6 IRRADIATION CURRENTS FOR SINGLE-THICKNESS SPECIMEN IN REVERSED POSITION

FROM LOW-VOLTAGE ELECTRODE			FROM HIGH-VOLTAGE ELECTRODE			FROM GUARD RING		
TIME (SEC)	CURRENT (A)	STD DEV (A)	TIME (SEC)	CURRENT (A)	STD DEV (A)	TIME (SEC)	CURRENT (A)	STD DEV (A)
3.	-7.94E-12	7.02E-12	3.	-5.40E-11	0.0	3.	9.34E-11	1.11E-11
15.	-1.04E-11	3.55E-12	15.	-5.80E-11	0.0	15.	9.03E-11	9.43E-12
30.	-1.03E-11	3.30E-12	30.	-5.70E-11	0.0	30.	9.02E-11	9.49E-12
45.	-9.97E-12	3.14E-12	45.	-5.60E-11	0.0	45.	9.05E-11	9.21E-12
60.	-9.60E-12	3.01E-12	60.	-5.50E-11	0.0	60.	9.08E-11	8.94E-12
75.	-9.25E-12	2.89E-12	75.	-5.45E-11	0.0	75.	9.12E-11	8.67E-12
90.	-8.87E-12	2.80E-12	90.	-5.35E-11	0.0	90.	9.20E-11	8.72E-12
105.	-8.53E-12	2.65E-12	105.	-5.25E-11	0.0	105.	9.27E-11	9.00E-12
120.	-8.18E-12	2.54E-12	120.	-5.15E-11	0.0	120.	9.30E-11	8.72E-12
150.	-7.65E-12	2.40E-12	150.	-5.00E-11	0.0	150.	9.44E-11	9.27E-12
180.	-7.03E-12	2.03E-12	180.	-4.35E-11	0.0	180.	9.52E-11	9.34E-12
240.	-6.20E-12	1.79E-12	240.	-4.59E-11	0.0	240.	9.62E-11	8.37E-12
300.	-5.43E-12	1.49E-12	300.	-4.35E-11	0.0	300.	9.72E-11	8.37E-12
360.	-4.82E-12	1.36E-12	360.	-4.15E-11	0.0	360.	9.82E-11	8.37E-12
420.	-4.22E-12	1.25E-12	420.	-3.98E-11	0.0	420.	9.89E-11	8.65E-12
480.	-3.72E-12	1.23E-12	480.	-3.83E-11	0.0	480.	9.96E-11	8.93E-12
540.	-3.29E-12	1.24E-12	540.	-3.69E-11	0.0	540.	1.00E-10	9.02E-12
600.	-2.91E-12	1.25E-12	600.	-3.57E-11	0.0	600.	1.01E-10	8.74E-12
660.	-2.56E-12	1.29E-12	660.	-3.46E-11	0.0	660.	1.01E-10	8.55E-12
720.	-2.26E-12	1.30E-12	720.	-3.37E-11	0.0	720.	1.01E-10	8.26E-12
780.	-1.98E-12	1.32E-12	780.	-3.28E-11	0.0	780.	1.02E-10	8.65E-12
840.	-1.71E-12	1.35E-12	840.	-3.20E-11	0.0	840.	1.02E-10	8.94E-12
900.	-1.47E-12	1.34E-12	900.	-3.14E-11	0.0	900.	1.03E-10	8.76E-12
960.	-1.25E-12	1.33E-12	960.	-3.07E-11	0.0	960.	1.03E-10	8.47E-12
1000.	-1.11E-12	1.33E-12	1000.	-3.04E-11	0.0	1000.	1.03E-10	8.30E-12

TABLE 9.4.7 POST-IRRADIATION CURRENTS FOR SINGLE-THICKNESS SPECIMEN IN NORMAL POSITION

FROM LOW-VOLTAGE ELECTRODE			FROM HIGH-VOLTAGE ELECTRODE			FROM GUARD RING		
TIME (SEC)	CURRENT (A)	STD DEV (A)	TIME (SEC)	CURRENT (A)	STD DEV (A)	TIME (SEC)	CURRENT (A)	STD DEV (A)
15.	1.30E-12	4.77E-13	15.	6.80E-13	5.69E-14	15.	1.51E-13	1.33E-13
18.	1.16E-12	4.05E-13	18.	5.35E-13	4.92E-14	18.	1.14E-13	1.19E-13
21.	1.06E-12	3.63E-13	21.	4.72E-13	8.10E-14	21.	8.21E-14	1.02E-13
24.	9.89E-13	3.23E-13	24.	4.20E-13	8.46E-14	24.	5.70E-14	8.80E-14
27.	9.43E-13	2.96E-13	27.	3.80E-13	8.46E-14	27.	3.85E-14	9.06E-14
30.	8.96E-13	2.71E-13	30.	3.45E-13	7.70E-14	30.	3.08E-14	8.17E-14
36.	7.86E-13	2.32E-13	36.	2.95E-13	7.12E-14	36.	2.01E-14	7.54E-14
42.	7.25E-13	2.04E-13	42.	2.57E-13	6.70E-14	42.	8.37E-15	6.94E-14
48.	6.76E-13	1.86E-13	48.	2.26E-13	6.21E-14	48.	2.00E-15	6.26E-14
54.	6.43E-13	1.73E-13	54.	2.08E-13	6.07E-14	54.	-5.03E-15	5.89E-14
60.	6.10E-13	1.60E-13	60.	1.90E-13	5.57E-14	60.	-9.06E-15	5.44E-14
66.	5.81E-13	1.43E-13	66.	1.74E-13	5.09E-14	66.	-1.64E-14	4.51E-14
72.	5.56E-13	1.35E-13	72.	1.60E-13	5.01E-14	72.	-2.15E-14	4.11E-14
78.	5.33E-13	1.26E-13	78.	1.49E-13	4.59E-14	78.	-2.65E-14	3.82E-14
84.	5.11E-13	1.15E-13	84.	1.43E-13	4.45E-14	84.	-2.68E-14	4.03E-14
90.	4.89E-13	1.11E-13	90.	1.35E-13	3.83E-14	90.	-3.02E-14	3.47E-14
96.	4.68E-13	9.79E-14	96.	1.31E-13	3.81E-14	96.	-3.59E-14	2.62E-14
102.	4.51E-13	8.79E-14	102.	1.29E-13	3.61E-14	102.	-3.62E-14	2.57E-14
108.	4.36E-13	8.16E-14	108.	1.25E-13	2.75E-14	108.	-3.69E-14	2.07E-14
114.	4.26E-13	7.06E-14	114.	1.21E-13	2.26E-14	114.	-3.92E-14	1.78E-14
120.	4.10E-13	7.30E-14	120.	1.17E-13	1.76E-14	120.	-4.32E-14	1.46E-14
135.	3.80E-13	5.54E-14	135.	1.05E-13	8.43E-15	135.	-4.63E-14	1.43E-14
150.	3.48E-13	5.38E-14	150.	1.01E-13	4.90E-15	150.	-4.96E-14	1.45E-14
165.	3.26E-13	4.38E-14	165.	9.85E-14	4.90E-15	165.	-4.63E-14	8.25E-15
180.	3.12E-13	3.07E-14	180.	9.25E-14	6.31E-15	180.	-4.96E-14	8.80E-15
210.	2.75E-13	1.93E-14	210.	8.35E-14	9.23E-15	210.	-5.06E-14	9.65E-15
240.	2.53E-13	8.33E-15	240.	8.00E-14	7.11E-15	240.	-4.96E-14	5.15E-15
270.	2.31E-13	1.37E-14	270.	8.25E-14	2.48E-14	270.	-4.49E-14	8.54E-15
300.	2.06E-13	1.27E-14	300.	8.55E-14	2.20E-14	300.	-3.82E-14	6.12E-15
330.	1.92E-13	1.20E-14	330.	8.85E-14	2.90E-14	330.	-3.12E-14	6.59E-15
360.	1.82E-13	1.44E-14	360.	8.15E-14	3.33E-14	360.	-2.71E-14	5.23E-15
420.	1.51E-13	1.51E-14	420.	8.70E-14	3.82E-14	420.	-2.41E-14	1.32E-14
480.	1.44E-13	2.92E-14	480.	8.40E-14	3.66E-14	480.	-2.35E-14	1.57E-14
540.	1.18E-13	1.60E-14	540.	9.05E-14	4.13E-14	540.	-2.01E-14	1.81E-14
600.	1.15E-13	2.59E-14	600.	9.65E-14	4.32E-14	600.	-1.44E-14	1.44E-14
660.	1.03E-13	2.33E-14	660.	9.80E-14	4.53E-14	660.	-8.71E-15	1.10E-14
720.	9.39E-14	2.15E-14	720.	9.45E-14	5.31E-14	720.	-8.04E-15	1.06E-14
780.	8.59E-14	2.42E-14	780.	9.30E-14	4.67E-14	780.	-5.36E-15	1.41E-14
840.	7.96E-14	2.41E-14	840.	8.90E-14	5.09E-14	840.	-3.01E-15	1.44E-14
900.	7.43E-14	2.55E-14	900.	9.35E-14	4.03E-14	900.	3.38E-16	1.35E-14
960.	7.29E-14	2.83E-14	960.	9.00E-14	4.25E-14	960.	3.37E-16	1.20E-14
1020.	6.49E-14	2.64E-14	1020.	9.10E-14	4.39E-14	1020.	2.69E-15	1.31E-14

TABLE 9.4.8 POST-IRRADIATION CURRENTS FOR SINGLE-THICKNESS SPECIMEN IN REVERSED POSITION

FROM LOW-VOLTAGE ELECTRODE			FROM HIGH-VOLTAGE ELECTRODE			FROM GUARD RING		
TIME (SEC)	CURRENT (A)	STD DEV (A)	TIME (SEC)	CURRENT (A)	STD DEV (A)	TIME (SEC)	CURRENT (A)	STD DEV (A)
15.	1.33E-12	3.52E-13	15.	1.09E-12	0.0	15.	1.11E-13	9.05E-14
18.	1.21E-12	3.16E-13	18.	9.10E-13	0.0	18.	7.58E-14	4.30E-14
21.	1.12E-12	2.81E-13	21.	7.80E-13	0.0	21.	5.83E-14	4.42E-14
24.	1.05E-12	2.51E-13	24.	6.95E-13	0.0	24.	4.96E-14	4.12E-14
27.	9.92E-13	2.23E-13	27.	6.20E-13	0.0	27.	4.76E-14	3.77E-14
30.	9.42E-13	1.98E-13	30.	5.70E-13	0.0	30.	4.16E-14	3.69E-14
36.	8.60E-13	1.63E-13	36.	4.90E-13	0.0	36.	3.62E-14	3.75E-14
42.	8.03E-13	1.56E-13	42.	4.40E-13	0.0	42.	2.88E-14	3.62E-14
48.	7.57E-13	1.41E-13	48.	3.92E-13	0.0	48.	2.21E-14	3.22E-14
54.	7.17E-13	1.31E-13	54.	3.59E-13	0.0	54.	1.98E-14	3.24E-14
60.	6.80E-13	1.26E-13	60.	3.32E-13	0.0	60.	1.61E-14	2.94E-14
66.	6.50E-13	1.16E-13	66.	3.05E-13	0.0	66.	9.38E-15	2.39E-14
72.	6.18E-13	1.08E-13	72.	2.89E-13	0.0	72.	1.67E-15	2.67E-14
78.	5.93E-13	1.03E-13	78.	2.66E-13	0.0	78.	-3.38E-16	2.35E-14
84.	5.73E-13	9.21E-14	84.	2.55E-13	0.0	84.	-1.69E-15	2.12E-14
90.	5.45E-13	8.71E-14	90.	2.41E-13	0.0	90.	-3.69E-15	2.11E-14
96.	5.22E-13	7.81E-14	96.	2.33E-13	0.0	95.	-5.70E-15	1.73E-14
102.	5.05E-13	7.85E-14	102.	2.20E-13	0.0	102.	-8.03E-15	1.67E-14
108.	4.88E-13	7.50E-14	108.	2.10E-13	0.0	108.	-1.04E-14	1.95E-14
114.	4.66E-13	7.94E-14	114.	1.94E-13	0.0	114.	-1.31E-14	2.05E-14
120.	4.52E-13	7.51E-14	120.	1.80E-13	0.0	120.	-1.61E-14	1.94E-14
135.	4.16E-13	6.60E-14	135.	1.81E-13	0.0	135.	-1.27E-14	1.73E-14
150.	3.92E-13	5.65E-14	150.	1.64E-13	0.0	150.	-1.27E-14	2.13E-14
165.	3.63E-13	4.94E-14	165.	1.55E-13	0.0	165.	-1.31E-14	2.50E-14
180.	3.37E-13	3.92E-14	180.	1.40E-13	0.0	180.	-1.91E-14	2.06E-14
210.	2.98E-13	2.27E-14	210.	1.27E-13	0.0	210.	-1.71E-14	2.00E-14
240.	2.69E-13	1.87E-14	240.	1.31E-13	0.0	240.	-1.31E-14	1.40E-14
270.	2.50E-13	1.76E-14	270.	1.21E-13	0.0	270.	-1.54E-14	1.95E-14
300.	2.26E-13	1.41E-14	300.	1.22E-13	0.0	300.	-7.04E-15	1.57E-14
330.	2.05E-13	8.66E-15	330.	1.11E-13	0.0	330.	-3.35E-15	1.14E-14
360.	1.91E-13	8.58E-15	360.	1.20E-13	0.0	360.	-1.01E-15	8.59E-15
420.	1.69E-13	1.05E-14	420.	1.13E-13	0.0	420.	1.14E-14	1.37E-14
480.	1.48E-13	7.82E-15	480.	1.10E-13	0.0	480.	1.44E-14	1.44E-14
540.	1.29E-13	1.43E-14	540.	1.15E-13	0.0	540.	1.68E-14	1.37E-14
600.	1.19E-13	1.08E-14	600.	1.12E-13	0.0	600.	1.44E-14	1.22E-14
660.	1.10E-13	1.51E-14	660.	1.04E-13	0.0	660.	1.94E-14	1.09E-14
720.	9.57E-14	1.71E-14	720.	1.03E-13	0.0	720.	2.28E-14	1.21E-14
780.	9.53E-14	2.91E-14	780.	1.03E-13	0.0	780.	2.51E-14	1.31E-14
840.	8.73E-14	2.00E-14	840.	1.00E-13	0.0	840.	2.31E-14	6.59E-15
900.	7.77E-14	1.94E-14	900.	1.00E-13	0.0	900.	2.95E-14	1.11E-14
960.	7.37E-14	1.51E-14	960.	1.03E-13	0.0	960.	2.55E-14	5.72E-15
1020.	6.57E-14	2.13E-14	1020.	1.05E-13	0.0	1020.	2.88E-14	8.13E-15

Appendix 9.5

Averaged Current Data at ±500V

TABLE 9.5.1 IRRADIATION CURRENTS FOR DOUBLE-THICKNESS SPECIMEN AT ±500 V

+500 V			-500 V		
TIME (SEC)	CURRENT (A)	STD DEV (A)	TIME (SEC)	CURRENT (A)	STD DEV (A)
3.	1.49E-10	1.23E-10	3.	-7.51E-11	2.84E-11
15.	1.44E-10	1.15E-10	15.	-7.81E-11	2.73E-11
30.	1.44E-10	1.11E-10	30.	-8.01E-11	2.71E-11
45.	1.46E-10	1.10E-10	45.	-8.08E-11	2.73E-11
60.	1.49E-10	1.10E-10	60.	-8.06E-11	2.74E-11
75.	1.50E-10	1.09E-10	75.	-8.03E-11	2.77E-11
90.	1.53E-10	1.10E-10	90.	-7.99E-11	2.80E-11
105.	1.54E-10	1.11E-10	105.	-7.92E-11	2.77E-11
120.	1.55E-10	1.10E-10	120.	-7.84E-11	2.75E-11
150.	1.58E-10	1.11E-10	150.	-7.74E-11	2.76E-11
180.	1.60E-10	1.11E-10	180.	-7.60E-11	2.79E-11
240.	1.62E-10	1.12E-10	240.	-7.40E-11	2.80E-11
300.	1.64E-10	1.13E-10	300.	-7.18E-11	2.73E-11
360.	1.67E-10	1.14E-10	360.	-6.94E-11	2.60E-11
420.	1.68E-10	1.14E-10	420.	-6.80E-11	2.55E-11
480.	1.68E-10	1.13E-10	480.	-6.68E-11	2.53E-11
540.	1.68E-10	1.13E-10	540.	-6.59E-11	2.49E-11
600.	1.70E-10	1.14E-10	600.	-6.48E-11	2.46E-11
660.	1.71E-10	1.14E-10	660.	-6.41E-11	2.45E-11
720.	1.71E-10	1.14E-10	720.	-6.35E-11	2.42E-11
780.	1.72E-10	1.14E-10	780.	-6.29E-11	2.39E-11
840.	1.72E-10	1.14E-10	840.	-6.25E-11	2.40E-11
900.	1.72E-10	1.14E-10	900.	-6.21E-11	2.35E-11
960.	1.73E-10	1.14E-10	960.	-6.14E-11	2.32E-11
1000.	1.73E-10	1.14E-10	1000.	-6.11E-11	2.31E-11

TABLE 9.5.2 POST-IRRADIATION CURRENTS FOR DOUBLE-THICKNESS SPECIMEN AT ±500 V

+500 V			-500 V		
TIME (SEC)	CURRENT (A)	STD DEV (A)	TIME (SEC)	CURRENT (A)	STD DEV (A)
15.	5.20E-12	2.88E-12	15.	-6.35E-12	3.08E-12
18.	4.96E-12	2.73E-12	18.	-6.12E-12	2.76E-12
21.	4.79E-12	2.62E-12	21.	-6.03E-12	2.66E-12
24.	4.64E-12	2.53E-12	24.	-5.95E-12	2.56E-12
27.	4.52E-12	2.42E-12	27.	-5.83E-12	2.45E-12
30.	4.40E-12	2.36E-12	30.	-5.76E-12	2.39E-12
36.	4.20E-12	2.22E-12	36.	-5.59E-12	2.23E-12
42.	4.03E-12	2.11E-12	42.	-5.45E-12	2.13E-12
48.	3.90E-12	2.05E-12	48.	-5.30E-12	2.01E-12
54.	3.77E-12	1.95E-12	54.	-5.19E-12	1.93E-12
60.	3.66E-12	1.87E-12	60.	-5.08E-12	1.85E-12
66.	3.57E-12	1.82E-12	66.	-4.98E-12	1.77E-12
72.	3.49E-12	1.76E-12	72.	-4.87E-12	1.69E-12
78.	3.40E-12	1.71E-12	78.	-4.80E-12	1.66E-12
84.	3.32E-12	1.65E-12	84.	-4.70E-12	1.57E-12
90.	3.26E-12	1.61E-12	90.	-4.62E-12	1.52E-12
96.	3.19E-12	1.55E-12	96.	-4.56E-12	1.48E-12
102.	3.14E-12	1.55E-12	102.	-4.48E-12	1.43E-12
108.	3.08E-12	1.51E-12	108.	-4.42E-12	1.39E-12
114.	3.03E-12	1.46E-12	114.	-4.35E-12	1.36E-12
120.	2.98E-12	1.43E-12	120.	-4.29E-12	1.32E-12
135.	2.87E-12	1.36E-12	135.	-4.15E-12	1.23E-12
150.	2.77E-12	1.29E-12	150.	-4.01E-12	1.13E-12
165.	2.67E-12	1.21E-12	165.	-3.89E-12	1.07E-12
180.	2.62E-12	1.16E-12	180.	-3.77E-12	9.95E-13
210.	2.47E-12	1.04E-12	210.	-3.58E-12	9.06E-13
240.	2.36E-12	9.58E-13	240.	-3.40E-12	8.15E-13
270.	2.25E-12	8.70E-13	270.	-3.25E-12	7.40E-13
300.	2.18E-12	8.18E-13	300.	-3.11E-12	6.82E-13
330.	2.11E-12	7.74E-13	330.	-2.98E-12	6.23E-13
360.	2.04E-12	7.24E-13	360.	-2.87E-12	5.74E-13
420.	1.92E-12	6.11E-13	420.	-2.68E-12	5.02E-13
480.	1.83E-12	5.57E-13	480.	-2.52E-12	4.30E-13
540.	1.74E-12	4.69E-13	540.	-2.36E-12	4.04E-13
600.	1.66E-12	4.37E-13	600.	-2.23E-12	3.73E-13
660.	1.60E-12	3.71E-13	660.	-2.14E-12	3.34E-13
720.	1.54E-12	3.31E-13	720.	-2.02E-12	3.09E-13
780.	1.49E-12	3.22E-13	780.	-1.94E-12	2.93E-13
840.	1.41E-12	2.75E-13	840.	-1.86E-12	2.54E-13
900.	1.38E-12	2.73E-13	900.	-1.78E-12	2.55E-13
960.	1.34E-12	2.38E-13	960.	-1.72E-12	2.30E-13
1020.	1.31E-12	2.53E-13	1020.	-1.64E-12	2.16E-13

TABLE 9.5.3 IRRADIATION CURRENTS FOR SINGLE-THICKNESS SPECIMEN AT ±500 V

+500 V			-500 V		
TIME (SEC)	CURRENT (A)	STD DEV (A)	TIME (SEC)	CURRENT (A)	STD DEV (A)
3.	2.40E-10	4.14E-11	3.	-5.94E-11	1.93E-11
15.	2.23E-10	4.06E-11	15.	-5.39E-11	1.84E-11
30.	2.25E-10	4.17E-11	30.	-5.68E-11	1.79E-11
45.	2.27E-10	4.27E-11	45.	-5.81E-11	1.82E-11
60.	2.29E-10	4.30E-11	60.	-5.90E-11	1.85E-11
75.	2.30E-10	4.30E-11	75.	-5.94E-11	1.87E-11
90.	2.30E-10	4.27E-11	90.	-5.97E-11	1.90E-11
105.	2.32E-10	4.27E-11	105.	-6.00E-11	1.94E-11
120.	2.33E-10	4.27E-11	120.	-6.00E-11	1.95E-11
150.	2.34E-10	4.36E-11	150.	-5.98E-11	1.98E-11
180.	2.34E-10	4.36E-11	180.	-5.96E-11	2.00E-11
240.	2.34E-10	4.43E-11	240.	-5.89E-11	2.07E-11
300.	2.36E-10	4.42E-11	300.	-5.84E-11	2.11E-11
360.	2.37E-10	4.40E-11	360.	-5.80E-11	2.13E-11
420.	2.38E-10	4.31E-11	420.	-5.75E-11	2.13E-11
480.	2.38E-10	4.34E-11	480.	-5.69E-11	2.11E-11
540.	2.38E-10	4.34E-11	540.	-5.68E-11	2.12E-11
600.	2.39E-10	4.40E-11	600.	-5.65E-11	2.12E-11
660.	2.39E-10	4.34E-11	660.	-5.60E-11	2.11E-11
720.	2.39E-10	4.34E-11	720.	-5.60E-11	2.12E-11
780.	2.40E-10	4.28E-11	780.	-5.58E-11	2.12E-11
840.	2.40E-10	4.31E-11	840.	-5.55E-11	2.11E-11
900.	2.41E-10	4.28E-11	900.	-5.55E-11	2.12E-11
960.	2.41E-10	4.28E-11	960.	-5.55E-11	2.12E-11
1000.	2.41E-10	4.31E-11	1000.	-5.53E-11	2.11E-11

TABLE 9.5.4 POST-IRRADIATION CURRENTS FOR SINGLE-THICKNESS SPECIMEN AT ±500 V

+500 V			-500 V		
TIME (SEC)	CURRENT (A)	STD DEV (A)	TIME (SEC)	CURRENT (A)	STD DEV (A)
15.	1.17E-11	4.49E-13	15.	-1.30E-11	1.21E-12
18.	1.15E-11	4.52E-13	18.	-1.29E-11	1.26E-12
21.	1.12E-11	4.23E-13	21.	-1.26E-11	1.24E-12
24.	1.10E-11	3.67E-13	24.	-1.24E-11	1.11E-12
27.	1.08E-11	3.71E-13	27.	-1.23E-11	1.06E-12
30.	1.06E-11	4.06E-13	30.	-1.21E-11	1.05E-12
36.	1.03E-11	3.35E-13	36.	-1.18E-11	1.00E-12
42.	1.01E-11	2.79E-13	42.	-1.15E-11	1.11E-12
48.	9.86E-12	2.82E-13	48.	-1.13E-11	9.93E-13
54.	9.72E-12	3.14E-13	54.	-1.10E-11	9.46E-13
60.	9.50E-12	2.48E-13	60.	-1.09E-11	7.41E-13
66.	9.36E-12	2.79E-13	66.	-1.07E-11	7.44E-13
72.	9.19E-12	2.53E-13	72.	-1.05E-11	7.69E-13
78.	9.06E-12	2.65E-13	78.	-1.03E-11	7.66E-13
84.	8.93E-12	2.56E-13	84.	-1.01E-11	7.08E-13
90.	8.79E-12	2.39E-13	90.	-9.97E-12	6.88E-13
96.	8.65E-12	2.32E-13	96.	-9.85E-12	7.15E-13
102.	8.53E-12	2.04E-13	102.	-9.75E-12	7.13E-13
108.	8.43E-12	2.06E-13	108.	-9.66E-12	7.34E-13
114.	8.32E-12	2.07E-13	114.	-9.54E-12	7.79E-13
120.	8.22E-12	2.09E-13	120.	-9.42E-12	7.73E-13
135.	7.98E-12	1.56E-13	135.	-9.11E-12	7.69E-13
150.	7.74E-12	1.57E-13	150.	-8.87E-12	7.69E-13
165.	7.55E-12	1.35E-13	165.	-8.61E-12	7.35E-13
180.	7.34E-12	1.38E-13	180.	-8.38E-12	7.08E-13
210.	6.99E-12	9.03E-14	210.	-7.95E-12	6.78E-13
240.	6.68E-12	9.41E-14	240.	-7.59E-12	6.73E-13
270.	6.44E-12	1.03E-13	270.	-7.21E-12	5.93E-13
300.	6.17E-12	8.93E-14	300.	-6.95E-12	6.10E-13
330.	5.96E-12	9.07E-14	330.	-6.62E-12	5.81E-13
360.	5.79E-12	8.15E-14	360.	-6.40E-12	5.54E-13
420.	5.41E-12	7.98E-14	420.	-5.95E-12	5.20E-13
480.	5.09E-12	8.24E-14	480.	-5.53E-12	4.63E-13
540.	4.82E-12	8.05E-14	540.	-5.19E-12	4.83E-13
600.	4.58E-12	6.29E-14	600.	-4.90E-12	4.07E-13
660.	4.36E-12	8.52E-14	660.	-4.64E-12	3.94E-13
720.	4.14E-12	8.10E-14	720.	-4.40E-12	3.54E-13
780.	3.99E-12	1.06E-13	780.	-4.20E-12	3.50E-13
840.	3.82E-12	1.08E-13	840.	-4.01E-12	3.32E-13
900.	3.67E-12	1.01E-13	900.	-3.83E-12	3.38E-13
960.	3.55E-12	1.00E-13	960.	-3.68E-12	3.11E-13
1020.	3.42E-12	1.20E-13	1020.	-3.52E-12	3.11E-13

Appendix 9.6

Current Generator Strengths

TABLE 9.6.1 IRRADIATION CURRENTS FOR DOUBLE-THICKNESS SPECIMEN IN NORMAL POSITION

L.V. TO H.V. ELECTRODE			GUARD RING TO H.V. ELECTRODE			COAXIAL CABLE		
TIME (SEC)	CURRENT (A)	STD DEV (A)	TIME (SEC)	CURRENT (A)	STD DEV (A)	TIME (SEC)	CURRENT (A)	STD DEV (A)
3.	1.34E-11	1.14E-11	3.	-1.59E-11	1.23E-11	3.	-1.12E-11	1.12E-11
15.	1.33E-11	1.13E-11	15.	-1.17E-11	1.17E-11	15.	-1.22E-11	1.11E-11
30.	1.47E-11	1.14E-11	30.	-9.73E-12	1.16E-11	30.	-8.96E-12	1.11E-11
45.	1.59E-11	1.14E-11	45.	-8.43E-12	1.16E-11	45.	-6.34E-12	1.12E-11
60.	1.69E-11	1.14E-11	60.	-7.41E-12	1.16E-11	60.	-4.03E-12	1.12E-11
75.	1.78E-11	1.14E-11	75.	-6.60E-12	1.15E-11	75.	-2.14E-12	1.11E-11
90.	1.85E-11	1.13E-11	90.	-5.86E-12	1.14E-11	90.	-4.20E-13	1.10E-11
105.	1.91E-11	1.13E-11	105.	-5.27E-12	1.14E-11	105.	1.04E-12	1.10E-11
120.	1.97E-11	1.12E-11	120.	-4.62E-12	1.13E-11	120.	2.46E-12	1.08E-11
150.	2.07E-11	1.10E-11	150.	-3.87E-12	1.11E-11	150.	4.64E-12	1.07E-11
180.	2.16E-11	1.09E-11	180.	-3.20E-12	1.11E-11	180.	6.50E-12	1.06E-11
240.	2.28E-11	1.06E-11	240.	-2.30E-12	1.09E-11	240.	9.40E-12	1.03E-11
300.	2.39E-11	1.04E-11	300.	-1.77E-12	1.06E-11	300.	1.17E-11	1.00E-11
360.	2.47E-11	1.02E-11	360.	-1.30E-12	1.05E-11	360.	1.35E-11	9.88E-12
420.	2.55E-11	1.01E-11	420.	-1.13E-12	1.03E-11	420.	1.50E-11	9.71E-12
480.	2.60E-11	9.90E-12	480.	-1.02E-12	1.02E-11	480.	1.62E-11	9.55E-12
540.	2.65E-11	9.75E-12	540.	-1.09E-12	1.00E-11	540.	1.72E-11	9.41E-12
600.	2.71E-11	9.65E-12	600.	-1.18E-12	9.89E-12	600.	1.81E-11	9.30E-12
660.	2.74E-11	9.50E-12	660.	-1.23E-12	9.75E-12	660.	1.89E-11	9.16E-12
720.	2.77E-11	9.41E-12	720.	-1.26E-12	9.64E-12	720.	1.99E-11	9.08E-12
780.	2.80E-11	9.29E-12	780.	-1.37E-12	9.51E-12	780.	2.01E-11	8.97E-12
840.	2.83E-11	9.25E-12	840.	-1.50E-12	9.46E-12	840.	2.06E-11	8.93E-12
900.	2.85E-11	9.12E-12	900.	-1.72E-12	9.36E-12	900.	2.10E-11	8.82E-12
960.	2.88E-11	9.12E-12	960.	-1.74E-12	9.34E-12	960.	2.14E-11	8.82E-12
1000.	2.88E-11	9.05E-12	1000.	-1.86E-12	9.26E-12	1000.	2.15E-11	8.75E-12

TABLE 9.6.2 IRRADIATION CURRENTS FOR DOUBLE-THICKNESS SPECIMEN IN REVERSED POSITION

L.V. TO H.V. ELECTRODE			GUARD RING TO H.V. ELECTRODE			COAXIAL CABLE		
TIME (SEC)	CURRENT (A)	STD DEV (A)	TIME (SEC)	CURRENT (A)	STD DEV (A)	TIME (SEC)	CURRENT (A)	STD DEV (A)
3.	2.27E-12	1.65E-11	3.	-2.63E-12	1.57E-11	3.	-1.53E-11	1.56E-11
15.	4.10E-12	1.73E-11	15.	-2.30E-12	1.61E-11	15.	-1.82E-11	1.60E-11
30.	6.66E-12	1.60E-11	30.	-4.33E-14	1.49E-11	30.	-1.49E-11	1.44E-11
45.	8.16E-12	1.61E-11	45.	5.63E-13	1.46E-11	45.	-1.25E-11	1.43E-11
60.	9.35E-12	1.61E-11	60.	1.15E-12	1.46E-11	60.	-1.04E-11	1.42E-11
75.	1.04E-11	1.62E-11	75.	1.48E-12	1.47E-11	75.	-8.49E-12	1.43E-11
90.	1.16E-11	1.62E-11	90.	1.72E-12	1.46E-11	90.	-6.75E-12	1.43E-11
105.	1.23E-11	1.64E-11	105.	1.99E-12	1.48E-11	105.	-5.35E-12	1.44E-11
120.	1.31E-11	1.64E-11	120.	2.32E-12	1.48E-11	120.	-3.96E-12	1.44E-11
150.	1.45E-11	1.65E-11	150.	2.87E-12	1.48E-11	150.	-1.63E-12	1.44E-11
180.	1.55E-11	1.66E-11	180.	3.13E-12	1.49E-11	180.	2.33E-13	1.44E-11
240.	1.72E-11	1.69E-11	240.	3.65E-12	1.51E-11	240.	3.18E-12	1.47E-11
300.	1.86E-11	1.72E-11	300.	3.97E-12	1.54E-11	300.	5.42E-12	1.50E-11
360.	1.95E-11	1.74E-11	360.	4.08E-12	1.56E-11	360.	7.11E-12	1.51E-11
420.	2.03E-11	1.75E-11	420.	4.29E-12	1.53E-11	420.	8.45E-12	1.53E-11
480.	2.08E-11	1.73E-11	480.	4.23E-12	1.55E-11	480.	9.63E-12	1.55E-11
540.	2.14E-11	1.80E-11	540.	4.25E-12	1.61E-11	540.	1.06E-11	1.56E-11
600.	2.17E-11	1.81E-11	600.	4.29E-12	1.63E-11	600.	1.14E-11	1.59E-11
660.	2.20E-11	1.81E-11	660.	4.15E-12	1.63E-11	660.	1.21E-11	1.58E-11
720.	2.24E-11	1.82E-11	720.	4.07E-12	1.64E-11	720.	1.27E-11	1.59E-11
780.	2.26E-11	1.82E-11	780.	4.04E-12	1.64E-11	780.	1.32E-11	1.59E-11
840.	2.27E-11	1.83E-11	840.	3.98E-12	1.64E-11	840.	1.36E-11	1.60E-11
900.	2.29E-11	1.82E-11	900.	3.87E-12	1.65E-11	900.	1.40E-11	1.60E-11
960.	2.31E-11	1.83E-11	960.	3.76E-12	1.65E-11	960.	1.44E-11	1.60E-11
1000.	2.32E-11	1.82E-11	1000.	3.65E-12	1.65E-11	1000.	1.46E-11	1.60E-11

TABLE 9.6.3 POST-IRRADIATION CURRENTS FOR DOUBLE-THICKNESS SPECIMEN IN NORMAL POSITION

L.V. TO H.V. ELECTRODE			GUARD RING TO H.V. ELECTRODE			COAXIAL CABLE		
TIME (SEC)	CURRENT (A)	STD DEV (A)	TIME (SEC)	CURRENT (A)	STD DEV (A)	TIME (SEC)	CURRENT (A)	STD DEV (A)
15.	4.91E-14	1.25E-13	15.	1.90E-12	1.03E-13	15.	2.55E-14	9.60E-14
18.	5.40E-14	1.32E-13	18.	1.77E-12	1.00E-13	18.	-6.70E-14	9.59E-14
21.	7.13E-14	1.35E-13	21.	1.68E-12	9.86E-14	21.	-1.21E-13	9.57E-14
24.	7.00E-14	1.30E-13	24.	1.58E-12	9.20E-14	24.	-1.65E-13	8.88E-14
27.	6.93E-14	1.26E-13	27.	1.51E-12	8.89E-14	27.	-1.95E-13	8.73E-14
30.	6.93E-14	1.21E-13	30.	1.45E-12	8.66E-14	30.	-2.15E-13	8.29E-14
36.	7.27E-14	1.12E-13	36.	1.32E-12	8.07E-14	36.	-2.36E-13	7.37E-14
42.	8.27E-14	1.11E-13	42.	1.23E-12	7.99E-14	42.	-2.41E-13	7.33E-14
48.	8.17E-14	1.09E-13	48.	1.16E-12	7.74E-14	48.	-2.44E-13	7.16E-14
54.	8.23E-14	1.03E-13	54.	1.08E-12	7.39E-14	54.	-2.49E-13	6.64E-14
60.	8.60E-14	9.92E-14	60.	1.01E-12	7.37E-14	60.	-2.45E-13	6.27E-14
66.	8.90E-14	9.50E-14	66.	9.61E-13	6.96E-14	66.	-2.39E-13	5.82E-14
72.	9.57E-14	9.01E-14	72.	9.06E-13	6.52E-14	72.	-2.32E-13	5.32E-14
78.	9.33E-14	8.78E-14	78.	8.77E-13	6.50E-14	78.	-2.33E-13	5.24E-14
84.	1.06E-13	8.35E-14	84.	8.20E-13	5.54E-14	84.	-2.20E-13	4.83E-14
90.	1.00E-13	8.14E-14	90.	7.93E-13	5.85E-14	90.	-2.22E-13	4.87E-14
96.	1.02E-13	8.10E-14	96.	7.66E-13	5.79E-14	96.	-2.18E-13	4.80E-14
102.	1.05E-13	7.71E-14	102.	7.36E-13	6.00E-14	102.	-2.13E-13	4.69E-14
108.	1.06E-13	7.49E-14	108.	7.09E-13	5.47E-14	108.	-2.11E-13	4.46E-14
114.	1.06E-13	7.50E-14	114.	6.83E-13	5.97E-14	114.	-2.10E-13	4.56E-14
120.	1.05E-13	7.38E-14	120.	6.59E-13	5.56E-14	120.	-2.07E-13	4.45E-14
135.	1.08E-13	6.77E-14	135.	5.97E-13	5.07E-14	135.	-1.98E-13	4.06E-14
150.	1.04E-13	6.67E-14	150.	5.54E-13	4.74E-14	150.	-1.91E-13	3.93E-14
165.	1.05E-13	6.72E-14	165.	5.14E-13	5.03E-14	165.	-1.85E-13	3.98E-14
180.	1.01E-13	6.57E-14	180.	4.79E-13	4.94E-14	180.	-1.80E-13	3.87E-14
210.	9.63E-14	5.71E-14	210.	4.16E-13	4.76E-14	210.	-1.68E-13	3.44E-14
240.	9.43E-14	5.69E-14	240.	3.63E-13	4.39E-14	240.	-1.55E-13	3.31E-14
270.	9.43E-14	5.26E-14	270.	3.24E-13	4.49E-14	270.	-1.43E-13	3.18E-14
300.	9.10E-14	5.29E-14	300.	2.91E-13	4.47E-14	300.	-1.30E-13	3.17E-14
330.	9.47E-14	4.56E-14	330.	2.56E-13	3.90E-14	330.	-1.19E-13	2.77E-14
360.	9.27E-14	4.48E-14	360.	2.31E-13	4.02E-14	360.	-1.10E-13	2.71E-14
420.	8.40E-14	3.93E-14	420.	1.92E-13	3.55E-14	420.	-9.20E-14	2.39E-14
480.	8.67E-14	3.64E-14	480.	1.59E-13	3.33E-14	480.	-7.93E-14	2.22E-14
540.	8.23E-14	3.26E-14	540.	1.36E-13	2.86E-14	540.	-6.67E-14	1.96E-14
600.	8.47E-14	2.86E-14	600.	1.14E-13	2.49E-14	600.	-5.83E-14	1.72E-14
660.	7.50E-14	2.46E-14	660.	9.80E-14	2.12E-14	660.	-5.00E-14	1.48E-14
720.	7.83E-14	2.60E-14	720.	8.53E-14	2.59E-14	720.	-4.47E-14	1.67E-14
780.	7.40E-14	2.83E-14	780.	7.30E-14	2.27E-14	780.	-3.70E-14	1.64E-14
840.	7.00E-14	2.09E-14	840.	6.13E-14	1.94E-14	840.	-3.30E-14	1.32E-14
900.	7.01E-14	2.07E-14	900.	5.71E-14	1.97E-14	900.	-2.62E-14	1.30E-14
960.	6.34E-14	2.11E-14	960.	5.09E-14	2.14E-14	960.	-2.59E-14	1.39E-14
1020.	6.63E-14	2.01E-14	1020.	4.28E-14	1.93E-14	1020.	-1.85E-14	1.28E-14

TABLE 9.6.4 POST-IRRADIATION CURRENTS FOR DOUBLE-THICKNESS SPECIMEN IN REVERSED POSITION

L.V. TO H.V. ELECTRODE			GUARD RING TO H.V. ELECTRODE			COAXIAL CABLE		
TIME (SEC)	CURRENT (A)	STD DEV (A)	TIME (SEC)	CURRENT (A)	STD DEV (A)	TIME (SEC)	CURRENT (A)	STD DEV (A)
15.	2.68E-13	2.52E-13	15.	2.02E-12	2.07E-13	15.	3.10E-14	2.03E-13
18.	2.37E-13	2.40E-13	18.	1.90E-12	2.06E-13	18.	-4.37E-14	2.04E-13
21.	2.31E-13	2.35E-13	21.	1.79E-12	1.97E-13	21.	-9.53E-14	1.98E-13
24.	2.22E-13	2.19E-13	24.	1.70E-12	1.73E-13	24.	-1.41E-13	1.77E-13
27.	2.24E-13	2.22E-13	27.	1.61E-12	1.80E-13	27.	-1.67E-13	1.79E-13
30.	2.25E-13	2.17E-13	30.	1.53E-12	1.74E-13	30.	-1.87E-13	1.77E-13
36.	2.15E-13	2.17E-13	36.	1.42E-12	1.69E-13	36.	-2.18E-13	1.68E-13
42.	2.20E-13	2.11E-13	42.	1.32E-12	1.61E-13	42.	-2.30E-13	1.60E-13
48.	2.11E-13	2.00E-13	48.	1.24E-12	1.49E-13	48.	-2.40E-13	1.49E-13
54.	2.08E-13	1.93E-13	54.	1.17E-12	1.40E-13	54.	-2.44E-13	1.40E-13
60.	1.96E-13	1.87E-13	60.	1.11E-12	1.35E-13	60.	-2.48E-13	1.34E-13
66.	1.99E-13	1.81E-13	66.	1.05E-12	1.29E-13	66.	-2.44E-13	1.29E-13
72.	1.92E-13	1.78E-13	72.	1.01E-12	1.25E-13	72.	-2.43E-13	1.25E-13
78.	1.85E-13	1.72E-13	78.	9.58E-13	1.21E-13	78.	-2.42E-13	1.21E-13
84.	1.88E-13	1.64E-13	84.	9.15E-13	1.16E-13	84.	-2.35E-13	1.15E-13
90.	1.82E-13	1.61E-13	90.	8.74E-13	1.13E-13	90.	-2.36E-13	1.13E-13
96.	1.73E-13	1.56E-13	96.	8.40E-13	1.07E-13	96.	-2.40E-13	1.06E-13
102.	1.64E-13	1.49E-13	102.	8.16E-13	1.01E-13	102.	-2.44E-13	1.00E-13
108.	1.57E-13	1.45E-13	108.	7.88E-13	9.85E-14	108.	-2.42E-13	9.75E-14
114.	1.67E-13	1.43E-13	114.	7.38E-13	9.48E-14	114.	-2.26E-13	9.42E-14
120.	1.67E-13	1.41E-13	120.	7.10E-13	9.11E-14	120.	-2.21E-13	9.05E-14
135.	1.62E-13	1.30E-13	135.	6.52E-13	8.85E-14	135.	-2.12E-13	8.77E-14
150.	1.56E-13	1.30E-13	150.	6.10E-13	8.08E-14	150.	-2.07E-13	7.99E-14
165.	1.43E-13	1.25E-13	165.	5.70E-13	7.85E-14	165.	-2.05E-13	7.75E-14
180.	1.45E-13	1.23E-13	180.	5.35E-13	7.47E-14	180.	-1.99E-13	7.37E-14
210.	1.36E-13	1.03E-13	210.	4.71E-13	6.54E-14	210.	-1.81E-13	6.32E-14
240.	1.27E-13	9.87E-14	240.	4.15E-13	6.10E-14	240.	-1.74E-13	5.92E-14
270.	1.16E-13	8.69E-14	270.	3.68E-13	5.66E-14	270.	-1.61E-13	5.32E-14
300.	1.12E-13	7.99E-14	300.	3.26E-13	4.96E-14	300.	-1.50E-13	4.67E-14
330.	1.03E-13	7.45E-14	330.	2.95E-13	4.66E-14	330.	-1.40E-13	4.32E-14
360.	9.77E-14	7.05E-14	360.	2.60E-13	4.55E-14	360.	-1.29E-13	4.12E-14
420.	8.80E-14	5.97E-14	420.	2.10E-13	3.64E-14	420.	-1.10E-13	3.32E-14
480.	8.10E-14	5.17E-14	480.	1.74E-13	3.31E-14	480.	-9.30E-14	2.86E-14
540.	7.43E-14	4.19E-14	540.	1.45E-13	2.34E-14	540.	-8.07E-14	2.36E-14
600.	7.20E-14	3.62E-14	600.	1.16E-13	2.67E-14	600.	-7.10E-14	2.09E-14
660.	6.60E-14	3.25E-14	660.	9.63E-14	2.57E-14	660.	-5.90E-14	2.03E-14
720.	6.17E-14	3.31E-14	720.	8.17E-14	2.60E-14	720.	-5.03E-14	1.99E-14
780.	6.35E-14	2.37E-14	780.	6.15E-14	2.16E-14	780.	-4.85E-14	1.54E-14
840.	5.73E-14	2.49E-14	840.	5.49E-14	1.99E-14	840.	-3.98E-14	1.55E-14
900.	5.85E-14	1.80E-14	900.	4.55E-14	1.83E-14	900.	-3.66E-14	1.30E-14
960.	5.81E-14	2.03E-14	960.	3.09E-14	1.85E-14	960.	-2.91E-14	1.33E-14
1020.	5.28E-14	1.77E-14	1020.	2.80E-14	2.00E-14	1020.	-2.00E-14	1.31E-14

TABLE 9.6.5 IRRADIATION CURRENTS FOR SINGLE-THICKNESS SPECIMEN IN NORMAL POSITION

L.V. TO H.V. ELECTRODE			GUARD RING TO H.V. ELECTRODE			COAXIAL CABLE		
TIME (SEC)	CURRENT (A)	STD DEV (A)	TIME (SEC)	CURRENT (A)	STD DEV (A)	TIME (SEC)	CURRENT (A)	STD DEV (A)
3.	5.97E-12	9.21E-12	3.	-7.38E-11	1.15E-11	3.	-6.13E-12	8.80E-12
15.	7.90E-12	8.13E-12	15.	-7.27E-11	1.13E-11	15.	-7.20E-12	7.49E-12
30.	9.20E-12	7.47E-12	30.	-7.17E-11	1.09E-11	30.	-6.20E-12	6.71E-12
45.	1.02E-11	7.33E-12	45.	-7.11E-11	1.11E-11	45.	-4.87E-12	6.49E-12
60.	1.10E-11	7.09E-12	60.	-7.06E-11	1.10E-11	60.	-3.67E-12	6.21E-12
75.	1.18E-11	6.86E-12	75.	-7.01E-11	1.09E-11	75.	-2.63E-12	5.99E-12
90.	1.23E-11	6.81E-12	90.	-6.99E-11	1.10E-11	90.	-1.67E-12	5.94E-12
105.	1.30E-11	6.69E-12	105.	-6.95E-11	1.10E-11	105.	-6.33E-13	5.83E-12
120.	1.35E-11	6.66E-12	120.	-6.94E-11	1.11E-11	120.	2.00E-13	5.83E-12
150.	1.42E-11	6.57E-12	150.	-6.92E-11	1.11E-11	150.	1.50E-12	5.79E-12
180.	1.47E-11	6.47E-12	180.	-6.93E-11	1.11E-11	180.	2.73E-12	5.74E-12
240.	1.59E-11	6.41E-12	240.	-6.85E-11	1.11E-11	240.	4.93E-12	5.75E-12
300.	1.68E-11	6.34E-12	300.	-6.83E-11	1.11E-11	300.	6.63E-12	5.75E-12
360.	1.74E-11	6.32E-12	360.	-6.81E-11	1.12E-11	360.	8.00E-12	5.79E-12
420.	1.80E-11	6.31E-12	420.	-6.79E-11	1.12E-11	420.	9.21E-12	5.81E-12
480.	1.84E-11	6.26E-12	480.	-6.77E-11	1.12E-11	480.	1.02E-11	5.80E-12
540.	1.88E-11	6.17E-12	540.	-6.76E-11	1.10E-11	540.	1.12E-11	5.75E-12
600.	1.91E-11	6.07E-12	600.	-6.75E-11	1.08E-11	600.	1.19E-11	5.67E-12
660.	1.95E-11	5.98E-12	660.	-6.74E-11	1.06E-11	660.	1.27E-11	5.59E-12
720.	1.99E-11	5.91E-12	720.	-6.75E-11	1.05E-11	720.	1.33E-11	5.52E-12
780.	2.04E-11	5.88E-12	780.	-6.74E-11	1.05E-11	780.	1.39E-11	5.52E-12
840.	2.05E-11	5.79E-12	840.	-6.75E-11	1.03E-11	840.	1.45E-11	5.43E-12
900.	2.07E-11	5.73E-12	900.	-6.73E-11	1.02E-11	900.	1.50E-11	5.39E-12
960.	2.09E-11	5.65E-12	960.	-6.76E-11	1.00E-11	960.	1.54E-11	5.33E-12
1000.	2.10E-11	5.68E-12	1000.	-6.74E-11	1.01E-11	1000.	1.57E-11	5.37E-12

TABLE 9.6.6 IRRADIATION CURRENTS FOR SINGLE-THICKNESS SPECIMEN IN REVERSED POSITION

L.V. TO H.V. ELECTRODE			GUARD RING TO H.V. ELECTRODE			COAXIAL CABLE		
TIME (SEC)	CURRENT (A)	STD DEV (A)	TIME (SEC)	CURRENT (A)	STD DEV (A)	TIME (SEC)	CURRENT (A)	STD DEV (A)
3.	1.84E-11	5.97E-12	3.	-8.29E-11	7.76E-12	3.	1.05E-11	4.38E-12
15.	1.87E-11	3.93E-12	15.	-8.30E-11	6.40E-12	15.	7.30E-12	3.36E-12
30.	1.79E-11	3.85E-12	30.	-8.26E-11	6.42E-12	30.	7.63E-12	3.35E-12
45.	1.81E-11	3.72E-12	45.	-8.23E-11	6.23E-12	45.	8.18E-12	3.24E-12
60.	1.83E-11	3.59E-12	60.	-8.21E-11	6.04E-12	60.	8.73E-12	3.14E-12
75.	1.84E-11	3.47E-12	75.	-8.20E-11	5.86E-12	75.	9.15E-12	3.05E-12
90.	1.87E-11	3.45E-12	90.	-8.21E-11	5.89E-12	90.	9.88E-12	3.05E-12
105.	1.91E-11	3.48E-12	105.	-8.21E-11	6.07E-12	105.	1.06E-11	3.13E-12
120.	1.93E-11	3.36E-12	120.	-8.19E-11	5.87E-12	120.	1.11E-11	3.03E-12
150.	1.99E-11	3.48E-12	150.	-8.21E-11	6.23E-12	150.	1.23E-11	3.19E-12
180.	2.03E-11	3.39E-12	180.	-8.20E-11	6.26E-12	180.	1.32E-11	3.19E-12
240.	2.09E-11	3.03E-12	240.	-8.15E-11	5.61E-12	240.	1.47E-11	2.85E-12
300.	2.15E-11	2.96E-12	300.	-8.11E-11	5.60E-12	300.	1.61E-11	2.83E-12
360.	2.21E-11	2.93E-12	360.	-8.03E-11	5.60E-12	360.	1.73E-11	2.83E-12
420.	2.25E-11	3.00E-12	420.	-8.06E-11	5.79E-12	420.	1.83E-11	2.91E-12
480.	2.29E-11	3.09E-12	480.	-8.04E-11	5.97E-12	480.	1.92E-11	3.00E-12
540.	2.32E-11	3.12E-12	540.	-8.01E-11	6.03E-12	540.	1.99E-11	3.03E-12
600.	2.37E-11	3.03E-12	600.	-8.02E-11	5.84E-12	600.	2.03E-11	2.94E-12
660.	2.38E-11	2.98E-12	660.	-7.97E-11	5.72E-12	660.	2.13E-11	2.88E-12
720.	2.39E-11	2.89E-12	720.	-7.93E-11	5.52E-12	720.	2.17E-11	2.79E-12
780.	2.44E-11	3.01E-12	780.	-7.96E-11	5.78E-12	780.	2.24E-11	2.92E-12
840.	2.45E-11	3.11E-12	840.	-7.92E-11	5.94E-12	840.	2.28E-11	3.01E-12
900.	2.48E-11	3.05E-12	900.	-7.96E-11	5.86E-12	900.	2.34E-11	2.95E-12
960.	2.49E-11	2.96E-12	960.	-7.93E-11	5.66E-12	960.	2.37E-11	2.86E-12
1000.	2.49E-11	2.91E-12	1000.	-7.92E-11	5.55E-12	1000.	2.38E-11	2.80E-12

TABLE 9.5.7 POST-IRRADIATION CURRENTS FOR SINGLE-THICKNESS SPECIMEN IN NORMAL POSITION

L.V. TO H.V. ELECTRODE			GUARD RING TO H.V. ELECTRODE			COAXIAL CABLE		
TIME (SEC)	CURRENT (A)	STD DEV (A)	TIME (SEC)	CURRENT (A)	STD DEV (A)	TIME (SEC)	CURRENT (A)	STD DEV (A)
15.	-5.90E-13	3.22E-13	15.	5.59E-13	1.83E-13	15.	7.10E-13	1.66E-13
18.	-5.57E-13	2.73E-13	18.	4.89E-13	1.57E-13	18.	6.03E-13	1.42E-13
21.	-5.22E-13	2.44E-13	21.	4.56E-13	1.41E-13	21.	5.38E-13	1.29E-13
24.	-5.00E-13	2.17E-13	24.	4.32E-13	1.25E-13	24.	4.89E-13	1.14E-13
27.	-4.83E-13	2.01E-13	27.	4.15E-13	1.16E-13	27.	4.54E-13	1.05E-13
30.	-4.72E-13	1.85E-13	30.	3.93E-13	1.09E-13	30.	4.24E-13	9.78E-14
36.	-4.19E-13	1.59E-13	36.	3.47E-13	9.67E-14	36.	3.67E-13	8.51E-14
42.	-3.95E-13	1.47E-13	42.	3.22E-13	8.52E-14	42.	3.30E-13	7.52E-14
48.	-3.75E-13	1.27E-13	48.	2.99E-13	7.76E-14	48.	3.01E-13	6.86E-14
54.	-3.61E-13	1.19E-13	54.	2.87E-13	7.26E-14	54.	2.82E-13	6.42E-14
60.	-3.46E-13	1.10E-13	60.	2.73E-13	6.71E-14	60.	2.64E-13	5.93E-14
66.	-3.35E-13	1.01E-13	66.	2.63E-13	6.02E-14	66.	2.46E-13	5.43E-14
72.	-3.24E-13	9.26E-14	72.	2.55E-13	5.53E-14	72.	2.31E-13	4.99E-14
78.	-3.14E-13	8.63E-14	78.	2.45E-13	5.14E-14	78.	2.18E-13	4.65E-14
84.	-3.02E-13	7.92E-14	84.	2.36E-13	4.91E-14	84.	2.09E-13	4.32E-14
90.	-2.91E-13	7.60E-14	90.	2.28E-13	4.55E-14	90.	1.98E-13	4.09E-14
96.	-2.80E-13	6.71E-14	96.	2.24E-13	3.91E-14	96.	1.88E-13	3.61E-14
102.	-2.70E-13	6.05E-14	102.	2.17E-13	3.61E-14	102.	1.81E-13	3.29E-14
108.	-2.61E-13	5.56E-14	108.	2.12E-13	3.18E-14	108.	1.75E-13	2.95E-14
114.	-2.57E-13	4.80E-14	114.	2.08E-13	2.74E-14	114.	1.69E-13	2.54E-14
120.	-2.49E-13	4.93E-14	120.	2.04E-13	2.69E-14	120.	1.61E-13	2.55E-14
135.	-2.34E-13	3.73E-14	135.	1.93E-13	2.10E-14	135.	1.46E-13	1.93E-14
150.	-2.15E-13	3.62E-14	150.	1.83E-13	2.04E-14	150.	1.33E-13	1.88E-14
165.	-2.00E-13	2.94E-14	165.	1.72E-13	1.57E-14	165.	1.26E-13	1.49E-14
180.	-1.94E-13	2.08E-14	180.	1.68E-13	1.20E-14	180.	1.18E-13	1.09E-14
210.	-1.72E-13	1.36E-14	210.	1.53E-13	9.53E-15	210.	1.03E-13	7.30E-15
240.	-1.59E-13	6.23E-15	240.	1.44E-13	5.01E-15	240.	9.45E-14	4.03E-15
270.	-1.41E-13	1.26E-14	270.	1.34E-13	1.10E-14	270.	8.95E-14	9.86E-15
300.	-1.22E-13	1.14E-14	300.	1.23E-13	9.40E-15	300.	8.44E-14	8.71E-15
330.	-1.09E-13	1.27E-14	330.	1.14E-13	1.13E-14	330.	8.31E-14	1.07E-14
360.	-1.03E-13	1.48E-14	360.	1.06E-13	1.26E-14	360.	7.88E-14	1.22E-14
420.	-7.97E-14	1.68E-14	420.	9.54E-14	1.63E-14	420.	7.13E-14	1.44E-14
480.	-7.59E-14	2.36E-14	480.	9.17E-14	1.85E-14	480.	6.82E-14	1.63E-14
540.	-5.52E-14	1.86E-14	540.	8.29E-14	1.92E-14	540.	6.28E-14	1.61E-14
600.	-4.93E-14	2.33E-14	600.	8.01E-14	1.93E-14	600.	6.57E-14	1.75E-14
660.	-3.39E-14	2.23E-14	660.	7.28E-14	1.85E-14	660.	6.41E-14	1.74E-14
720.	-3.39E-14	2.30E-14	720.	6.82E-14	2.04E-14	720.	6.01E-14	1.94E-14
780.	-2.81E-14	2.29E-14	780.	6.32E-14	1.99E-14	780.	5.78E-14	1.82E-14
840.	-2.44E-14	2.33E-14	840.	5.82E-14	2.12E-14	840.	5.52E-14	1.94E-14
900.	-1.83E-14	2.21E-14	900.	5.57E-14	1.83E-14	900.	5.60E-14	1.65E-14
960.	-1.85E-14	2.42E-14	960.	5.41E-14	1.89E-14	960.	5.44E-14	1.78E-14
1020.	-1.20E-14	2.33E-14	1020.	5.02E-14	1.92E-14	1020.	5.29E-14	1.76E-14

TABLE 9.6.8 POST-IRRADIATION CURRENTS FOR SINGLE-THICKNESS SPECIMEN IN REVERSED POSITION

L.V. TO H.V. ELECTRODE			GUARD RING TO H.V. ELECTRODE			COAXIAL CABLE		
TIME (SEC)	CURRENT (A)	STD DEV (A)	TIME (SEC)	CURRENT (A)	STD DEV (A)	TIME (SEC)	CURRENT (A)	STD DEV (A)
15.	-4.86E-13	2.37E-13	15.	7.33E-13	1.32E-13	15.	8.44E-13	1.21E-13
18.	-4.78E-13	2.11E-13	18.	6.56E-13	1.09E-13	18.	7.32E-13	1.06E-13
21.	-4.67E-13	1.88E-13	21.	5.94E-13	9.82E-14	21.	6.53E-13	9.48E-14
24.	-4.52E-13	1.66E-13	24.	5.49E-13	8.81E-14	24.	5.98E-13	8.49E-14
27.	-4.39E-13	1.49E-13	27.	5.08E-13	7.85E-14	27.	5.53E-13	7.54E-14
30.	-4.24E-13	1.33E-13	30.	4.76E-13	7.04E-14	30.	5.18E-13	6.71E-14
36.	-3.98E-13	1.09E-13	36.	4.26E-13	5.98E-14	36.	4.62E-13	5.58E-14
42.	-3.79E-13	1.05E-13	42.	3.95E-13	5.73E-14	42.	4.24E-13	5.34E-14
48.	-3.67E-13	9.46E-14	48.	3.68E-13	5.17E-14	48.	3.90E-13	4.82E-14
54.	-3.52E-13	8.80E-14	54.	3.45E-13	4.97E-14	54.	3.65E-13	4.50E-14
60.	-3.37E-13	8.40E-14	60.	3.27E-13	4.63E-14	60.	3.43E-13	4.31E-14
66.	-3.29E-13	7.77E-14	66.	3.12E-13	4.18E-14	66.	3.21E-13	3.95E-14
72.	-3.15E-13	7.29E-14	72.	3.01E-13	4.02E-14	72.	3.03E-13	3.71E-14
78.	-3.07E-13	6.91E-14	78.	2.87E-13	3.77E-14	78.	2.86E-13	3.52E-14
84.	-2.98E-13	6.18E-14	84.	2.77E-13	3.38E-14	84.	2.75E-13	3.15E-14
90.	-2.86E-13	5.85E-14	90.	2.65E-13	3.23E-14	90.	2.62E-13	2.99E-14
96.	-2.72E-13	5.24E-14	96.	2.55E-13	2.85E-14	96.	2.50E-13	2.67E-14
102.	-2.66E-13	5.26E-14	102.	2.47E-13	2.84E-14	102.	2.39E-13	2.68E-14
108.	-2.59E-13	5.04E-14	108.	2.40E-13	2.82E-14	108.	2.29E-13	2.53E-14
114.	-2.50E-13	5.34E-14	114.	2.29E-13	2.98E-14	114.	2.18E-13	2.73E-14
120.	-2.47E-13	5.05E-14	120.	2.21E-13	2.82E-14	120.	2.05E-13	2.59E-14
135.	-2.21E-13	4.44E-14	135.	2.07E-13	2.47E-14	135.	1.95E-13	2.27E-14
150.	-2.11E-13	3.93E-14	150.	1.94E-13	2.36E-14	150.	1.81E-13	2.01E-14
165.	-1.96E-13	3.33E-14	165.	1.85E-13	2.32E-14	165.	1.67E-13	1.82E-14
180.	-1.84E-13	2.13E-14	180.	1.72E-13	1.70E-14	180.	1.53E-13	1.22E-14
210.	-1.61E-13	1.65E-14	210.	1.52E-13	1.53E-14	210.	1.35E-13	1.01E-14
240.	-1.40E-13	1.34E-14	240.	1.42E-13	1.17E-14	240.	1.29E-13	7.95E-15
270.	-1.31E-13	1.34E-14	270.	1.34E-13	1.43E-14	270.	1.19E-13	8.76E-15
300.	-1.12E-13	1.03E-14	300.	1.21E-13	1.15E-14	300.	1.14E-13	7.03E-15
330.	-1.01E-13	6.95E-15	330.	1.08E-13	8.25E-15	330.	1.04E-13	4.83E-15
360.	-8.77E-14	6.40E-15	360.	1.04E-13	6.40E-15	360.	1.03E-13	4.05E-15
420.	-7.22E-14	8.36E-15	420.	8.54E-14	9.79E-15	420.	9.68E-14	5.75E-15
480.	-5.72E-14	7.07E-15	480.	7.64E-14	9.95E-15	480.	9.08E-14	5.46E-15
540.	-4.21E-14	1.06E-14	540.	7.01E-14	1.03E-14	540.	8.69E-14	6.60E-15
600.	-3.72E-14	1.17E-14	600.	6.74E-14	9.87E-15	600.	8.18E-14	6.92E-15
660.	-3.22E-14	1.13E-14	660.	5.84E-14	8.93E-15	660.	7.78E-14	6.46E-15
720.	-2.19E-14	1.21E-14	720.	5.10E-14	9.99E-15	720.	7.34E-14	7.02E-15
780.	-2.08E-14	1.39E-14	780.	4.94E-14	1.51E-14	780.	7.45E-14	1.07E-14
840.	-1.72E-14	1.35E-14	840.	4.70E-14	7.93E-15	840.	7.01E-14	7.02E-15
900.	-8.63E-15	1.35E-14	900.	3.96E-14	9.83E-15	900.	6.91E-14	7.45E-15
960.	-6.30E-15	1.02E-14	960.	4.19E-14	6.31E-15	960.	6.74E-14	5.38E-15
1020.	8.00E-16	1.45E-14	1020.	3.77E-14	8.93E-15	1020.	6.65E-14	7.60E-15

Appendix 9.7

T-Test for Corrected Post-Irradiation Currents at ±500V

The t-value for the difference between two means may be found from the following formula (25)

$$t = \frac{|\bar{x}_1 - \bar{x}_2|}{\bar{s}(x)(1/n_1 + 1/n_2)^{1/2}} \qquad (9.7.1)$$

where

$\bar{x}_1$, $\bar{x}_2$ = the two means being compared

n_1, n_2 = the number of samples of which $\bar{x}_1$ and $\bar{x}_2$ are, respectively, the means

$\bar{s}(x)$ = the pooled estimate of the standard deviation from both sets of data.

The value of $\bar{s}(x)$ is defined by

$$\bar{s}^2(x) = \frac{(n_1-1)s^2(x_1) + (n_2-1)s^2(x_2)}{(n_1-1) + (n_2-1)} \qquad (9.7.2)$$

where $s(x_1)$ and $s(x_2)$ are the standard deviations associated with $\bar{x}_1$ and $\bar{x}_2$, respectively.

The null hypothesis is that the true means μ_1 and μ_2, of which $\bar{x}_1$ and $\bar{x}_2$ are the estimators, are equal.

Then, t is calculated from Eq. (9.7.1) and is compared to tabulated values for the degrees of freedom equal to $n_1 + n_2 - 2$, i.e., the total degrees of freedom available for calculating the pooled estimate of the standard deviation. If the calculated t is larger than the tabulated t at a preselected probability or significance level α, then it is concluded that the null hypothesis is false, i.e., the population mean estimated by $\bar{x}_1$ is significantly different from the population mean estimated by $\bar{x}_2$, with the α chance of being wrong.

The calculated t-values for the corrected post-irradiation currents at ±500V are given in Tables 9.7.1 and 9.7.2.

Table 9.7.1 T-Values for Double-Thickness Specimen

Time {sec}	I_{+500} {pA}	$-I_{-500}$ {pA}	t
15	5.22 ± 2.88	6.33 ± 3.08	.452
18	5.08 ± 2.73	6.00 ± 2.76	.409
21	4.98 ± 2.63	5.84 ± 2.67	.396
24	4.87 ± 2.54	5.71 ± 2.57	.403
27	4.78 ± 2.43	5.57 ± 2.46	.392
30	4.68 ± 2.37	5.48 ± 2.39	.408
36	4.51 ± 2.22	5.28 ± 2.23	.424
42	4.35 ± 2.11	5.13 ± 2.13	.445
48	4.23 ± 2.05	4.98 ± 2.02	.450
54	4.10 ± 1.95	4.86 ± 1.93	.477
60	3.99 ± 1.87	4.75 ± 1.85	.497
66	3.90 ± 1.82	4.65 ± 1.77	.513
72	3.82 ± 1.76	4.54 ± 1.69	.513
78	3.73 ± 1.71	4.47 ± 1.66	.542
84	3.65 ± 1.65	4.37 ± 1.57	.552
90	3.58 ± 1.61	4.30 ± 1.52	.559
96	3.51 ± 1.55	4.24 ± 1.48	.588
102	3.46 ± 1.55	4.16 ± 1.43	.577
108	3.40 ± 1.51	4.10 ± 1.39	.594
114	3.35 ± 1.46	4.03 ± 1.36	.596
120	3.29 ± 1.43	3.97 ± 1.32	.604
135	3.18 ± 1.36	3.84 ± 1.23	.629
150	3.06 ± 1.29	3.71 ± 1.13	.655
165	2.96 ± 1.21	3.60 ± 1.07	.684
180	2.90 ± 1.16	3.49 ± 1.00	.664
210	2.73 ± 1.04	3.32 ± 0.91	.731
240	2.61 ± 0.96	3.15 ± 0.82	.743
270	2.49 ± 0.97	3.01 ± 0.74	.794
300	2.40 ± 0.82	2.89 ± 0.69	.790
330	2.32 ± 0.78	2.77 ± 0.63	.767
360	2.24 ± 0.73	2.67 ± 0.58	.791
420	2.10 ± 0.61	2.50 ± 0.51	.890
480	2.00 ± 0.56	2.35 ± 0.43	.877
540	1.89 ± 0.47	2.21 ± 0.41	.896
600	1.80 ± 0.44	2.09 ± 0.38	.852
660	1.72 ± 0.37	2.01 ± 0.34	1.000
720	1.66 ± 0.33	1.90 ± 0.31	.890
780	1.60 ± 0.32	1.83 ± 0.30	.900
840	1.51 ± 0.28	1.76 ± 0.26	1.120
900	1.48 ± 0.27	1.68 ± 0.26	.956
960	1.43 ± 0.24	1.63 ± 0.23	.995
1020	1.40 ± 0.25	1.55 ± 0.22	.825

Table 9.7.2 T-Values for Single-Thickness Specimen

Time {sec}	I_{+500} {pA}	$-I_{-500}$ {pA}	t
15	10.40 ± 0.66	14.30 ± 1.30	4.64
18	10.30 ± 0.61	14.10 ± 1.32	4.43
21	10.10 ± 0.56	13.70 ± 1.29	4.34
24	10.00 ± 0.49	13.40 ± 1.16	4.67
27	9.86 ± 0.48	13.20 ± 1.10	4.89
30	9.70 ± 0.49	13.00 ± 1.08	4.79
36	9.51 ± 0.41	12.60 ± 1.03	4.82
42	9.37 ± 0.35	12.20 ± 1.13	4.18
48	9.18 ± 0.34	12.00 ± 1.01	4.54
54	9.08 ± 0.36	11.60 ± 0.96	4.33
60	8.89 ± 0.30	11.50 ± 0.76	5.58
66	8.78 ± 0.32	11.30 ± 0.76	5.27
72	8.63 ± 0.29	11.10 ± 0.78	5.04
78	8.53 ± 0.29	10.80 ± 0.78	4.81
84	8.42 ± 0.28	10.60 ± 0.72	4.93
90	8.30 ± 0.26	10.50 ± 0.70	5.02
96	8.18 ± 0.25	10.30 ± 0.72	4.84
102	8.08 ± 0.22	10.20 ± 0.72	4.89
108	7.99 ± 0.22	10.10 ± 0.74	4.72
114	7.89 ± 0.22	9.97 ± 0.78	4.42
120	7.81 ± 0.22	9.83 ± 0.78	4.33
135	7.60 ± 0.17	9.49 ± 0.77	4.15
150	7.39 ± 0.17	9.22 ± 0.77	4.01
165	7.22 ± 0.14	8.94 ± 0.74	3.95
180	7.03 ± 0.14	8.69 ± 0.71	3.99
210	6.71 ± 0.09	8.22 ± 0.68	3.82
240	6.43 ± 0.09	7.84 ± 0.67	3.61
270	6.21 ± 0.10	7.44 ± 0.59	3.54
300	5.96 ± 0.09	7.16 ± 0.61	3.35
330	5.77 ± 0.09	6.81 ± 0.58	3.07
360	5.61 ± 0.08	6.58 ± 0.55	3.01
420	5.26 ± 0.08	6.10 ± 0.52	2.77
480	4.94 ± 0.08	5.67 ± 0.46	2.71
540	4.70 ± 0.08	5.31 ± 0.48	2.14
600	4.46 ± 0.07	5.01 ± 0.41	2.30
660	4.26 ± 0.09	4.74 ± 0.40	2.08
720	4.05 ± 0.08	4.49 ± 0.36	2.13
780	3.89 ± 0.11	4.29 ± 0.35	1.85
840	3.74 ± 0.11	4.09 ± 0.33	1.72
900	3.60 ± 0.10	3.90 ± 0.34	1.51
960	3.48 ± 0.10	3.75 ± 0.31	1.45
1020	3.36 ± 0.12	3.58 ± 0.31	1.19

Appendix 9.8

Experimental I-V Data During Neutron Irradiation

Table 9.8.1 I-V Data for Dark Conductivity

Applied Voltage {V}	$I \times 10^{13}$ {A}	Applied Voltage {V}	$I \times 10^{13}$ {A}
0	+ 0.30		
+ 100	+ 1.90	- 100	- 2.90
+ 200	+ 2.90	- 200	- 3.90
+ 300	+ 3.95	- 300	- 4.85
+ 400	+ 5.25	- 400	- 6.15
+ 500	+ 6.35	- 500	- 7.45
+ 600	+ 7.25	- 600	- 8.65
+ 700	+ 8.65	- 700	- 9.40
+ 800	+10.00	- 800	-10.50
+ 900	+10.90	- 900	-12.00
+1000	+12.60	-1000	-13.30
+ 900	+ 9.70	- 900	-10.00
+ 800	+ 7.50	- 800	- 8.70
+ 700	+ 5.95	- 700	- 6.70
+ 600	+ 4.60	- 600	- 5.15
+ 500	+ 3.60	- 500	- 3.70
+ 400	+ 2.55	- 400	- 2.45
+ 300	+ 1.50	- 300	- 1.40
+ 200	+ 0.30	- 200	- 0.35
+ 100	- 0.70	- 100	+ 0.70
0	- 1.85	0	+ 1.90

Table 9.8.2 I-V Data for Position 1

Applied Voltage {V}	$I \times 10^9$ {A}
+1000	+2.22
+ 900	+2.06
+ 800	+1.87
+ 700	+1.68
+ 600	+1.47
+ 500	+1.25
+ 400	+1.03
+ 300	+0.81
+ 200	+0.56
+ 100	+0.30
0	+0.03
- 100	-0.22
- 200	-0.48
- 300	-0.68
- 400	-0.90
- 500	-1.10
- 600	-1.30
- 700	-1.47
- 800	-1.65
- 900	-1.82
-1000	-1.96

Table 9.8.3 I-V Data for Position 2

Applied Voltage {V}	$I \times 10^{11}$ {A}
+1000	+4.05
+ 900	+3.92
+ 800	+3.78
+ 700	+3.62
+ 600	+3.42
+ 500	+3.20
+ 400	+2.91
+ 300	+2.52
+ 200	+1.98
+ 100	+1.19
0	-0.06
- 100	-1.09
- 200	-1.75
- 300	-2.28
- 400	-2.69
- 500	-3.02
- 600	-3.25
- 700	-3.43
- 800	-3.58
- 900	-3.69
-1000	-3.78

Table 9.8.4 I-V Data for Position 3

Applied Voltage {V}	$I \times 10^{12}$ {A}
+1000	+1.90
+ 900	+1.45
+ 800	+1.16
+ 700	+0.94
+ 600	+0.65
+ 500	+0.29
+ 400	-0.10
+ 300	-0.40
+ 200	-0.62
+ 100	-1.00
0	-1.30
- 100	-1.55
- 200	-1.80
- 300	-1.99
- 400	-2.16
- 500	-2.31
- 600	-2.45
- 700	-2.56
- 800	-2.64
- 900	-2.67
-1000	-2.73

Table 9.8.5 I-V Data for Position 4

Applied Voltage {V}	$I \times 10^{13}$ {A}
+1000	+3.62
+ 900	+3.36
+ 800	+3.19
+ 700	+2.31
+ 600	+1.40
+ 500	+0.47
+ 400	-0.32
+ 300	-0.99
+ 200	-1.64
+ 100	-2.33
0	-3.02
- 100	-3.40
- 200	-3.75
- 300	-3.91
- 400	-4.07
- 500	-4.13
- 600	-4.15
- 700	-4.15
- 800	-4.15
- 900	-4.18
-1000	-4.18

Appendix 9.9

Reference Source Data

Table 9.9.1 Reference Source Activity Data

Source	Half-Life	Initial Activity {μCi}	Date
^{133}Ba	7.5 y	1.24	8 July 1969
^{57}Co	270 d	2.16	8 July 1969
^{60}Co	5.27 y	1.25	8 July 1969
^{22}Na	2.60 y	1.80	8 July 1969
^{109}Cd	470 d	9.54	8 July 1969
^{137}Cs	30 y	1.58	8 July 1969
^{54}Mn	314 d	3.29	8 July 1969

Table 9.9.2 Reference Source Gamma Data

Source	Gamma Energy {MeV}	% Occurrence
^{133}Ba	0.356	71.0
	0.382	7.56
	(0.360 avg.)	
^{57}Co	0.122	88.8
	0.136	10.98
	(0.124 avg.)	
^{60}Co	1.173	99.0
	1.332	99.13
^{22}Na	1.275	100.
^{109}Cd	0.088	100.
^{137}Cs	0.6616	93.5
^{54}Mn	0.8353	100.

Appendix 9.10

Calculation of NaI Detector Efficiency

Present activity is given by

$$A(t) = A_o e^{-\lambda t} \tag{9.10.1}$$

where A_o is the measured activity at some time, λ is the decay constant, and t is the elasped time since the activity was measured.

The decay constant is given by

$$\lambda = \frac{\ell n\ 2}{t_{1/2}} \tag{9.10.2}$$

where $t_{1/2}$ is the half-life.

The number of gammas appearing per second is just the present activity times the fractional occurrence of that particular gamma.

The measured count rate for a particular gamma is the total number of counts under its photopeak in the reference spectrum divided by the counting live time, and multiplied by two, since only one-half the gammas are counted in a 2π geometry.

The efficiency for that particular gamma energy is then

$$\varepsilon = \frac{\text{measured count rate}}{\text{calculated count rate}} . \tag{9.10.3}$$

Table 9.10 NaI Detector Efficiency vs. Gamma Energy

E_γ {MeV}	ε {%}
0.088	40.7
0.124	69.8
0.360	23.8
0.662	25.4
0.835	18.5
1.173	13.4
1.276	9.26
1.332	11.5

Appendix 9.11

Gold Foil Irradiation Data

Table 9.11 Foil Weights and Irradiation Times

Position	Bare	Covered	wt {g}	Time In	Time Out
1	X		0.5007	1538 14 Dec 72	1542 14 Dec 72
		X	0.4989		
2	X		0.4784	1458 16 Dec 72	1658 16 Dec 72
		X	0.4782		
3	X		0.4940	1712 16 Dec 72	0816 17 Dec 72
		X	0.4883		
4	X		0.4794	0840 17 Dec 72	0910 19 Dec 72
		X	0.4792		

Appendix 9.12

Gold Foil Counting Data

Table 9.12.1 Single Detector Foil Counting Data

Foil Wt {g}	Time Begun	Counting Time	Counts-Background for .412 MeV Photopeak
0.5007	1516 15 Dec 72	4 min	609420
	1523 15 Dec 72	4 min	609090
0.4989	1530 15 Dec 72	10 min	205551
	1542 15 Dec 72	10 min	207011
0.4784	1642 18 Dec 72	10 min	58388
	1655 18 Dec 72	10 min	57659
0.4782	1720 18 Dec 72	10 Min	5095
	1733 18 Dec 72	10 min	4933
0.4940	1115 18 Dec 72	10 min	9271
	1154 18 Dec 72	10 min	8966
0.4883	1309 18 Dec 72	10 min	0
	1321 18 Dec 72	10 min	0
0.4794	1417 19 Dec 72	10 min	0
	1429 19 Dec 72	10 min	0
0.4792	1504 19 Dec 72	10 min	0
	1517 19 Dec 72	10 min	0

Table 9.12.2 Coincidence Counting Data

Foil Wt {g}	Time Begun	Counting Time	N_γ	N_β	$N_{\beta\gamma}$
0.5007	1351 15 Dec 72	350.44 sec	37847	836366	5115
	1400 15 Dec 72	350.22 sec	37690	831618	5114
0.4989	1408 15 Dec 72	1340.42 sec	23637	486057	3001
	1432 15 Dec 72	1340.22 sec	23474	483533	2951
0.4784	1424 18 Dec 72	2000.25 sec	13081	186766	1244
	1458 18 Dec 72	2000.20 sec	13135	185677	1151
0.4782	1533 18 Dec 72	2025.29 sec	5245	20633	122
	1611 18 Dec 72	2001.06 sec	5043	20387	128
0.4940	0924 18 Dec 72	3000.23 sec	9310	47547	266
	1016 18 Dec 72	3000.00 sec	9196	47586	308
0.4883	1347 18 Dec 72	1000.60 sec	2405	3333	14
	1404 18 Dec 72	1000.14 sec	2319	3381	16
0.4974	1540 19 Dec 72	100.00 sec	252	408	0
0.4972	1542 19 Dec 72	100.00 sec	244	234	0

Appendix 9.13

Calculation of Foil Activity Using Single Detector Data

If $N_r(t)$ is the number of radioactive atoms present at time t, R(t) is the rate of production of the radioactive species, and λ is the decay constant for that species, then the equation governing $N_r(t)$ is

$$\frac{dN_r}{dt} = R(t) - \lambda N_r(t) \ . \tag{9.13.1}$$

R(t) is given by

$$R(t) = \int_{\substack{\text{foil} \\ \text{volume}}} dV \int N_p(x,y,z,t)\ \sigma_a(E)\ \phi(x,y,z,E,t)\ dE$$

where N_p is the number of parent atoms per cm^3, σ_a is the activation cross section of the parent atom, and ϕ is the neutron flux.

If the flux is constant in time, and the small decrease in N_p is neglected, then R is constant in time. Equation (9.13.1) then becomes

$$\frac{dN_r}{dt} + \lambda N_r(t) = R \ . \tag{9.13.2}$$

The solution to this differential equation is

$$N_r(t) = \frac{R}{\lambda}\ (1 - e^{-\lambda t}) \ . \tag{9.13.3}$$

The activity A(t) is defined by

$$A(t) \equiv \lambda N_r(t) = R(1 - e^{-\lambda t}) \ . \tag{9.13.4}$$

As $t \to \infty$, the saturation activity is given by

$$A_s = A(\infty) = \lim_{t\to\infty} R(1 - e^{-\lambda t}) = R. \tag{9.13.5}$$

Thus,

$$A(t) = \lambda N_r(t) = A_s(1 - e^{-\lambda t}) \ . \tag{9.13.6}$$

For single detector counting the number of counts measured between time t_1 and time t_2 (measured from the end of irradiation) is

$$C = \varepsilon \int_{t_1}^{t_2} A_o e^{-\lambda t} dt + B = \frac{\varepsilon A_o}{\lambda} (e^{-\lambda t_1} - e^{-\lambda t_2}) + B \qquad (9.13.7)$$

where ε is the detector efficiency, A_o is the activity at the end of irradiation, and B is the number of background counts from time t_1 to time t_2.

Then, from Eqs. (9.13.6) and (9.13.7), the saturation activity is given by

$$A_s = \frac{\lambda(C - B)}{\varepsilon(1 - e^{-\lambda t_o})(e^{-\lambda t_1} - e^{-\lambda t_2})} \qquad (9.13.8)$$

where t_o is the time of irradiation.

The mean saturation activity for each foil is determined by averaging the saturation activities for the two different counts of each foil.

Table 9.13 Mean Saturation Activity for Each Foil Using Single Detector Data

Foil Wt {g}	Saturation Activity $\{sec^{-1}\}$
0.5007	2.12×10^{7}
0.4989	2.88×10^{6}
0.4784	3.52×10^{4}
0.4782	3.06×10^{3}
0.4940	6.32×10^{2}
0.4883	~ 0
0.4974	~ 0
0.4972	~ 0

Appendix 9.14

Calculation of Foil Activity Using Coincidence Data

Define: $N \equiv$ number decays

$N_\beta \equiv \varepsilon_\beta N$ = number of β^- detector counts

$N_\gamma \equiv \varepsilon_\gamma N$ = number of γ detector counts

$N_{\beta\gamma} \equiv \varepsilon_\beta \varepsilon_\gamma N$ = number of coincident counts

where ε_β and ε_γ are the absolute efficiencies for the β^- and the γ detectors. Then,

$$N_{\beta\gamma} = \frac{N_\beta}{N} \times \frac{N_\gamma}{N} \times N = \frac{N_\beta N_\gamma}{N} \tag{9.14.1}$$

or

$$N = \frac{N_\beta N_\gamma}{N_{\beta\gamma}} . \tag{9.14.2}$$

N is also given by

$$N = \int_{t_1}^{t_2} A_o \, e^{-\lambda t} \, dt = \frac{A_o}{\lambda} \left(e^{-\lambda t_1} - e^{-\lambda t_2}\right) \tag{9.14.3}$$

where all symbols are defined as in Appendix 9.13.

Then, from Eqs. (9.13.6) and (9.14.3), the saturation activity is given as

$$A_s = \frac{\lambda C}{\left(1 - e^{-\lambda t_o}\right)\left(e^{-\lambda t_1} - e^{-\lambda t_2}\right)} . \tag{9.14.4}$$

Table 9.14 Mean Saturation Activity for Each Foil Using Coincidence Data

Foil Wt {g}	Saturation Activity $\{sec^{-1}\}$
0.5007	3.13×10^{7}
0.4989	5.31×10^{6}
0.4784	8.09×10^{4}
0.4782	3.31×10^{4}
0.4940	4.56×10^{3}
0.4883	4.98×10^{3}*
0.4974	~0
0.4972	~0

*This data point was thrown out in later calculations. Insufficient counts were measured for reasonable counting statistics to apply.

Appendix 9.15

Calculation of Thermal Flux from Foil Activities

Let N_T be the number of target atoms in a foil given by

$$N_T = \frac{Wt\ N_o}{W} \tag{9.15.1}$$

where Wt is the foil weight {g}, N_o is Avagandro's number, and W is the atomic weight of the foil {g/gram atom}.

The saturation activity of the foil can be expressed as

$$A_s = N_T\left\{\int_{thermal} vn(v)\ \frac{\sigma_{oa}\ v_o}{v}\ dv + \int_{epithermal} vn(v)\ \sigma_a(v)\ dv\right\} \tag{9.15.2}$$

if 1/v cross sections are assumed in the thermal energy range, where v is the neutron speed, v_o is the speed of 0.025 eV neutrons, σ_{oa} is the activation cross section of the parent atom for 0.025 eV neutrons, $\sigma_a(v)$ is the activation cross section for neutrons having speed v, and n(v) is the density of neutrons having speed v. Then,

$$A_s = A_{st} + A_{se} = N_T\ n_{th}\ v_o \sigma_{oa} + A_{se} \tag{9.15.3}$$

where A_{st} is the saturation activity due to thermal neutrons, A_{se} is the saturation activity due to epithermal neutrons, and n_{th} is the density of thermal neutrons.

Cadmium covers may be used to absorb all neutrons with energies below 0.4 eV. Then A_{se} is given by

$$A_{se} = F_{Cd}\ A_s(Cd) \tag{9.15.4}$$

where $A_s(Cd)$ is the saturation activity of the cadmium covered foil, and F_{Cd} is a correction factor to account for epithermal neutron absorption in the cadmium cover. For gold foils with thin cadmium covers, $F_{Cd} \simeq 1$, so that

$$A_{st} \simeq A_s - A_s(Cd)\ . \tag{9.15.5}$$

Note that flux depression is the foil itself is also neglected.

From Eq. (9.15.3)

$$A_{st} = N_T \, n_{th} \, v_o \sigma_{oa} \tag{9.15.6}$$

so that

$$n_{th} = \frac{A_s - A_s(Cd)}{N_T \, v_o \sigma_{oa}} \, . \tag{9.15.7}$$

To obtain the thermal neutron flux, multiply n_{th} by $\bar{v}$, the average neutron velocity, where

$$\bar{v} = \frac{1}{n} \int_0^\infty vn(v) \, dv \, . \tag{9.15.8}$$

If the neutron spectrum can be approximated by a Maxwellian distribution, $\bar{v}$ is given by

$$\bar{v} = (8kT/\pi m_n)^{1/2} \tag{9.15.9}$$

where k is the Boltzmann constant, T is the absolute temperature of the medium, and m_n is the rest mass of the neutron. For T = 293.16°K, $\bar{v} = 2.48 \times 10^5$ cm sec^{-1}.

Then

$$\phi_{th} = \bar{v} n_{th} = \frac{\bar{v}[A_s - A_s(Cd)]}{v_o \, N_T \, \sigma_{oa}} \, . \tag{9.15.10}$$

Since the bare and the covered foils are not the same weight, Eq. (9.15.10) must be corrected. Let N_{Tb} be the number of atoms in the bare foil and N_{Tc} be the number of atoms in the covered foil. Consider the activity per atom:

$$\frac{A_{st}}{N_T} = \frac{A_s}{N_{Tb}} - \frac{A_s(Cd)}{N_{Tc}} \, . \tag{9.15.11}$$

Use N_{Tb} as a basis: $N_T \equiv N_{Tb}$. Then

$$A_{st} = N_{Tb}\left[\frac{A_s}{N_{Tb}} - \frac{A_s(Cd)}{N_{Tc}}\right] \quad (9.15.12)$$

or

$$A_{st} = A_s - \frac{N_{Tb}}{N_{Tc}} A_s(Cd) \ . \quad (9.15.13)$$

But N_{Tb}/N_{Tc} is just the ratio of the foil weights. Define the weight ratio w_r as

$$w_r \equiv \frac{\text{wt of bare foil}}{\text{wt of covered foil}} \ . \quad (9.15.14)$$

The corrected equation for the thermal flux then becomes

$$\phi_{th} = \frac{\bar{v}[A_s - w_r A_s(Cd)]}{v_o N_{Tb} \sigma_{oa}} \ . \quad (9.15.15)$$

The calculated thermal flux at each position is given in Table 4.2.

RADIATION-INDUCED CURRENTS AND CONDUCTIVITY IN POLYETHYLENE

by

JEFFREY CLAIR RYMAN

B.S., Kansas State University, 1969

AN ABSTRACT OF A MASTER'S THESIS

submitted in partial fulfillment of the

requirements for the degree

MASTER OF SCIENCE

Department of Nuclear Engineering

KANSAS STATE UNIVERSITY
Manhattan, Kansas

1974

ABSTRACT

An investigation was undertaken of the radiation-induced currents in both single- and double-thickness polyethylene sheet specimens under short-circuit conditions. It is believed the basic mechanisms are an electron injection current and a conduction current controlled by a time-dependent spatially non-uniform charge distribution within the specimen. The short-circuit currents were found to represent a reproducible physical phenomenon. An attempt to model the short-circuit currents in terms of fictitious current generators within the specimen was successful during irradiation, but failed during post-irradiation recovery.

For the double-thickness specimen, subtraction of the post-irradiation short-circuit currents from the recovery currents observed at ±500V resulted in corrected currents which may be analyzed in terms of standard post-irradiation recovery models.

In addition, a polyethylene specimen was exposed to neutron and gamma radiation using the Kansas State University ^{252}Cf facility. The steady-state electrical conductivity was measured at four different fast-neutron flux levels. It was found that the steady-state conductivity, corrected for dark conductivity, was proportional to the 0.77 ± 0.09 power of the fast-neutron flux.